NOVA SCHOOL OF SCIENCE & TECHNOLOGY

CHEMISTRY DEPARTMENT

ACTIVE DRESSINGS BASED ON NATURAL POLYMERS FOR WOUND TREATMENT

JOÃO RICARDO ANTUNES DOS SANTOS SOARES PEREIRA

Master in Biotechnology

DOCTORATE IN CHEMICAL AND BIOLOGICAL ENGINEERING

NOVA University Lisbon

April 2024

NOVA SCHOOL OF SCIENCE & TECHNOLOGY

CHEMISTRY DEPARTMENT

ACTIVE DRESSINGS BASED ON NATURAL POLYMERS FOR WOUND TREATMENT

JOÃO RICARDO ANTUNES DOS SANTOS SOARES PEREIRA

Master in Biotechnology

Adviser: Maria Filomena Andrade de Freitas
Assistant Professor, NOVA School of Science and Technology (FCT NOVA)

Co-advisers: Jorge Alexandre de Carvalho Silva
Associate Professor, NOVA School of Science and Technology (FCT NOVA)

Examination Committee:

Chair: Maria da Ascensão Carvalho Fernandes Miranda Reis,
Full Professor, NOVA School of Science and Technology (FCT NOVA)

Rapporteurs: Liliana Sofia Carvalho Tomé,
Assistant Professor, Faculty of Sciences and Technology of University of Coimbra (FCT UC)
Viviana Pinto Ribeiro,
Full Researcher, Catholic University of Porto

Adviser: Maria Filomena Andrade de Freitas,
Assistant Professor, NOVA School of Science and Technology (FCT NOVA)

Members: Vítor Manuel Delgado Alves,
Assistant Professor, School of Agriculture of University of Lisbon (ISA UL)
Henrique Martiniano Vazão de Almeida,
Full Researcher, NOVA School of Science and Technology (FCT NOVA)

DOCTORATE IN CHEMICAL AND BIOLOGICAL ENGINEERING

NOVA University Lisbon
April 2024

Active Dressings Based On Natural Polymers For Wound Treatment

To my Family and Friends who help me become a better version of myself every day…

ACKNOWLEDGMENTS

A realização de um projeto de doutoramento é uma jornada longa, cheia de desafios e obstáculos que testam constantemente as nossas capacidades de perseverança, resiliência, espírito crítico e dedicação. Durante este árduo caminho é fácil de pensar que atravessamos tudo sozinhos de uma forma penosa, pesada e, por vezes, desmotivadora. Contudo, temos sempre à nossa volta pessoas que tornam esta aventura muito mais satisfatória, leve e motivadora. No fundo, pessoas com a capacidade especial de tornar a floresta tenebrosa que nós próprios criámos num trilho verde, luminoso, simpático e que nem sequer damos conta que o estamos a atravessar. Posso dizer que fui um sortudo no que toca às pessoas que me puderam acompanhar durante o meu percurso. Conheci pessoas que admiro, que me fizeram crescer e que levo comigo para sempre. E por isso não posso deixar de vos agradecer. Já dizia Antoine de Saint Éxupérie: "Aqueles que passam por nós não vão sós. Deixam um pouco de si, levam um pouco de nós." e, portanto, partirei para a minha próxima aventura de barriga cheia com um pouco de todos vós no coração.

Um Muito Obrigado a todos.

Gostaria de começar por dedicar um agradecimento especial, a uma pessoa que admiro muito, à Professora Doutora Filomena Freitas, que ao longo de todos estes anos me ajudou, orientou, ensinou e depositou a sua confiança em mim para demonstrar que seria capaz de desenvolver este e qualquer outro trabalho científico. Agradecer todas as oportunidades que me foi dando ao longo do meu percurso. E por último um muito obrigado pela orientação excecional, por toda a transmissão de conhecimento científico, espírito crítico e por ser um

exemplo a seguir em dedicação, simpatia, calma e perseverança. Espero que tenha gostado de trabalhar comigo o quanto eu gostei de trabalhar consigo.

Quero estender o meu agradecimento à Professora Doutora Maria Ascensão Reis, por ser uma pessoa admirável e por provar que é possível ser uma líder exemplar, ter boa disposição e profissionalismo. Um muito obrigado pela disponibilização de todos os recursos e, por me deixar fazer parte do Biochemical Engineering Group (BIOENG) há 7 anos, um grupo incrivelmente acolhedor.

Gostaria ainda de agradecer ao Professor Doutor Jorge Silva pela co-orientação, acolhimento e integração no seu grupo de investigação e pela partilha de conhecimentos, conselhos e propostas que ajudaram a enriquecer bastante o conteúdo desta dissertação.

Queria agradecer também às instituições que me acolheram para o desenvolvimento deste doutoramento, a Unidade de Ciências Biomoleculares Aplicadas (UCIBIO) um laboratório associado ao Instituto para a Saúde e Bioeconomia (i4HB) e o Centro de Investigação de Materiais (CENIMAT) um laboratório associado ao instituto de Nanoestruturas, Nanomodelação e Nanofabricação (i3N). Não esquecendo o agradecimento à Fundação para a Ciência e Tecnologia (FCT I. P.) pelo suporte financeiro (SFRH/BD/147518/2019) que me permitiu desenvolver este trabalho de investigação científica.

Um enorme obrigado ao grupo BIOENG que, juntamente com as suas pessoas, me fizeram sempre sentir em casa. Começando pelo laboratório de culturas puras (Lab 407) por me terem acolhido de uma forma tão carinhosa e por contribuírem para aquilo que sou hoje. Deste grupo levo pessoas que começaram como colegas de trabalho e que rapidamente evoluíram para uma grande amizade. À Diana Araújo um obrigado por todos os ensinamentos, partilhas, desabafos, devaneios e por mostrar que a dedicação e a resiliência superam quase tudo o que nos aparece à frente. Obrigado por seres um exemplo "Pai". À Patrícia Reis por ser a minha companheira não só de curso e de laboratório, como também uma amiga que esteve sempre disponível para me ajudar. Gostei muito de fazer este percurso contigo, muito obrigado por tudo "Sis". À Rita Bernardino por todas as conversas e discussões de gabinete, por ser uma pessoa muito ponderada sempre com uma opinião bastante acertada nos mais diversos temas e que me ajudou a ter uma perspetiva diferente em relação aos meus obstáculos. À Patrícia Freitas pelo sentido de humor e boa disposição e por me desafiar sempre a querer resolver

problemas e a melhorar o que já está implementado, uma pessoa com um espírito de proatividade inigualável. À Ana Teresa pela alegria, entusiasmo e companheirismo dentro e fora do laboratório e pela partilha dos desafios, ideias e obstáculos que o doutoramento possui. À Cátia Gil por ser uma pessoa muito humana, dedicada e com uma intensidade de trabalho admirável. À Asiyah Esmail, Francisco Santos, Thomas Rodrigues e Bruno Serafim pelas discussões, dúvidas e repostas que me ajudaram a expandir os meus horizontes não só acerca do meu trabalho, mas também a quanto àquilo que me rodeia. À Marta Catalão, Beatriz Almeida, Maria Batista pelas gargalhadas e pelo ótimo ambiente que vivemos dentro e fora do laboratório. À Eliana Guarda pela amizade, boa disposição e sentido de humor que fazem alegrar o dia de todas as pessoas que a rodeiam. Por ser uma das pessoas com o coração mais puro e bondoso que conheço, tendo uma proatividade e disponibilidade incansáveis em querer ajudar em tudo o que pode. A lista de nomes é infinita, mas não poderia de deixar de mencionar algumas pessoas (Marta Rodrigues, João Carvalho, Elsa Mestre, Elisabete Freitas, Bárbara Almeida, Cristiana Torres, Fernando Silva, Mariana Matos, Mónica Carvalheira, Bruno Marreiros, Joana Fradinho).

Um agradecimento especial ao Soft Biofunctional Materials Group (SBMG) por me terem acolhido de uma forma tão carinhosa e pelo conhecimento transmitido. Um obrigado muito grande à Doutora Tânia Vieira pelos conselhos, conhecimento, bom ambiente e por todas as conversas e sorrisos que partilhamos, sem ti teria sido tudo mais difícil. Um agradecimento à Sofia Pádua pelas discussões e troca de ideias bastante produtivas e impactantes no desenvolvimento deste trabalho. À Catarina e à Ana Filipa pela alegria, boa disposição e simpatia partilhadas no laboratório, sem vocês não teria sido igual.

Quero deixar um obrigado especial a todos os meus amigos que de uma forma ou de outra estiveram presentes durante este meu percurso ao André Gutierres, Hugo Monteiro, Filipa Quinaz, João Matos, Rodrigo Duarte, Ana Isabel, Maria Clara, Sandro Casaleiro, Tiago Moreira, Tatiana Vitorino, Matilde Moreira, Joana Freitas, Nuno Coutinho, Mariana Paiva, Joana Vaz, Dário Valezim, Carolina Rodrigues, Miguel Nogueira, Juliana Almeida, Gonçalo Santos, Inês Paulo, Miguel Palhas, Marta Fernandes, Catarina Chaparro, Bernardo Barros, Teresa Duarte e Duarte Baptista.

Gostaria ainda de agradecer à minha Família com quem partilhei muitos dos desafios de ser estudante de doutoramento, António Pereira, Maria Celeste Pereira, Ana Filipa Pereira, Bruno Pereira, Filipa Caseiro, Clarinha, Margarida Antunes, Adelino Santos, Fátima Bau, José Bau, Maria Ana Bau, João Pedro Bau nenhum agradecimento escrito conseguirá refletir o que sinto por me terem apoiado durante todo este tempo, por isso, do fundo do meu coração um muito obrigado por estarem presentes. E porque a Família não é só a de sangue, mas também a que acolhemos, um agradecimento especial Carla Figueiras, José Pedro Saldanha, Joaquim Figueiras, Amélia Figueiras, Elsa Figueiras, Fernando Félix, David Félix, Maria Lapão vocês são a família que não sabia que precisava.

Por fim e o meu maior agradecimento vai para a Beatriz Santos, porque muitas vezes estamos tão focados em terminar este projeto, esta grande etapa da nossa vida que nos esquecemos que não a estamos a viver sozinhos e que os nossos problemas passam a ser o problema com quem dividimos uma vida. Por isso, muito obrigado por suportares todos os meus desabafos, todas as minhas preocupações, por me fazeres acreditar que sou capaz de fazer tudo a que me comprometo, por me dares força para continuar, por fazeres de mim uma pessoa melhor, por dares 150% de ti quando eu só pude dar 50% de mim, adorei partilhar este caminho contigo e mal posso esperar pelas nossas próximas aventuras.

Um Muito Obrigado a todos!

"O valor das coisas não está no tempo que elas duram,

mas na intensidade com que acontecem.

Por isso existem momentos inesquecíveis,

coisas inexplicáveis e pessoas incomparáveis."

- Fernando Pessoa -

Abstract

The skin is one of the human organs responsible for sensory detection, temperature regulation, and water balance. Skin damage can lead to wounds that if not treated properly may cause serious health complications. The conventional wound healing products, made from non-biodegradable synthetic materials, usually have low biocompatibility and only offer mechanical protection or exudate removal, without actively helping the wound healing process. To address these limitations, developing new natural, biocompatible, biodegradable, and bioactive materials is crucial to create an optimal environment for proper wound regeneration, minimizing any adverse secondary effects. In this context, this dissertation proposes the use of natural polymers (polyhydroxyalkanoate (PHA) and exopolysaccharide (EPS)) to develop porous structures for wound treatment. To achieve this, four biopolymers were produced: the EPS FucoPol and three different types of PHA: (poly(3-hydroxybutyrate) (P(3HB)), poly(3-hydroxybutyrate-co-3-hydroxyvalerate-co-3-hydroxyhexanoate) (P(3HB-co-3HV-co-3HHx) and a medium chain length PHA (mcl-PHA)), characterized by their distinct physical, chemical and functional properties. The PHAs had distinct molecular weights (ranging from 0.4 to 9.2 x10^5 Da), different crystallinities (from 18.2 to 85.5%), diverse melting points (between 44.9 and 174.2 °C), various glass transition temperatures (from -46 to 4.1 °C), but similar degradation temperatures (around 275 °C). FucoPol was an amorphous exopolysaccharide had a molecular weight of 1.4 x10^6 Da, was rich in fucose (34.3 mol%) and had a high degradation temperature (240 °C). All the produced biopolymers were non-cytotoxic towards fibroblasts and keratinocytes. The inherent structural properties of PHA polymers, as well as their lack of cytotoxicity, makes them suitable materials to develop porous structures for wound treatment applications. Given

this, different PHA porous structures were developed, based on two different strategies: the emulsion templating technique followed by solvent evaporation and the hot-pressing salt leaching method. Generally, the porous structures achieved by these procedures were macroscopically white and opaque, with thicknesses ranging from 160 to 700 μm, and porosity values from 49.8 to 87.1%. The morphological appearance of these structures resembled those of porous scaffolds attained with synthetic polymers, such as, poly(lactic acid) (PLA), poly(caprolactone) (PCL) and poly(ethylene terephthalate) (PET), which are examples of polymers commonly used in wound dressing applications. The PHA scaffolds were shown to be capable of sustaining fibroblast adhesion and proliferation. The adhesion values achieved for all PHA structures ranged from 25% to 46%, where P(3HB) emulsion templated scaffold achieved the highest fibroblast population after 7 days of cell cultivation (311%). PHAs are biocompatible and biodegradable polymers with good structural properties, however, they usually lack biological activity. To confer this bioactivity to the developed scaffolds, FucoPol (a natural bioemulsifier) was added to these structures, due to its proven ability to promote *in vitro* migration of keratinocytes, which supports its use in wound treatment. The resulting FucoPol:PHA structures were porous materials with improved bioactive properties. FucoPol revealed to improve biological features, increasing fibroblast population values after 7 days from 311% to 325% and from 145% to 340% for P(3HB) and P(3HB-co-3HV-co-3HHx) emulsion templated scaffolds, respectively. This behaviour was also observed in the hot-pressing salt leaching scaffolds with an increase from 178% to 333% for P(3HB) and from 80% to 121% for P(3HB-co-3HV-co-3HHx) porous structures. Some of these proliferation profiles revealed to be superior to the ones described in the literature for scaffolds produced with PCL, poly(urethane) (PU) and chitosan. These results also suggested that the most promising PHA polymer to produce 3D scaffolds was the homopolymer P(3HB), while the emulsion templating technique showed to be the most favourable strategy to produce porous structures.

This dissertation revealed that it is possible to achieve porous scaffolds based on two natural polymers (PHA and FucoPol), through two different methods, with biological properties suitable for soft tissue engineering purposes or in skin regeneration for wound treatment applications.

Keywords: Poly(hydroxyalkanoate) (PHA), FucoPol, porous scaffold, emulsion templating, hot-pressing salt leaching, tissue engineering, wound management

RESUMO

A pele é um dos órgãos humanos responsável pela deteção sensorial, regulação da temperatura e equilíbrio de água. Danos causados à pele podem levar a feridas que, se não forem tratadas adequadamente, podem causar graves complicações de saúde. Os produtos convencionalmente usados no tratamento de feridas, feitos de materiais sintéticos são geralmente não biodegradáveis, apresentam baixa biocompatibilidade e oferecem apenas proteção mecânica ou remoção de exsudato, sem ajudar ativamente no processo de cicatrização de feridas. Para ultrapassar estas limitações, a produção de novos materiais naturais, biocompatíveis, biodegradáveis e bioativos é crucial para criar um ambiente ideal para a regeneração adequada da ferida, minimizando quaisquer efeitos secundários adversos. Posto isto, esta dissertação propõe a utilização de polímeros naturais (polihidroxialcanoato (PHA) e exopolissacárido (EPS)) no desenvolvimento de estruturas porosas para tratamento de feridas. Para isso, foram produzidos quatro biopolímeros: o EPS FucoPol e três tipos diferentes de PHA: poli(3-hidroxibutirato) (P(3HB), poli(3-hidroxibutirato-co-3-hidroxivalerato-co-3-hidroxihexanoato) (P(3HB-co-3HV-co-3HHx) e um PHA de cadeia média (mcl-PHA), característicos pelas suas propriedades físicas, químicas e funcionais distintas. Os PHAs tinham pesos moleculares distintos (variando de 0,4 a 9,2 x10^5 Da), diferentes cristalinidades (de 18,2 a 85,5%), diversos pontos de fusão (entre 44,9 e 174,2 °C) e temperaturas de transição vítrea (de -46 a 4,1 °C), mas temperaturas de degradação semelhantes (em torno de 275 °C). Por outro lado, FucoPol é um exopolissacárido amorfo com peso molecular de 1,4 x10^6 Da, rico em fucose (34,3 mol%) e com uma alta temperatura de degradação (240 °C). Todos os biopolímeros produzidos não eram citotóxicos para fibroblastos nem para queratinócitos. As propriedades estruturais inerentes dos PHA,

bem como a sua falta de citotoxicidade, torna-os materiais adequados para desenvolver estruturas porosas para aplicações na área do tratamento de feridas. Posto isto, diferentes estruturas porosas de PHA foram desenvolvidas, com base em duas estratégias distintas: a técnica da emulsão seguida de evaporação do solvente e o método de prensagem a quente seguido da lixiviação de sal. Na generalidade, as estruturas porosas obtidas por estes procedimentos eram macroscopicamente brancas e opacas, com espessuras entre os 160 a 700 μm e com valores de porosidade entre os 49,8 a 87,1%. As aparências morfológicas destas estruturas eram semelhantes às estruturas porosas obtidas com polímeros sintéticos, como ácido polilático (PLA), policaprolactona (PCL) e polietileno tereftalato (PET), que são exemplos de polímeros normalmente utilizados no tratamento de feridas. As estruturas de PHA mostraram ser capazes de sustentar a adesão e proliferação de fibroblastos. Os valores de adesão alcançados para todas as estruturas de PHA variaram entre os 25% e os 46%, onde a estrutura obtida pelo método da emulsão usando o P(3HB) alcançou a maior população de fibroblastos após 7 dias de cultivo (311%). Os PHAs são polímeros biocompatíveis e biodegradáveis com boas propriedades estruturais, porém geralmente não possuem atividade biológica. Para conferir esta bioatividade às estruturas desenvolvidas, foi adicionado FucoPol (um bioemulsionante natural) a estes materiais, devido à sua comprovada capacidade de promover a migração *in vitro* de queratinócitos, demonstrando a sua utilização no tratamento de feridas. As estruturas FucoPol:PHA resultantes eram materiais porosos com melhores propriedades bioativas. O FucoPol revelou melhorar as características biológicas, aumentando os valores da população de fibroblastos após 7 dias de 311% para 325% e de 145% para 340% para estruturas obtidas pelo método da emulsão usando P(3HB) e P(3HB-co-3HV-co-3HHx), respetivamente. Este comportamento também foi observado nas estruturas obtidas pelo método de prensagem a quente com lixiviação de sal verificando-se um aumento de 178% para 333% para o P(3HB) e de 80% para 121% para o P(3HB-co-3HV-co-3HHx). Alguns destes perfis de proliferação revelaram ser superiores aos descritos na literatura para estruturas produzidas com PCL, poliuretano (PU) e quitosano. Estes resultados também sugeriram que o polímero PHA mais promissor para produzir estruturas 3D foi o homopolímero P (3HB) e que a técnica da emulsão demonstrou ser a estratégia mais favorável para produzir estas estruturas porosas.

Esta dissertação revelou que usando dois tipos de polímeros naturais (PHA e FucoPol), e dois métodos de produção diferentes, é possível obter estruturas porosas com propriedades biológicas adequadas para utilização em engenharia de tecidos, ou na regeneração da pele para aplicações no tratamento de feridas.

Palavras-chave: Poli(hidroxialcanoato) (PHA), FucoPol, estrutura porosa, emulsão, prensagem a quente com lixiviação de sal, engenharia de tecidos, tratamento de feridas

CONTENTS

LIST OF FIGURES

List of Tables

Acronyms

ANOVA	Analysis of variance
DMEM	Dulbecco's Modified Eagle's Medium
DMSO	DiMethyl SulfOxide
DSC	Differential Scanning Calorimetry
EPS	ExoPolySaccharide
FBS	Fetal Bovine Serum
FDA	Food and Drug Administration
FID	Flame Ionization Detector
GC	Gas Chromatography
GPC	Gel Permeation Chromatography
GTA	GluTarAldehyde
HaCaT	*in vitro* spontaneously transformed keratinocytes from histologically normal skin
HDPE	High Density Poly(Ethylene)
HFFF2	Human Caucasian Foetal Foreskin Fibroblasts from a 14- to 18-week-old human foetus
HPLC	High Performance Liquid Chromatography

LDPE	Low Density Poly(Ethylene)
mcl-PHA	Medium Chain Length - Poly(HydxroxyAlkanoate)
PBS	Phosphate Buffered Saline
PCL	Poly(CaproLactone)
PDI	PolyDispersity Index
PEG	Poly(Ethylene Glycol)
PEO	Poly(Ethylene Oxide)
PET	Poly(Ethylene Terephthalate)
PHA	Poly(HydxroxyAlkanoate)
PLA	Poly(Lactic Acid)
PLGA	Poly(Lactic-co-Glycolic Acid)
PPO	Poly(Propylene Oxide)
PTFE	Poly(Tetra Fluoro Ethylene)
PU	Poly(Urethane)
P(3HB)	Poly(3-HydroxyButyrate)
P(3HB-co-3HHx)	Poly(3-HydroxyButyrate-co-3-HydroxyHexanoate)
P(3HB-co-3HV)	Poly(3-HydroxyButyrate-co-3-HydroxyValerate)
P(3HB-co-3HV-co-3HHx)	Poly(3-HydroxyButyrate-co-3-HydroxyValerate-co-3-HydroxyHexanoate)
P(3HB-co-4HB)	Poly(3-HydroxyButyrate-co-4-HydroxyButyrate)
P(3HO)	Poly(3-HydroxyOctanoate)
P(4HB)	Poly(4-HydroxyButyrate)
RID	Refractive Index Detector

ROS	Reactive Oxygen Species
scl-PHA	Short Chain Length - Poly(HydxroxyAlkanoate)
SCPL	Solvent-Casting Particulate Leaching
SEC	Size Exclusion Chromatography
SEM	Scanning Electron Microscopy
TCP	Tissue Culture Plate
TFA	TriFluoroacetic Acid
TGA	Thermal Gravimetric Analysis
XRD	X-Ray Diffraction
3HB	3-HydroxyButyrate
3HV	3-HydroxyValerate
3HHx	3-HydroxyHexanoate
3HO	3-HydroxyOctanoate
3HD	3-HydroxyDecanoate
3HDd	3-HydroxyDodecanoate
3HTd	3-HydroxyTetradecanoate

VARIABLES

M_n	Number average molecular weight (Da)
mol%	Molar percentage
M_w	Average molecular weight (Da)
T_{deg}	Degradation temperature (°C)
T_g	Glass transition temperature (°C)
T_m	Melting temperature (°C)
v/v	Volume per volume
X_c	Crystallinity index (%)
w/v	Weight per volume

1

GENERAL INTRODUCTION

The content of this chapter is included in the following book chapter publications: "Concórdio-Reis, P., Pereira, J. R., Esmail, A., Araújo, D., Ramos, K., & Freitas, F. Wound healing approaches based on polysaccharide-nanoparticles biocomposites in Recent advances in nanomedicines mediated wound healing (Submitted)", and "Rebocho, A. T.; Pereira, J. R.; Torres, C. A.; Freitas, F.; Reis, M.A. Linking the Properties of Polyhydroxyalkanoates (PHA) to Current and Prospective Applications. In The Handbook of Polyhydroxyalkanoates; CRC Press, 2020; pp 203−220".

1.1 Wound Healing

1.1.1 Skin

The skin is one the human organs responsible for sensory detection, thermoregulation of body temperature, and maintaining the fluid balance (A. Sharma et al., 2023). It is also the primary layer of protection for the human body against physical and thermal injuries, being a well-organized and stratified tissue composed of three layers: the subcutaneous layer (hypodermis), the dermis, and the epidermis (Figure 1.1). Each layer has different cell lines in its composition, for instance, the epidermis comprises melanocytes, keratinocytes, Merkel and Langerhans cells (Figure 1.1A), while the dermis has fibroblasts, neutrophils, adipocyte, dendritic, Mast and T cells (Figure 1.1B) (Massella et al., 2019; Sadeghi-Aghbash et al., 2023). These cells establish important interactions among them to form a functional connective tissue.

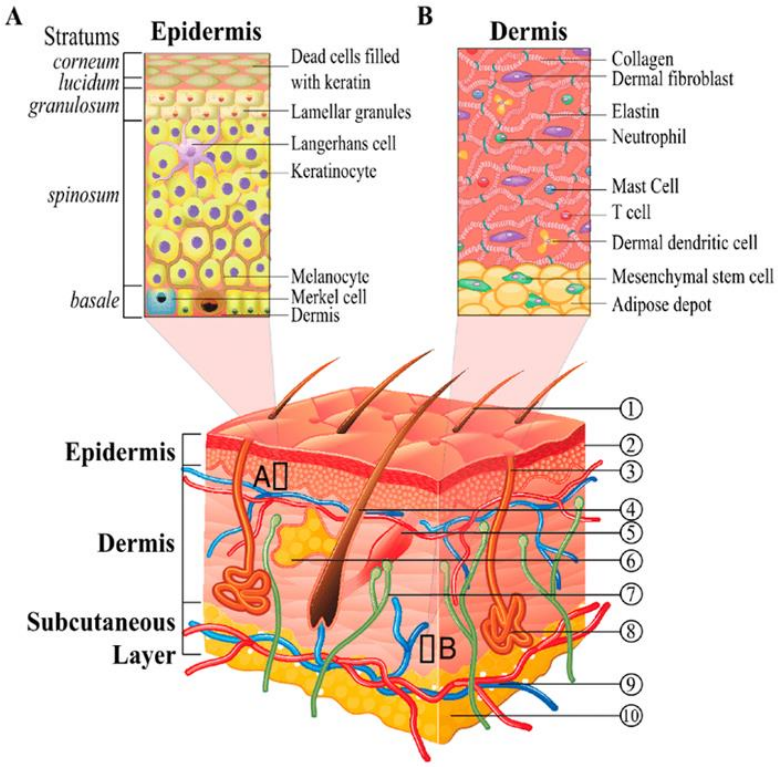

Figure 1.1 - Schematic representation of the skin. **A** and **B** are the highlighted and detailed structures of the epidermis and dermis, respectively. **1** is a hair strand; **2** is the stratum corneum; **3** is a sweat-pore; **4** is an hair follicle; **5** is the arrector pili muscle; **6** is a sebaceous gland; **7** is a nerve ending; **8** is the eccrine sweat gland; **9** is the subcutaneous vascular plexus and **10** is the subcutaneous adipose depot (Gaur et al., 2017).

1.1.2 Wound Healing Process

Sometimes skin is submitted to physical damages which can result in wounds. According to Sadeghi-Aghbash et al., 2022, there are different types of wounds based on: their cause (traumatic or surgical), mode of injury (abrasion, burn, laceration, degloving, etc.), depth of the injury (epidermis, dermis, or full skin), contamination (clean, contaminated, or dirty), presence of necrosis in the wounded tissue or their healing time (acute or chronic) (Niculescu & Grumezescu, 2022; Sadeghi-Aghbash et al., 2023). Usually, such injuries trigger a natural physiological reaction called the wound healing process, that is composed of four stages: hemostasis, inflammation, proliferation, and remodelling (Figure 1.2). This well-organized and sequenced procedure involves different cell lines (such as, platelets, macrophages, fibroblast, epithelial and endothelial cells), as well as regulatory molecules, growth factors, cytokines, and extracellular matrix components (Borbolla-Jiménez et al., 2023; Criollo-Mendoza et al., 2023). Complications during the wound healing process can lead to inflammation, pain, infections, scar tissue or chronical wound formation (Borbolla-Jiménez et al., 2023; Sadeghi-Aghbash et al., 2023).

1.1.2.1 Hemostasis

Hemostasis is the first step in the wound healing process, and it starts within a few minutes after an injury occurs. In this stage, platelets are triggered (through a cascade signalling activation) to form blood clots (composed of fibrin, thrombospondin, vitronectin, and fibronectin), producing an hemostatic plug that prevents blood loss (Figure 1.2A) (Borbolla-Jiménez et al., 2023; Criollo-Mendoza et al., 2023). Additionally, this cascade signalling induces the release of various proteins, enzymes, and other biological molecules (e.g., vasoconstrictors), which also help in the bleeding stoppage and are needed throughout the whole wound healing process. The expression of immune mediators and growth factors (such as transforming growth factor-β, TGF-β, and platelet-derived growth factor, PDGF) initiates the tissue repair and recruit monocytes and neutrophils to the wounded area to initiate the inflammatory phase (Borbolla-Jiménez et al., 2023; Criollo-Mendoza et al., 2023; Koehler et al., 2018).

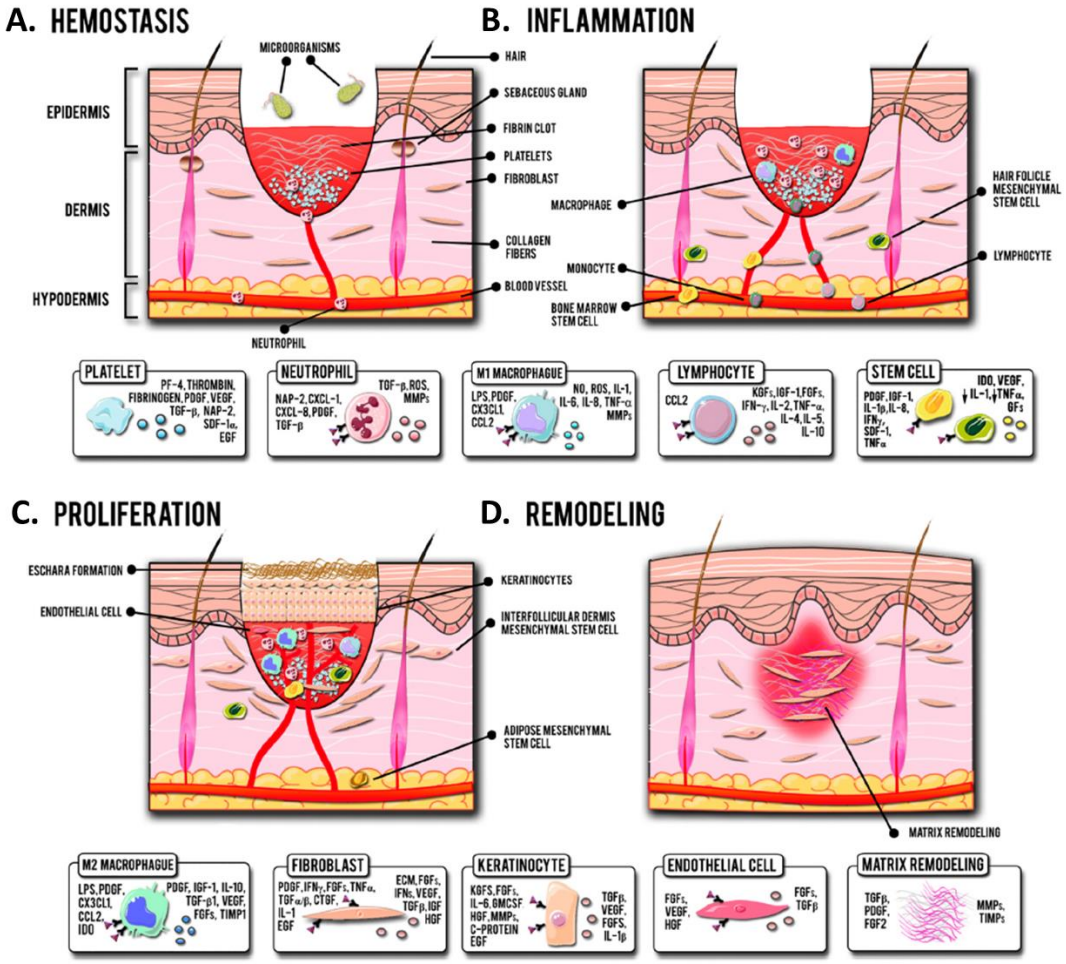

Figure 1.2 - Stages of the wound healing process, where, **A** is the hemostasis phase, **B** is the inflammation stage, **C** is the proliferation step, and **D** is the remodeling phase [Reproduced with permission from (Las Heras et al., 2020)].

1.1.2.2 Inflammation

After bleeding control and hemostasis is established, the inflammatory phase begins. In this step, neutrophils and monocytes are moved into the wounded area to promote an immune barrier against microorganisms to prevent infections (Figure 1.2B). Initially, neutrophile cells start to eliminate bacteria, foreign debris, and damaged cells through phagocytose and begin to secrete cytokines, which will help to promote monocytes differentiation into macrophages (Figure 1.2B). Afterwards, these leukocyte cells will remain in the affected area continuously removing bacteria and devitalized tissue, while releasing more cytokines (such as interleukins IL-1 and IL-6) and various growth factors (including insulin-like growth factor-1, IGF-1 and fibroblast growth factor, FGF), which are crucial for recruiting fibroblast and epithelial cells needed in the transition to the proliferation phase (Borbolla-Jiménez et al., 2023; Koehler et al.,

2018; Criollo-Mendoza et al., 2023). All this activity usually leads to pain, redness and swelling of the wounded area after a few days from the injury (Sadeghi-Aghbash et al., 2023).

1.1.2.3 Proliferation

The proliferation step aims to reduce the wounded area, as well as restore tissues' structure and function. In this phase, fibroblasts migrate to the affected region and begin to secret collagen, fibronectins, and proteoglycans to replace the previously formed fibrin clots (Borbolla-Jiménez et al., 2023; Criollo-Mendoza et al., 2023). This collagen deposition causes the wound to contract and is crucial for the development of new extracellular matrices. Meanwhile, the formation of new granular tissue and angiogenesis are occurring, essentially mediated by fibroblast and endothelial cells, respectively. Macrophages are also present in this step, In which, together with fibroblasts, keratinocytes and endothelial cells, they secret the growth factors and cytokines needed in this stage (Figure 1.2C) (Koehler et al., 2018). While the re-epithelization progresses, keratinocytes and fibroblasts start to establish important connections to promote the epidermal regeneration. These two cell lines will proliferate and differentiate to restore the proper function of the epidermal tissue (Borbolla-Jiménez et al., 2023; Criollo-Mendoza et al., 2023). This process can take several weeks, depending on the size of the wounded area.

1.1.2.4 Remodelling

The remodelling phase is the last stage of the wound healing process. This step aims to produce a normal tissue with uniform texture, structure, and shape (Sadeghi-Aghbash et al., 2023). To achieve this, the vascularization in the affected area is reduced and the differentiated fibroblasts (myofibroblasts) start to express the smooth muscle actin (SMA) to restore the mechanical strength of the skin tissue (Borbolla-Jiménez et al., 2023). During this maturation process, granulated tissue formed previously during the proliferation phase evolves into a scar and the reorganization of the collagen fibres will also help to recover the tissue initial tensile strength (Figure 1.2D) (Criollo-Mendoza et al., 2023; Koehler et al., 2018). The correct remodelling of the skin tissue is known to last from several weeks to months, depending on the wound's area and depth.

1.2 Wound Dressings

Wound care usually includes assessing, cleansing, and disinfecting wounds, together with implementing interventions to promote healing, generally by using dressing products. Wound dressings are materials applied over a wound to protect it and promote healing. The purpose of these products is to care the local wound environment to help wound healing (Balusamy et al., 2017; Dhivya et al., 2015; Holloway & Harding, 2022). The selection of the correct dressing material (e.g. foam, hydrogel, film, hydrocolloid, sponge, or mesh) to be applied locally in the wound bed is crucial for a successful healing process. However, wound patients occasionally present some pathological conditions (e.g. diabetes, vascular disease, auto-immune limitations), as well as other factors that could negatively affect the wound healing process (e.g. age, smoking, malnutrition, protein, vitamins, mineral deficiency or polypharmacy) Figure 1.3 (Dhivya et al., 2015; Holloway & Harding, 2022). In some of these cases, it is could be crucial to have a systemic pharmaceutical (e.g. anti-inflammatory, antibiotic, vascular, or auto-immune medical drug) that could improve the patient's overall health conditions to enhance the wound healing process (Holloway & Harding, 2022).

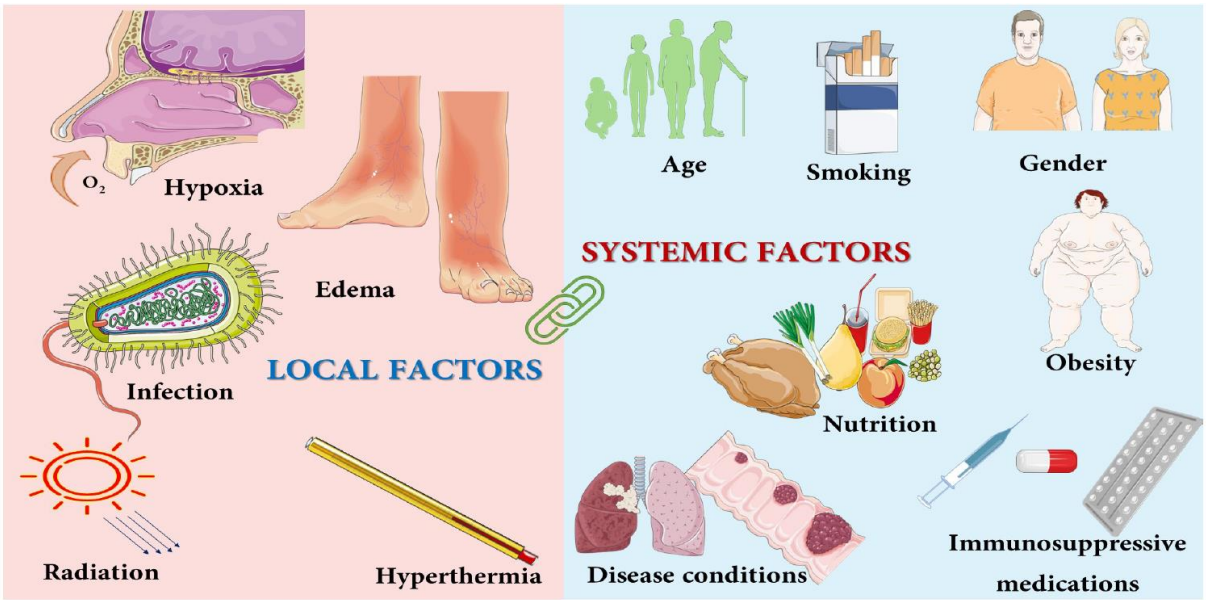

Figure 1.3 - Factors affecting wound healing (Rani Raju et al., 2022).

Wounds and especially chronic wounds usually require several dressing changes and provides physical limitations to patients which decreases their life quality (Koehler et al., 2018). Nowadays, these wounds are becoming be more frequent and are incredibly difficult to heal

(Kuddushi et al., 2023). Chronic and complex acute wounds often require patient hospitalization for wound treatment. This increases the spending costs on wound management materials which could lead to an economic pressure on the health care systems (Koehler et al., 2018). Moreover, the global market size of wound dressing materials has reached 12.4 billion USD in 2021, and it is expected to have an annual growth rate of 5.3% from 2022 to 2030 (Shi et al., 2023). For these reasons, it is essential to develop new enhanced materials for wound management applications, to reduce the treatment costs associated with wound healing management while improving the patient's life quality (Kuddushi et al., 2023; Shi et al., 2023).

1.2.1 Properties of wound dressings

To develop the best material for wound management, it is imperative to consider what are the requirements needed for a proper healing procedure. It has already been established that for each type of wound, there is an appropriate treatment procedure, which may involve the use of wound dressing materials. This means that for each type of wound there is an ideal structured material that will help in a specific way the wound healing process, therefore it is essential to apply the correct wound treatment on the proper injury (Dhivya et al., 2015). To achieve this, dressing materials are decisive to provide the assistance needed in wound treatment. An ideal wound dressing product should help the wound healing process in one or more phases of the four-stage procedure described above (Hemostasis, Inflammation, Proliferation and Remodelling). Such materials should improve the bleeding stoppage, thus preventing major blood losses, help in the signalling process, provide a good structure for macrophage diffusion and cellular proliferation (preventing infections and enhancing tissue regeneration, respectively), or even, help in the remodelling step to prevent the formation of scar tissue (Sadeghi-Aghbash et al., 2023; W. Wang et al., 2023). For these reasons, most dressing materi- also should fulfil certain requirements to consider their use as wound management products. They should protect the wound from physical injuries, absorb secretions while providing an adequate moist, prevent infections, stimulate growth factors, should not provoke adverse reactions (i.e., toxic, or allergic), if necessary, reduce necrosis on the wound surface, and, in general, accelerate the healing process (Castro et al., 2021; Santamaria et al., 2023). Dressing materials should also have some mechanical stability and elasticity, not only to adapt and adhere

well to the wound's surface, but also to guaranty their durability throughout the treatment process (Koehler et al., 2018).

1.2.2 Types of wound dressings

To achieve the necessary requirements of wound dressings, different structured materials have been developed over the years, such as hydrogels, fibres (including micro and nanofibers), hydrocolloids, meshes, foams, sponges, and films Figure 1.4 (Nguyen et al., 2023; A. Sharma et al., 2023; Z. Shen et al., 2023). These biomaterials can be divided into two different types, namely passive/traditional or interactive/modern/advanced wound dressings (Figure 1.4) (Dhivya et al., 2015; Kuddushi et al., 2023; Nguyen et al., 2023).

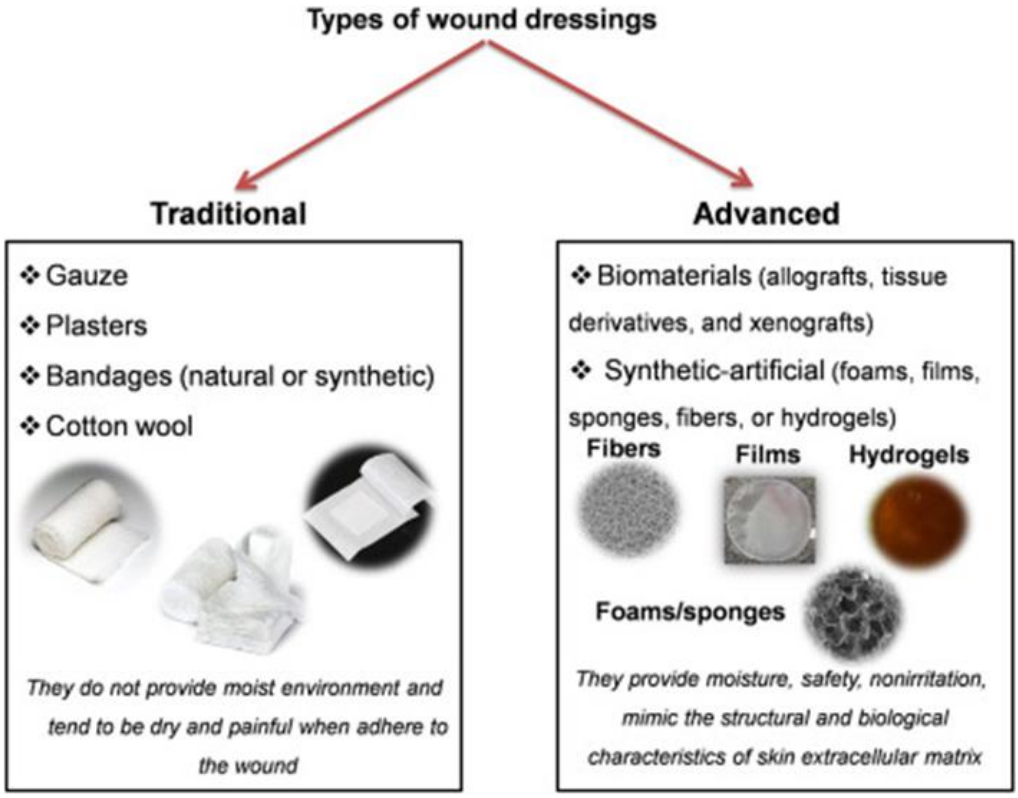

Figure 1.4 - Types of wound dressings: passive/traditional and interactive/modern/advanced [Reproduced with permission from (Özcan Bülbül et al., 2022)].

Passive/traditional dressings are usually meant for providing physical protection of the wound and, in general, have no active Impact on improving the wound healing process. Such dressings are frequently made of cotton (gauze), plaster or even wool, which may results in extremely absorbable materials that excessively dry the wound, consequently compromising the wound healing process (Figure 1.4). Also, the exudate absorbed by these materials may

easily be contaminated with bacteria causing wound infections through moisture transfer. These types of dressings adhere and adapt well to the wound surface, but they may cause pain or additional injury upon removal (Kuddushi et al., 2023; Pang et al., 2023; W. Wang et al., 2023; J. Zhu et al., 2023).

On the other hand, interactive/modern wound dressings are structured materials such as films, fibres, foams, hydrogels, or hydrocolloids that besides providing protection to the wound, also offer the precise water, oxygen, and carbon dioxide permeation. These are important dressing properties that are required for a correct moisturizing of the wound to prevent bacterial infections (Figure 1.4) (Kuddushi et al., 2023; Nguyen et al., 2023). To attain these structures, polymeric materials (synthetic or natural) are often used in the development of interactive/modern wound dressings. Also, some of these products can be loaded with pharmaceuticals drugs or with inorganic materials such as, ceramics, metals (e.g. micro- or nano- particles of Ag, Au, Fe, Ce), and nanocarbons, to further enhance their biological and structural properties. In this view, some natural biopolymers, due to their intrinsic properties, can be considered as bioactive products, which suggests their use in interactive/modern wound dressings, improving, even more, the wound healing process (Ali et al., 2023; Anwer et al., 2023; Kuddushi et al., 2023; Sadeghi-Aghbash et al., 2023).

1.2.3 Polymeric dressings

Polymeric dressings are materials based on polymers (synthetic or natural) applied over a wound to protect it and promote healing (Holloway & Harding, 2022). Over the past few years, a wide range of materials based on synthetic polymers have been developed for wound management applications and numerous of these products are currently available in the market. For instance, poly(ethylene glycol) (PEG) can be found in Coseal® (produced by Baxter), Neoheal® hydrogel (developed by Kikgel), poly(caprolactone) (PCL) is the major component of PURASORB® PC (from Corbion), poly(vinylpyrrolidone) (PVP) is present also in Neoheal® hydrogel (by Kikgel) and in Exufiber® (from Mölnlycke), poly(lactic-co-glycolic acid) (PLGA) is a compound of VICRYL™ (polyglactin 910) Woven Mesh (made by Johnson & Johnson MedTech) and poly(urethane) (PU) can be found in many different products, such as, Tromboguard® (from Tricomed), Simpurity™ Hydrogel (by Safe n Simple Medical), Allevyn® (produced by

Smith&Nephew), Hydrosorb® (developed by Hartmann), Lyofoam® and Mepilex® (from Mölnlycke) - Table 1.1 (Tiwari et al., 2023). These materials are known for their resistance, flexibility, structure, long shelf-life, moisturizing agent, and gas barrier/permeability properties. Synthetic polymers can also help the wound healing process by acting as structured materials to harbour cell growth or to provide physical protection to the injured area. However, the use of these polymers revealed to be challenging due to their inherent absence of biological activity, non-biodegradability, high hydrophobicity, and possible responses from the immune system, which could lead to severe allergic reactions - Table 1.1 (Borbolla-Jiménez et al., 2023; Sadeghi-Aghbash et al., 2023; Zahra et al., 2023). Given this, more natural polymers are being studied over the recent years due to their inherent biocompatibility, biodegradability, and lack of antigenicity.

Natural polymers, due to their biodegradability, biocompatibility and structural properties, together with the inherent biological activity that many of them exhibit, can easily outperform the synthetic polymers currently used in the commercially available wound dressings products, enhancing the healing properties of these materials while improving the wellbeing of wound patients. In fact, many polymers obtained from microorganisms (e.g. bacteria, fungi, microalgae) have been reported to have antioxidant, antimicrobial and/or anti-inflammatory activity (Borbolla-Jiménez et al., 2023; Sadeghi-Aghbash et al., 2023; Tiwari et al., 2023), while other biopolymers can be formulated into polymeric matrices, such as hydrogels, films or nanoparticles (Kuddushi et al., 2023; Nguyen et al., 2023). Furthermore, enhanced biomaterials can be obtained from such polymeric matrices by their loading with pharmaceutical active drugs or inorganic materials (e.g., metallic nanoparticles) (Borbolla-Jiménez et al., 2023; Dam et al., 2023; Song et al., 2023). Given this, biopolymers synthesized by microorganisms arise as promising candidates for the development of structures that can satisfy all requirements needed to produce an improved topical dressing material and ultimately outperform the synthetic polymers currently used in wound healing systems (Solanki et al., 2023).

Biopolymers, such as alginate, collagen, chitosan, chitin, cellulose, silk fibroin or hyaluronic acid are known to be moisture retentive and haemostatic agents with antimicrobial properties and minimum inflammatory reactions (Pino et al., 2023). Given this, some of these natural biopolymers can also be found in commercially available products for wound management

applications. For example, alginate is present in various wound dressing materials namely, Kaltostat (from ConvaTec), AlgiSite M (by Smith&Nephew), Algicell (developed by Derma Sciences) and TegadermTM Alginate (produced by 3M). Collagen is commercialized by Southwest Technologies Inc. as Stimulen collagen gel. Chitosan is the major component in numerous materials, namely, Chitosorb (manufactured by Chitotech), ChitoGauzePro (from HemCon), Kyto-Cell (by Protex Healthcare), Opticell (commercialized by Medline) and Maxiocel® (from Axio Biosolutions). A derivative of cellulose (carboxymethyl cellulose) is also found in some products, such as, Eurocell® Hydro (produced by eurofarm), AQUACEL Ag® (from ConvaTec), AquaRite Extra CMC (developed by DermaRite) and CMC Fiber dressing (from Gentell). Hyaluronic acid is an important compound in these materials Hyalomatrix (by Medline), Hyalofill® (from ConvaTec), HYALO4 Regen (produced by Fidia) and Restore Hydrogel (developed by Hollister Wound Care) - Table 1.1 (Pino et al., 2023; Yang & Wang, 2023). These biomaterials usually adhere well to the wound's surface, keeping it with the proper moisture and preventing blood loss by activating coagulation factors. This promotes the adhesion and aggregation of platelets, which helps the first step of the wound healing process. Also, some of these biopolymers could even regulate the growth factors activity and enhance the performance of inflammatory cells. This prevents bacterial infections and stimulates cell migration, fibroblast proliferation, granular tissue formation, collagen deposition, neovascularization, and re-epithelialization, helping, at the same time, the second and third phases of the wound healing process (Pino et al., 2023; Yang & Wang, 2023). The main disadvantages of these materials are usually the biopolymers' production costs, short shelf-life and the uncontrollable degradation rates under physiological conditions (too fast or too slow) - Table 1.1 (Sadeghi-Aghbash et al., 2023; Zahra et al., 2023; J. Zhu et al., 2023). Natural biopolymers, despite of all their disadvantages, present a significant benefit in terms of biological activity when compared with synthetic materials.

Table 1.1 - Polymeric materials used in skin regeneration and wound healing adapted from (Gianino et al., 2018; Tiwari et al., 2023; Vach Agocsova et al., 2023; Yang & Wang, 2023).

Polymers		Advantages	Drawbacks	Commercially available wound dressing
Synthetic	Poly(ethylene glycol) (PEG)	Hydrophilic, flexible and compatible qualities; Surface modifier allowing for better grip in the contact layer; High growth factor affinity;	Poor cellular adhesion Limitations on the use of antibiotics and other drugs in PEG necessitate the use of composite materials	Coseal®, Neo-heal® hydrogel
	Poly(lactic-co-glycolic acid) (PLGA)	Food and drug administration (FDA) approved for drug delivery, suture applications; Ratio of lactide to glycolide units can modify release of drugs and growth factors; Cytocompatible and stimulates fibroblast adhesion, spreading, and proliferation; High processability;	Hydrophobic in nature; Properties fail to match with extracellular matrix or collagen requiring additional antimicrobial agents;	BioDegmer® PGLA, VICRYL™ (polyglactin 910) Woven Mesh
	Poly(urethane) (PU)	Semipermeable membrane that prevents bacteria from entering; Provides a moist environment; Delivers bioactive substances for fighting infection; Drainage properties that decrease the risk of swelling;	Non-absorbing; Lack of adherence property;	Tromboguard®, Simpurity™ Hydrogel, Allevyn®, Lyofoam®, Mepilex®, Hydrosorb®
	Poly (caprolactone) (PCL)	FDA approved for suture applications; Fibrous structure similar to ECM architecture; Water retention capacities used to capture wound exudate; Resistant to many solvents allowing for slow and controlled degradation;	Lack of antimicrobial property; Poor cell adhesion due to hydrophobic surface;	PURASORB® PC
Natural	Chitosan	Antimicrobial and hemostatic properties; Functional derivatives allowing for modified and versatile effects; Drug delivery ability;	Low mechanical strength; Less porous in structure; Poor water solubility (due to its rigid crystalline structure); Crosslinking may affect its intrinsic properties;	Chitosorb, ChitoGauzePro, HemCon, KytoCell, Opticell, Medline, Maxiocel

Hyaluronic Acid	Lubricative and water absorptive; Bi products promote epithelial cell migration; Improves collagen deposition and angiogenesis; Popular drug delivery system and vehicle for growth factors	Difficult to control the viscosity for electrospinning;	Hyalomatrix, LaserSkin®, Hyalograft®, Hyal04 Regen
Alginate	Tissue adhesion; Lubricative; Promotes tissue granulation;	Lack of mechanical strength; Poor stability resulting in ion leaching;	Tegaderm, Kaltostat, AlgiSite M, Algicell
Cellulose	Readily available with low cost; Fiber and foam materials; Creates a gel-like material, forming a moist environment; Releases GFs to stimulate fibroblast proliferation;	Lack of mechanical strength; Poor antibacterial property deficient water vapour and oxygen permeability;	AQUACEL Ag®, AquaRite Extra CMC, Gentell CMC Fiber dressing
Dextran	Lubricative; Promotes cell adhesion, migration and proliferation; Antithrombotic properties;	High cost; Its use as protein drug delivery systems is restricted because of their high permeability, which can cause the prior release of drug that are captured in them;	SurgiClot® Hemostatic Dressing
Poly(lactic acid) (PLA)	Mechanical strength; High processability;	Poor flexibility; Slow degradation rate; Strong hydrophobicity; Chemically inert; Low heat resistance;	No formulation available for wound dressings
Poly(hydroxyalkanoate) (PHA)	Natural human metabolite; Great mechanical and structural properties; Flexibility;	Crystallinity; High hydrophobicity; Thermal stability;	No formulation available for wound dressings

1.2.3.1 Poly(hydroxyalkanoates) (PHAs)

Poly(hydroxyalkanoates) (PHAs) are water insoluble, biodegradable, and biocompatible polyesters that many bacteria accumulate intracellularly as carbon and energy storage compounds. Their physical properties range from brittle, rigid and highly crystalline bio-thermoplastics (e.g., poly(3-hydroxybutyrate), P(3HB)), to amorphous, rubbery, or sticky elastomers (e.g., medium-chain-length poly(hydroxyalkanoate), mcl-PHA), depending on their monomeric composition (Figure 1.5) (Pereira et al., 2019). Moreover, terpolyesters (e.g., poly(3-hydroxybutyrate-co-3-hydroxyvalerate-co-3-hydroxyhexanoate), P(3HB-co-3HV-co-3HHx)) are considered one of the most promising additions to the PHAs family since they combine short-chain length (scl) and medium-chain length (mcl) monomers into novel materials with interesting properties (Meléndez-Rodríguez et al., 2021; Silva et al., 2022). This versatility makes PHAs attractive materials for use in a wide range of applications, including bioplastics, fine chemicals, biomedicine, tissue engineering and wound management (Diniz et al., 2023). The intrinsic structural properties of PHAs makes them great candidates as suitable alternative materials for the development of new bio-based dressings for wound management, as they could be used to develop novel scaffolds with improved properties to harbour cell adhesion, proliferation, and differentiation (Kalia et al., 2023; Pereira et al., 2023). The use of PHAs have been previously suggested in the literature for several wound management applications. These polyesters were studied to act as dressing structures for tissue regeneration, for instance P(3HB) and poly(3-hydroxybutyrate-co-3-hydroxyvalerate) (P(3HB-co-3HV) were used to produce scaffolds with improved properties for fibroblast adhesion and proliferation (Kalia et al., 2023). Keratinocyte and myoblast cells also revealed to have greater proliferation in materials based on poly(3-hydroxyoctanoate) (P3HO) (Kalia et al., 2023). Mcl-PHA polymers were suggested to serve as adhesives materials for wound closure (Diniz et al., 2023; Yousefi & Wnek, 2024). Moreover, some poly(4-hydroxybutyrate) (P(4HB)) based products (namely, GalaFLEX™ and Phasix™) has been approved for repair and reinforcement of soft tissue by the food and drug administration (FDA). TephaFLEX™ and TephaELAST™ are also examples of P(4HB) and poly(3-hydroxybutyrate-co-4-hydroxybutyrate) (P(3HB-co-4HB)) based materials, respectively, with FDA approval for biomedical use as implant material (Yousefi & Wnek, 2024).

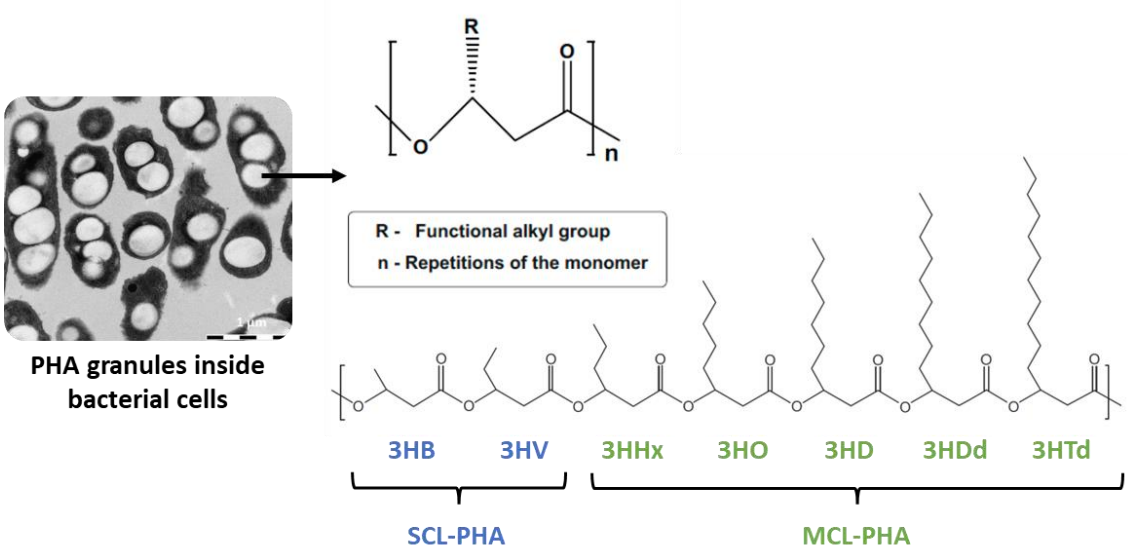

Type of PHA Polymer	Alkyl "R" Groups	N° of carbon atoms	PHA Monomers
Short-Chain-Length PHA SCL-PHA	CH_3	C_4	3-Hydroxybutyrate (3HB)
	CH_2-CH_3	C_5	3-Hydroxyvalerate (3HV)
Medium-Chain-Length PHA MCL-PHA	$(CH_2)_2$-CH_3	C_6	3-Hydroxyhexanoate (3HHx)
	$(CH_2)_4$-CH_3	C_8	3-Hydroxyoctanoate (3HO)
	$(CH_2)_6$-CH_3	C_{10}	3-Hydroxydecanoate (3HD)
	$(CH_2)_8$-CH_3	C_{12}	3-Hydroxydodecanoate (3HDd)
	$(CH_2)_{10}$-CH_3	C_{14}	3-Hydroxytetradecanoate (3HTd)

Figure 1.5 - Scanning electron microscopy (SEM) image of PHA granule inside the bacterial cell and a schematic representation of the general molecular structure of PHA polymers [adapted with the permission from (Obruca et al., 2020; Peregrina et al., 2021)].

1.2.3.2 Polysaccharides

Polysaccharides are high molecular weight carbohydrate polymers that can be produced by microorganisms, namely bacteria, fungi, yeast, and microalgae (Concórdio-Reis et al., 2022; Concórdio-Reis, Reis, et al., 2020). These biopolymers can have countless applications as structuring agents, based on their ability to form polymeric structures (i.e., emulsions, gels, films, micro- and nanoparticles) or as biological active materials that can be used to develop new pharmaceuticals or even to replace some products currently available in the market (Yildiz & Karatas, 2018; Yu et al., 2018). Generally, the most common monomers found in microbial polysaccharides are glucose, galactose, and mannose. However, sometimes it is also possible to find arabinose, rhamnose, fucose, amino sugars, and uronic acids in these biopolymers. Given the diversity of their composition, microbial polysaccharides have a wide range of different molecular structures that can display distinct physical and chemical properties. There are

several microbial polysaccharides currently commercialized, such as xanthan (produced by *Xanthomonas* sp.), dextran (produced by genera of *Leuconostoc*, *Streptococcus*, *Weisella*, *Pediococcus* and *Lactobacillus*), hyaluronic acid (produced by *Streptococcus zooepidemicus*) and pullulan (produced by *Aureobasidium pullulans*). Most of these biopolymers have high-value applications in food, cosmetics, pharmaceuticals, and medicine (Freitas et al., 2021; Vach Agocsova et al., 2023).

FucoPol which is a high molecular weight heteropolysaccharide secreted by *Enterobacter* A47 (DSM 23139) composed of fucose, galactose, glucose, and glucuronic acid. This exopolysaccharide (EPS) has already been studied for its film and hydrogel forming capacity, flocculating, thickening, emulsifying, anti-inflammatory, antioxidant, anti-aging, UV protective, cryoprotective and, even, wound healing ability (Araújo et al., 2023; Baptista et al., 2023; Concórdio-Reis, Pereira, et al., 2020; Fialho et al., 2021; Guerreiro et al., 2020, 2021). These properties are advantageous for wound dressing applications, since this eco-friendly, non-toxic, biodegradable, and bioactive polysaccharide could be used to develop new bio-based products with enhanced performance for wound healing purposes (Concórdio-Reis, Pereira, et al., 2020).

1.2.4 Biocomposite dressings

Biocomposites are biocompatible or eco-friendly composite structures (Haraguchi, 2014). They consist in a blend of natural materials with other inorganic (e.g. ceramics, metals or nanocarbons), synthetic (e.g. polymers or pharmaceutical drugs) or natural (e.g. polymers, proteins, sugar, lipids) compounds to develop a product that combines the properties of the starting components (Borbolla-Jiménez et al., 2023; Ferrari et al., 2022; Haraguchi, 2014). Recently, this technique has been studied to produce various materials for wound treatment purposes using, both, synthetic polymers (e.g., PVA, PCL, PEG) and natural biopolymers (e.g., alginate, cellulose, hyaluronic acid) (Farazin et al., 2023; A. Sharma et al., 2023; Xu et al., 2023; Zahra et al., 2023). A good example of these strategy are the blends of PCL with chitosan or with collagen to produce scaffolds to harbour cell growth for bone tissue engineering and wound healing applications, respectively (Anaya Mancipe et al., 2023; Gautam et al., 2023). Such scaffolds combined the great structural features of PCL with the biological properties of chitosan (e.g. mucoadhesive, antioxidant, antibacterial, proliferative and haemostatic effects) or collagen (e.g.

reduced immunogenicity, promotes blood coagulation, cellular adhesion and proliferation) (Anwer et al., 2023; Kuddushi et al., 2023; Sadeghi-Aghbash et al., 2023). In line with this, it is possible to combine two natural polymers with distinct properties to develop a hybrid material. Such biocomposites are biocompatible, biodegradable, from biological origin and contribute to a sustainable development of wound management products, by reducing their environmental impact while contributing to a circular economy. One great example of this was the development of a hybrid film of lignin and chitosan (two natural polymers) for wound management applications (Pothal et al., 2023). The produced film exhibited excellent antioxidant activity with no toxicity towards fibroblast cells. Additionally, when the loaded with the antibiotic neomycin sulphate, it showed significant antimicrobial activity against gram-negative and gram-positive bacteria (Pothal et al., 2023). From this perspective, another good opportunity could be the development of hybrid structures composed of natural polymers with great structural features with biopolymers that possess some biological activity. This would result in a biocomposite that is, at the same time, biologically active and has unique structural properties. One promising approach could be combining PHAs and polysaccharides to attain a natural structured product for wound dressing applications. The production of biocomposites using PHA and polysaccharides has been previously reported in the literature, where P(3HB) and chitosan were used to produce structures through electrospinning. These scaffolds were studied to assess the proliferation and differentiation of stem cells from human exfoliated deciduous teeth into odontoblast-like cells (Khoroushi et al., 2018). The addition of chitosan showed to increase the hydrophilicity and cell viability, when compared with scaffolds only produced by P(3HB) (Khoroushi et al., 2018; Zhuikova et al., 2022). P(3HB) and P(4HB) were also blended with small amounts of chitosan and hyaluronic acid to develop novel absorbable films suitable for use as a tissue engineering scaffolds for keratinocytes as a therapy for replacement of damaged skin (Peschel et al., 2008). The addition of these polysaccharides promoted the proliferation of keratinocytes in the scaffolds when compared with the structures only produced by both PHAs (Peschel et al., 2008; Zhuikova et al., 2022). These results suggest that the use of PHA and polysaccharides could be an interesting approach to develop new dressing materials for wound treatment purposes.

1.3 Motivation

PHAs are well-known biobased and biodegradable polyesters, which are an ecological and promising alternative to some of the most used conventional petroleum-derived plastics. As mentioned before, their physical properties range from brittle, rigid and highly crystalline bio-thermoplastics to amorphous, rubbery, or sticky elastomers. The diverse properties found in these products, makes them attractive materials for a wide range of applications, including packaging, fine chemicals, biomedicine, and tissue engineering. Also, due to their intrinsic structural features, PHAs are great candidates for the development of new biobased dressings for wound management. FucoPol, on the other hand, is an hydrophilic EPS that have unique properties that include film and hydrogel forming capacity, as well as flocculating, thickening, emulsifying, anti-inflammatory, antioxidant, anti-aging, UV protective, cryoprotective and, even, wound healing ability. The diverse properties found in this microbial polysaccharide makes it suitable to a wide range of applications in the food industry, the pharmaceutical field, the medical area, and as cosmetic products. Together, PHAs and FucoPol can be used to develop hybrid materials with enhanced structural and bioactive features for wound management applications. These biodegradable and biocompatible structures could even outperform the properties of synthetic and petroleum-derived materials, contributing, not only, to the reduction of the environmental impact associated with the manufacture of wound care products, but also, to a circular economy. Therefore, this PhD work aimed to develop an active wound dressing material based on natural polymers (PHAs and FucoPol) for wound management applications. The main idea was to produce a hybrid material combining the inherent structural properties of PHA polymers with the intrinsic biological activity of FucoPol. To achieve this, three different types of PHA polymers with distinct properties (P(3HB), P(3HB-co-3HV-co-3HHx) and mcl-PHA), together with the polysaccharide FucoPol were studied to create a biocomposite material by using two separated methods (the emulsion templating technique and the hot-pressing salt leaching process). This work is in line with a bio-based economy idea where novel value-added bioproducts are produced, providing new solutions for sustainable bioprocesses. This dissertation is also within the "Goals of the United Nations 2030 Agenda for Sustainable Development" by promoting healthy lives and well-being for all at all ages (Goal 3). Due to the inherent biocompatibility and biodegradability of the material produced in this project, it

ensures a sustainable consumption and production of polymeric structured materials with potential application in the biomedical field (Goal 12) contributing to a more sustainable city (Goal 11) while protecting the environment.

1.4 Thesis Outline

The work developed in this dissertation is sequentially organized in five chapters. Each chapter (with the exception of Chapters 1 and 5) contains: a small summary and an introduction which provides information about the content and the contextualization of that section, followed by a detailed description of the materials and methods used, together with results presentation and a thorough discussion, and the general conclusions of that sector. More specifically, the content of each chapter is listed below:

Chapter 1 - General Introduction and Motivation - presents an overview of the state of the art, the motivation, and the outline of this dissertation. This chapter provides some insights on the previously reported information while clarifying key concepts for a better understanding of this dissertation.

Chapter 2 - Biopolymer Characterization - reports the production and characterization procedures used in each biopolymer, contemplating the information about three different PHA polymers (P(3HB), P(3HB-co-3HV-co-3HHx) and mcl-PHA) and the extracellular bacterial polysaccharide FucoPol.

Chapter 3 - Development of Polymeric Structures - describes the development and characterization of structured porous materials using PHA polymers, namely, P(3HB) and P(3HB-co-3HV-co-3HHx), with two different strategies: the emulsion templated technique and the hot-pressing salt leaching method.

Chapter 4 - Development of Active Wound Dressings - investigates the addition of FucoPol in the porous structures previously attained by PHA polymers, (P(3HB) and P(3HB-co-3HV-co-3HHx)).

Chapter 5 - General Conclusions and Future Perspectives - reviews the main outcomes of this dissertation and proposes some suggestions for future research studies.

The work developed during this PhD resulted in 2 book chapters (1 submitted and 1 published), 2 research papers, published in peer-reviewed international scientific journals, as well as 3 oral communications and 2 poster presentations in international conferences.

2

BIOPOLYMERS CHARACTERIZATION

The contents presented in this chapter are partly included in the publication "Pereira, J. R., Rafael, A. M., Esmail, A., Morais, M., Matos, M., Marques, A. C., Reis, M. A. M., & Freitas, F. (2023). Preparation of Porous Scaffold Based on Poly(3-hydroxybutyrate-co-3-hydroxyvalerate-co-3-hydroxyhexanoate) and FucoPol. *Polymers*, *15*(13), 2945. https://doi.org/10.3390/polym15132945".

2.1 Summary

This chapter describes the production of microbial polymers used in subsequent chapters for the development of wound dressing materials. Three types of PHA namely, P(3HB), P(3HB-co-3HV-co-3HHx), an mcl-PHA, and the extracellular polysaccharide FucoPol were produced in bioreactor cultivation runs. The P(3HB) homopolymer and the mcl-PHA were produced by the bacteria *Cupriavidus necator* DSM 428 and *Pseudomonas chlororaphis* subsp. *aurantiaca* DSM 19603, respectively, using fructose as the sole carbon source. The P(3HB-co-3HV-co-3HHx) terpolymer was produced by a mixed microbial culture (MMC) using fermented fruit pulp as carbon source. The PHAs were recovered from the biomass by Soxhlet extraction with chloroform and purified using a standardized procedure of polymer precipitation in ice-cold ethanol. FucoPol was produced by *Enterobacter* A47 using glycerol as carbon source. This polysaccharide was recovered from the cultivation broth by a standardized diafiltration/ultrafiltration procedure. All the biopolymers were characterized in terms of their physical properties. Briefly, the produced P(3HB) had molecular weight (M_w) of 9.2×10^5 Da together with a polydispersity index (PDI) of 2.9. It had a temperature of melting (T_m) of 174.2 °C, glass transition (T_g) of 4.1 °C and a degradation (T_{deg}) of 276.6 °C with a crystallinity index (X_c) of 85.5%. The P(3HB-co-3HV-co-3HHx) terpolymer had a composition of 59 mol% of 3HB, 20 mol% of 3HV and 21 mol% of 3HHx. It had M_w of 0.9×10^5 Da with a PDI of 2.2. Had two melting points at 108.5 °C (T_{m1}) and at 159.7 °C (T_{m2}), a T_g at -3.8 °C and a T_{deg} at 275.5 °C with a X_c of 26.2%. The attained mcl-PHA had a composition of 4 mol% of 3HHx, 24 mol% of 3HO, 61 mol% of 3HD, 6 mol% of 3HDd and 5 mol% of 3HTd. Had M_w of 0.4×10^5 Da with a PDI of 1.7. Had a T_m value of 44.9 °C, a T_g of -46 °C and a T_{deg} at 274 °C with a X_c of 18.2%. All the PHAs produced revealed to be non-cytotoxic against fibroblasts and keratinocytes. FucoPol was composed of fucose (34.33 mol%), glucose (33.12 mol%), galactose (26.21 mol%) and glucuronic acid (9.93 mol%). It was an amorphous biopolymer with a M_w of 1.4×10^6 Da and a PDI of 1.2 together with a T_{deg} around 240 °C. FucoPol is known to be non-cytotoxic against several cell lines including fibroblasts and keratinocytes.

2.2 Introduction

PHAs are a well-known group of water insoluble, biobased, biocompatible, and biodegradable polyesters, which are an ecological and promising alternative to some of the most used conventional petroleum-derived plastics. These natural polymers are accumulated intracellularly by many bacteria as carbon and energy storage compounds. Their physical properties range from brittle, rigid and highly crystalline bio-thermoplastics (e.g. P(3HB)) to amorphous, rubbery, or sticky elastomers (e.g. mcl-PHA), depending on their monomeric composition (Pereira et al., 2019). Some PHAs, such as the terpolyesters P(3HB-co-3HV-co-3HHx), join scl- and mcl- monomers in the same macromolecule, creating a novel material with very interesting properties (Meléndez-Rodríguez et al., 2021; Silva et al., 2022). This versatility makes PHAs suitable to a wide range of applications in biomedicine, namely, drug carrier, tissue engineering, adhesives, and wound treatment (Diniz et al., 2023). More specifically, different types of PHA polymers, namely, P(3HB), P(3HB-co-4HB) P(3HB-co-3HV), poly(3-hydroxybutyrate-co-3-hydroxyhexanoate) (P(3HB-co-3HHx)), poly(3-hydroxyocatnoate) (P(3HO)), and mcl-PHA have already been tested for their biocompatibility and applicability as scaffold materials for biomedical applications (Diniz et al., 2023; Ladhari et al., 2023; Tawonsawatruk et al., 2023). These polyesters proved to be safe to use in various cell lines, including mouse or human skin fibroblasts and keratinocytes (Casula et al., 2023; Chen et al., 2023; Liu et al., 2024; T. G. Volova et al., 2019).

FucoPol is a fucose-rich EPS secreted by the bacteria *Enterobacter A47*. It has various distinct properties, namely, film and hydrogel forming capacity, UV protective and cryoprotective ability, and it is a flocculating, thickening and emulsifying agent (Baptista, Pereira, et al., 2022). Moreover, FucoPol has been also reported to promote the *in vitro* migration of keratinocytes, suggesting its use for wound healing applications (Concórdio-Reis, Pereira, et al., 2020). This polysaccharide was shown to be non-cytotoxic towards various cell lines, including human skin keratinocytes and mouse fibroblasts (Concórdio-Reis, Pereira, et al., 2020; Guerreiro et al., 2020). Fucose is a rare sugar which imparts bioactive properties to the biopolymer. Fucose, among other distinctive features is known to have an antitumor effect helping specially in intestinal diseases, the ability to regulate microbial virulence and anti-aging properties (Y. Wang et al., 2024). Moreover, polysaccharides comprising fucose in their composition are known to have improved biological activity since they can promote proliferation of human skin

fibroblasts and protect cellular death against reactive oxygen species (ROS) (Y. Wang et al., 2024). A great example of bioactive polysaccharide containing fucose is fucoidan, which is known to exhibit antiviral, anti-atherosclerotic, anti-inflammatory, and immune-regulation effects (Baptista, Torres, et al., 2022a; Y. Wang et al., 2024). These are important properties that could help the wound healing process, which supports the use of FucoPol in the development of wound dressing materials.

Given this, the present chapter aimed to produce and characterize the exopolysaccharide FucoPol and three different types of PHA polymers (P(3HB), P(3HB-co-3HV-co-3HHx) and mcl-PHA) in terms of their composition, molecular mass distribution, thermal properties, crystallinity, functional groups and cytotoxicity effect against fibroblasts and keratinocytes, envisaging their use as wound dressing materials in the subsequent Chapters.

2.3 Materials and Methods

2.3.1 Biopolymer production, extraction and purification

P(3HB) homopolymer was obtained by the cultivation of *Cupriavidus necator* DSM 428 in a 10 L bioreactor (BioStat B-plus, Sartorius, Germany) with the production process described by (Rebocho et al., 2020) using fructose as the sole carbon source. Mcl-PHA was produced by *Pseudomonas chlororaphis* subsp. *aurantiaca* DSM 19603 in 10 L bioreactor (BioStat B-plus, Sartorius, Germany) with the procedure described in (Pereira et al., 2021) using fructose as the sole carbon source. The terpolymer P(3HB-co-3HV-co-3HHx) produced by MMC in a 100 L bioreactor, using fermented fruit pulp as feedstock, as described by (Silva et al., 2022). To recover the biopolymers from the biomass the cultivation broth was recovered and centrifuged (13 131 ×g, for 20 min, 4 °C) to separate the bacterial cells from the cell-free supernatant. For extraction of the PHAs, the cell pellets thus obtained were resuspended in deionized water and centrifuged again under the same conditions. This process was repeated until a clean supernatant was achieved. The washed biomass was then freeze dried in a ScanVac CoolSafeTM, LaboGene, Lillerød, Denmark), at -110 °C for 48 h. The PHA was extracted from the dried biomass by Soxhlet extraction with chloroform (250 mL) (99.5 %, Sigma-Aldrich, USA), at 80 °C for 48 h, and purified by precipitation in ice-cold ethanol (1:10, v/v) under vigorous stirring, from which the precipitate was recovered and left in a fume hood, at room temperature, for solvent evaporation, as described by Pereira et al. (2019).

FucoPol was obtained via cultivation of the bacterium *Enterobacter A47* (DSM 23139) in a 10 L bioreactor (BioStat B-plus, Sartorius, Germany) using glycerol as the sole carbon source, as described by (Concórdio-Reis, Reis, et al., 2020). FucoPol was extracted and purified using the procedure described by Baptista et al. (2022). Briefly, at the end of the fermentation process the cultivation broth was recovered, diluted with deionized water in a 1:3 (v/v) ratio and centrifuged (13 000 ×g, for 45 min, 4 °C) for cell removal. The cell pellet was discarded, and the cell-free supernatant was subjected to a thermal treatment (70 °C, for 1 h) followed by centrifugation (13 000 ×g, for 45 min, 4 °C) for protein denaturation and removal, this step was repeated twice. The resulting treated cell-free supernatant was purified by diafiltration with a crossflow module (Sartocon Slide Holder, Sartorius, Germany) using a membrane with a surface

area of 100 cm^2 and cut-off 100 000 Da (Hydrosart ultrafiltration cassette, Sartorius, Germany). The system was operated in a diafiltration mode by continuously adding deionized water to the retentate's vessel to maintain a constant volume. This procedure removes salts and molecules with molecular weight lower than 100 000 Da. When the retentate's conductivity reached a value below 200 S/cm, water addition to the vessel was suspended and the retentate was concentrated by operating the module in an ultrafiltration mode. At the end of this process, the concentrated retentate was freeze-dried (ScanVac CoolSafeTM, LaboGene, Lillerød, Denmark), at -110 °C for 48 h.

All the produced biopolymers were stored in closed flask at room temperature until use.

2.3.2 Biopolymer Characterization

2.3.2.1 Composition

The PHAs composition was determined by gas chromatography (GC). Samples (1.5 mg) were mixed with 2 mL benzoic acid methyl ester (Sigma-Aldrich, USA) in chloroform (99.5 %, Sigma-Aldrich, USA) (1 g/L) and 2 mL 20% (v/v) sulphuric acid (Honeywell, USA) in methanol (Fisher Chemical, USA), and heated at 100 °C, for 4 h. After cooling, 1 mL of deionized water was added and mixed in a vortex. After phase separation the aqueous phase was retrieved and another 1 mL of deionized water was added and mixed, after phase separation the organic phase was recovered, passed through molecular sieves, filtered using poly(tetrafluoroethylene) (PTFE) syringe filters of 0.2 µm pore (Labfil, China) into a vail and analysed by GC with a flame ionization detector (FID) (TRACE 1300, Thermo Scientific, USA) and with a column of 60 m, 0.53 mmID, 1 µM df, Crossbond, Stabilwax (Restek, USA). The injection volume was 1.0 µL, with a running time of 32 min, constant pressure of 14.50 psi and helium as carrier gas. The heating ramp followed a 20 °C/min rate until 100 °C, 3 °C/min until 155 °C and again 20 °C/min until 220 °C. The standards used for this analysis were 3-hydroxybutyric acid (for 3-hydroxybutyrate, 3HB) (97%, Thermo Scientific, USA), 3-hydroxyvaleric acid (for 3-hydroxyvalerate, 3HV) (98%, MedChemExpress, USA) and Methyl-3-hydroxyhexanoic acid (for 3-hydroxyhexanoate, 3HHx) (97%, Sigma-Aldrich, USA) with concentrations between 0.05 and 1.0 g/L, for determination of the composition of P(3HB) and P(3HB-co-3HV-co-3HHx). For the mcl-PHA it was used as a standard a polymer with the following composition, validated by GC–MS (Rebocho et al., 2019): 3

mol% 3-hydroxyhexanoate (3HHx), 17 mol% 3-hydroxyoctanoate (3HO), 57 mol% 3-hydroxydecanoate (3HD), 11 mol% 3-hydroxydodecanoate (3HDd) and 12 mol% 3-hydroxytetradecanoate (3HTd), with concentrations ranging from 0.08 to 1.6 g/L (Pereira et al., 2021). The standards were prepared with the same protocol used for sample preparation. All the samples were prepared in triplicates.

FucoPol's composition was determined by high performance liquid chromatography (HPLC) using a Carbopac PA10 column (Thermo Scientific, Dionex, USA), equipped with an amperometric detector. Samples of FucoPol (1 g/L, 5 mL) was hydrolysed with 0.1 mL trifluoroacetic acid (TFA, 99%, Sigma-Aldrich, USA) at 120 ℃ for 2 h. L-Fucose (Biosynth, Switzerland), D(+)-glucose anhydrous (Scharlau, Spain), D(+)-galactose (98%, Alfa Aesar, USA) and D(+)-glucuronic acid (98%, Alfa Aesar, USA) were used as standards. All the samples were prepared in triplicates.

2.3.2.2 Fourier-Transform Infrared Spectroscopy

The biopolymers were characterized via Fourier-transform infrared spectroscopy (FT-IR) with a spectrum two spectrometer (PerkinElmer, USA) equipped with the attenuated total reflectance (ATR) accessory. The spectra were recovered based on five scans between a resolution of 4000 and 400 cm^{-1} at room temperature.

2.3.2.3 Molecular Mass Distribution

Number and average molecular weights, M_n and M_w, respectively, and the polydispersity index (PDI = M_w/M_n) of the P(3HB), P(3HB-co-3HV-co-3HHx) and mcl-PHA samples were determined by a gel permeation and size exclusion chromatography (GPC/SEC) System (KNAUER Smartline, Germany), using a Phenomenex Phenogel Linear Liquid Chromatographic Column 300×7.8 mm (Phenomenex, USA) coupled with the refractive index detector (RID) Waters2414 (Waters, USA). The samples were dissolved in chloroform (concentration range: 0.3 – 0.4%, w/v) and monodisperse polystyrene standards (370 – 2520,000 Da) were used. The solutions were injected (100 µL) and the analysis was performed at 30 °C, with a flow rate of 1 mL/min of chloroform as mobile phase (Appendix A.1). FucoPol's M_n, M_w and PDI were determined using the same GPC/SEC system (KNAUER Smartline, Germany) and column (Phenomenex, USA), using 0.1 M $LiNO_3$ as eluent, at a flow rate of 0.6 mL/min. FucoPol (50 µL) solution (0.5%, w/v, in

0.1 M $LiNO_3$) were injected and detected in RID Waters2414 (Waters, USA). M_w and M_n were calculated using a calibration curve generated with pullulan standards (P50 to P80) (Appendix A.1).

2.3.2.4 X-Ray Diffraction

The crystalline structure of the biopolymers was analysed by X-ray diffraction (XRD) using a PANalytical's X'Pert PRO MRD diffractometer (PANalytical B.V., Netherlands), with a monochromatic Cu Kα radiation source (wavelength 1.540598 Å). Data were acquired in a range between 10° and 90° (2θ) with a scanning step size of 0.03°, in continuous mode and operating at 45 kV with 40 mA. The degree of crystallinity was calculated according to the following equation (1):

$$\text{Crystallinity index (\%)} = A_{cryst}/A_{total} \times 100 \qquad (1)$$

Here, A_{Cryst} is the sum of the area under crystalline peaks; and A_{Total} is the total area under the diffractogram. The peak deconvolution was done using the X'Pert HighScore Plus software (Malvern Panalytical). The area under the deconvoluted peaks was used for the calculation of crystallinity (S. Park et al., 2010).

2.3.2.5 Thermal Properties

2.3.2.5.1 Differential Scanning Calorimetry

Differential Scanning Calorimetry (DSC) was performed in a DSC Q2000 (TA instruments, USA), by placing the PHA samples in aluminium hermetic pans and analysing them with a heating and cooling speed of 10 °C/min from room temperature until 100 °C, then from 100 to -100 °C followed by two heating cycles within a temperature range of -100 and 200 °C (Appendix A.2). The melting temperatures (T_m) were determined by analysing the endotherm peak's temperature and area, respectively, during the first heating cycle. The glass transition (T_g) was analysed by endothermic slope observed during the last heating ramp. All heating cycles from all samples are shown in Appendix A.2.

2.3.2.5.2 Thermal Gravimetric Analysis

Thermogravimetric Analysis (TGA) was performed in a Thermogravimetric Analyzer Setaram Labsys EVO (Steram, France) with a weighing precision of +/- 0.01 %, using aluminium crucibles to place the samples (8.8 - 20.8 mg) and analysing them with a temperature range between 25

°C and 500 °C, at 10 °C/min, in Argon atmosphere. The degradation temperature (T_{deg}) was considered the point where the sample had 5 % of mass loss (in the case of FucoPol, this weight loss was only measured after 150 °C due to water mass loss). The maximum degradation temperature was considered the value after the major mass loss.

2.3.2.6 Cell Testing

2.3.2.6.1 Cell culture and media

Fibroblast cells (HFFF2, Human Caucasian Foetal Foreskin Fibroblasts from a 14- to 18-week-old human foetus, ECACC, UK) were cultured in low-glucose with stable glutamine and sodium pyruvate (Biowest, USA) supplemented with penicillin (100 U/mL) (Life Technologies, USA), streptomycin (100 μg/mL) (Life Technologies, USA) and 10% FBS (Fetal Bovine Serum, Biowest, USA). Keratinocyte cells (HaCaT, *in vitro* spontaneously transformed keratinocytes from histologically normal skin, AddexBio, USA) were cultured in Dulbecco's Modified Eagle Medium (DMEM) with high glucose content (DMEM – high glucose, with 4.5 g/L glucose, stable glutamine, and sodium pyruvate (Biowest, USA) supplemented with 100 U/mL with penicillin (Life Technologies, USA), 100 μg/mL streptomycin (Life Technologies, USA) and 10% FBS (Biowest, USA).

2.3.2.6.1 Cytoxicity Test

HFFF2 and HaCaT cells were cultivated in a 96-well microplate. HFFF2 and HaCaT cells were seeded at a density of 20,000 and 25,000 cells/cm^2, respectively, and incubated during 24 h at 37 °C, 5% CO_2 in a humidified atmosphere incubator (MCO-19AIC(UV) Sanyo, Japan). For the cytotoxicity assessment it was used the extract method in accordance with the International Standard ISO 10993-5. To prepare the extracts the PHA samples were previously sterilized in ethanol 70% and after complete evaporation (24 h to 72 h) they were exposed to the growth media for each cell line (Low- and high-glucose DMEM for HFFF2 and HaCaT, respectively) at a concentration range of 1.5 – 50 mg/mL of the tested PHA sample (P(3HB), P(3HB-co-3HV-co-3HHx) and mcl-PHA), during 48 h. The cells were then exposed to the prepared extracts for 48 h while using low-glucose or high-glucose DMEM supplemented with 10% of dimethyl sulfoxide (DMSO, Supelco, USA) as the positive control, whereas the negative control was low-glucose or high-glucose DMEM, depending on the cell line (HFFF2 or HaCaT, respectively). After 48 h, a colorimetric viability assay was performed where the well volumes were discarded

and 100 μL of a resazurin: low/high-glucose DMEM solution (50% of resazurin (Alfa Aesar, USA) in phosphate buffered saline (PBS) (Amresco, VWR Chemicals, USA) solution at 0.04 mg/mL + 50% of Low/high-glucose DMEM) were added and incubated during 4 h at 37 °C, 5% CO_2 in a humidified atmosphere incubator (MCO-19AIC(UV) Sanyo, Japan). Cell viability was assessed through the reduction of resazurin into resorufin by viable cells and measuring the optical density in a microplate reader (ELX 800UV, BioTek, USA) at 570 and 600 nm, respectively. The corrected absorbance (was obtained by subtracting the absorbance measured at 600 nm from the one measured at 570 nm and subtracting the medium control) is proportional to cell viability. The combined standard uncertainty was calculated by propagation of uncertainties.

2.4 Results and Discussion

2.4.1 Biopolymers Characterization

2.4.1.1 Composition

Cupriavidus necator DSM 428 is a well-known producer of P(3HB) homopolymers capable of using different carbon sources including industrial wastes (Esmail, Pereira, Sevrin, et al., 2021). In this study, this bacterium was used to produce a 3-hydroxybutyrate (3HB) homopolymer using fructose as the sole carbon source (Table 2.1). P(3HB) is one of the most studied PHA polymers in the literature. Besides *C. necator*, there are several reports of different bacterial strains that can produce this homopolymer, such as, *Bacillus, Alcaligenes, Burkholderia, Halomonas, Rhizobium* and recombinant *Escherichia coli* (Diniz et al., 2023; Ladhari et al., 2023). It is also possible to attain P(3HB) using different strategies using MMC (Queirós et al., 2014; M. Y. Shen et al., 2023; Zhou et al., 2022). This biopolyester is even commercially available under various trademark names for instance, BIOCYCLE, Minerv-PHA, COFCO PHA and YOOP produced by PHB Industrial S.A. (Brazil), Bio-On (Italy), COFCO (China) and Mango Materials (USA), respectively (Koller & Mukherjee, 2022; Yousefi & Wnek, 2024).

The P(3HB-co-3HV-co-3HHx) biopolymer accumulated by the MMC cells was composed of 58.95 ± 1.30 mol% 3HB, 19.82 ± 1.26 mol% 3HV and 21.24 ± 0.84 mol% 3HHx (Table 2.1). Similar monomer ratios (59 - 71 mol% 3HB, 9 - 16 mol% 3HV and 13 - 32 mol% 3HHx) have been reported previously for other terpolyesters synthesized by MMC using fermented fruit pulp as the sole carbon source (Meléndez-Rodríguez et al., 2021; Silva et al., 2022). Also, a P(3HB-co-3HV-co-3HHx) synthesized by the recombinant strain *C. necator* P(3HB)-4 fed with crude palm kernel oil as main substrate and valerate as co-substrate displayed lower 3HHx contents (2 - 12 mol%) with 3HB and 3HV contents in the range of 66 - 94 mol% and 3 - 32 mol%, respectively (Bhubalan et al., 2010; Ye et al., 2010). The recombinant *C. necator* Re2133/pCB81 was also reported to synthesize P(3HB-co-3HV-co-3HHx) with a monomer composition within the same ranges (53 - 81 mol% 3HB, 2 - 34 mol% 3HV and 9 - 45 mol% 3HHx) by cultivation on tung oil and on fructose with different concentrations of butyrate or propionate (Jung et al., 2019; Lee et al., 2021). Lower 3HV contents were reported for the biopolymers produced by the recombinant *C. necator* Re2133/pCB81 and P(3HB)-4 (2 and 3

mol%, respectively) (Bhubalan et al., 2010; Lee et al., 2021). For those strains, the 3HHx content varied within 9 - 45 and 2 - 12 mol%, respectively (Table 2.1). The observed variability of P(3HB-co-3HV-co-3HHx) monomers' content is a result of the distinct microbial PHA-producing systems that were fed with different substrates, thus translating into biopolymers with different composition.

The mcl-PHA synthesized by *P. chlororaphis* subsp. *aurantiaca* DSM 19603 was composed of 3HHx (3.83 ± 0.11 mol%), 3HO (23.59 ± 0.53 mol%), 3HD (61.14 ± 0.47 mol%), 3HDd (6.51 ± 0.15 mol%) and 3HTd (4.93 ± 0.06 mol%). Similar monomeric composition has been reported previously for the same bacterial strain grown on different carbon sources, although with distinct relative monomeric proportions (Table 2.1) (de Meneses et al., 2020; Pereira et al., 2019, 2021). Other *P. chlororaphis* strains were also able to achieve mcl-PHAs with distinct monomeric ratios (Table 2.1). More specifically, mcl-PHAs enriched with 3HD monomers were reported for *P. chlororaphis* 555 (44 – 56 mol%) (Cerrone et al., 2015; Walsh et al., 2015), *P. citronellolis* sp. (32-68 mol%) (Cruz, Araújo, et al., 2016; Muhr, Rechberger, Salerno, Reiterer, Schiller, et al., 2013; Rebocho et al., 2019), *P. putida* sp. (44 - 61 mol%) (Ma et al., 2009; G.-Y. Tan et al., 2014), and *P. mediterranea* CFBP 5447 (61 mol%) (Pappalardo et al., 2014) (Table 2.1). On the other hand, polymers synthesized by *P. chlororaphis* strains DSM 50083 and PA23 (Muhr, Rechberger, Salerno, Reiterer, Malli, et al., 2013; P. K. Sharma et al., 2017) were enriched in 3HO monomers (46 and 49 mol%, respectively). The presence of 3HDd and 3HTd were detected in polymers synthesized by *P. chlororaphis* subsp. *aurantiaca* DSM 19603 (10 - 43 mol% and 11 - 17 mol%, respectively), *P. chlororaphis* HS21 (1 mol% and 11 mol%, respectively), *P. chlororaphis* PA23 (10 and 3 mol%, respectively), *P. resinovorans* NRRL B-2649 (9 - 18 mol% and 1 - 15 mol%, respectively), *P. citronellolis* NRRL B-2504 (5 - 14 mol% and 1 - 4 mol%, respectively) (Table 2.1). It is also noticed that 3HO and 3HD are frequently the predominant monomers in the reported mcl-PHA polymers, while 3HDd and 3HTd are only detected in the polyesters synthesized by some bacterial strains. These differences are, not only, associated with the bacterial strains used during the mcl-PHA production process, but also, with the substrates used for the bioreactor cultivation. As reported by several authors, the composition of the mcl-PHA is highly influenced by the carbon sources supplied to the cultures (G.-Y. Tan et

al., 2014). This is a useful feature since it grants the opportunity to attain mcl-PHA with tailored composition, that will impact the biopolymers final properties.

The exopolysaccharide FucoPol was synthesized by *Enterobacter A47* in a standardized bioreactor procedure using glycerol. This polysaccharide was composed of fucose (34.33 ± 2.05 mol%), glucose (33.12 ± 2.02 mol%), galactose (26.21 ± 2.04 mol%) and glucuronic acid (9.93 ± 1.06 mol%). These values are within the ones reported previously (30 – 36 mol% fucose; 25 - 34 mol% glucose; 22 – 29 mol% galactose; 9 – 10 mol% glucuronic acid) (Concórdio-Reis et al., 2018). FucoPol is also known to have acetate (3.5–6.8 wt.%), pyruvate (3.7–14 wt.%) and succinate (0.6–3 wt.%) as acyl groups, giving this polymer a polyanionic character, due to these negatively charged groups, allowing the formation of gel structures through physical cross-linking via electrostatic interaction with cations (i.e. Fe^{3+} and Cu^{2+}) (Araújo et al., 2023).

Table 2.1 - Composition, molecular mass distribution, thermal properties and crystallinity of the PHA polymers by different microbial sources (3HB, 3-hydroxybutyrate; 3HV, 3-hydroxyvalerate; 3HHx, 3-hydroxyhexanoate; 3HO, 3-hydroxyoctanoate; 3HD, 3-hydroxydecanoate; 3HDd, 3-hydroxydodecanoate; 3HTd, 3-hydroxytetradecanoate; M_w, molecular weight; PDI, polydispersity index; T_g, glass transition temperature; T_m, melting temperature; T_{deg}, degradation temperature; X_c, crystallinity index; n.a., data not available; n.d., not detected).

P(3HB) Polymers

Microbial source	Composition (mol%)							M_w ($\times 10^5$ Da)	PDI	T_g (°C)	T_{m1} (°C)	T_{m2} (°C)	T_{deg} (°C)	X_c (%)	References
	3HB	3HV	3HHx	3HO	3HD	3HDd	3HTd								
	100	*n.d.*	*n.d.*	*n.d.*	*n.d.*	*n.d.*	*n.d.*	*9.2*	*2.9*	*4.1*	*174.2*	*n.d.*	*276.6*	*85.5*	*This study*
	100	n.d.	n.d.	n.d.	n.d.	n.d.	n.d.	5.0	2.0	n.d.	176	n.d.	293	n.a.	(Rebocho et al., 2020)
C. necator DSM 428	100	n.d.	n.d.	n.d.	n.d.	n.d.	n.d.	5.2	1.8	n.d.	176	n.d.	293	52.4	(Esmail, Pereira, Sevrin, et al., 2021)
	100	n.d.	n.d.	n.d.	n.d.	n.d.	n.d.	n.a.	n.a.	5.8	177	n.d.	n.a.	n.a.	(Hernández-Herreros et al., 2023)
	84	6	n.d.	n.d.	n.d.	n.d.	n.d.	0.8	1.8	40.3	167	n.d.	269	64.3	(Ribeiro et al., 2023)
	100	n.d.	n.d.	n.d.	n.d.	n.d.	n.d.	9.2	2.5	n.d.	178	n.d.	295	76	(T. G. Volova et al., 2016)
C. necator B10646	100	n.d.	n.d.	n.d.	n.d.	n.d.	n.d.	7.1	3.4	n.d.	168	n.d.	278	78	(N. O. Zhila et al., 2023)
	100	n.d.	n.d.	n.d.	n.d.	n.d.	n.d.	6.5	3.7	n.d.	158	n.d.	261	74	
B. cereus RCL02	100	n.d.	n.d.	n.d.	n.d.	n.d.	n.d.	n.a.	n.a.	n.a.	171	n.d.	279	n.a.	(Andler et al., 2023)
A. vinelandii OP	100	n.d.	n.d.	n.d.	n.d.	n.d.	n.d.	n.a.	n.a.	n.a.	180	n.d.	275	n.a.	
	100	n.d.	n.d.	n.d.	n.d.	n.d.	n.d.	n.a.	n.a.	4	177	n.d.	n.a.	n.a.	
	94	6	n.d.	n.d.	n.d.	n.d.	n.d.	3.4	2.8	-7	171	n.d.	n.a.	n.a.	(Derippe et al., 2024)
Halomonas sp. SF2003	89	11	n.d.	n.d.	n.d.	n.d.	n.d.	3.3	2.9	-7	172	n.d.	n.a.	n.a.	
	85	15	n.d.	n.d.	n.d.	n.d.	n.d.	4.9	1.4	-0.2	n.a.	n.a.	n.a.	43	
	77	23	n.d.	n.d.	n.d.	n.d.	n.d.	4.7	1.4	-1	n.a.	n.a.	n.a.	36	(Fosse et al., 2023)
	73	27	n.d.	n.d.	n.d.	n.d.	n.d.	5.3	1.2	-2.5	n.a.	n.a.	n.a.	43	

Cont. - Terpolymers - P(3HB-co-3HV-co-3HHx)

Microbial source	Composition (mol%)							M_w ($\times 10^5$ Da)	PDI	T_g (°C)	T_{m1} (°C)	T_{m2} (°C)	T_{deg} (°C)	X_c (%)	References
	3HB	3HV	3HHx	3HO	3HD	3HDd	3HTd								
	59	*20*	*21*	*n.d.*	*n.d.*	*n.d.*	*n.d.*	*0.9*	*2.2*	*-3.8*	*108.5*	*159.7*	*275.5*	*26.2*	*This study*
Mixed microbial consortium	59	9	32	n.d.	n.d.	n.d.	n.d.	n.a.	n..a.	n.a.	n.a.	n.a.	n.a.	n.a.	(Silva et al., 2022)
	71	16	13	n.d.	n.d.	n.d.	n.d.	n.a.	n.a.	0.2	111	173	266	22.6	(Meléndez-Rodríguez et al., 2021)
C. necator B-10646	97.1	1.6	0.3	n.d.	n.d.	n.d.	n.d.	7.5	5.6	n.a.	160	168	284	71	(N. O. Zhila et al., 2023)
	64-93*	1-25*	0-5*	n.d.*	n.d.*	n.d.*	n.d.*	4.4-8.2*	3.0-6.0*	-8.6 to -0.7*	166-173*	n.d.*	259-286*	30-45*	(T. G. Volova et al., 2016)*
Recombinant *C. necator* Re2133/pCB81	57-70	11-34	9-19	n.d.	n.d.	n.d.	n.d.	n.a.	n.a.	-2.8	70-133	n.d.	n.a.	5.4-13.4	(Jung et al., 2019)
	53	2	45	n.d.	n.d.	n.d.	n.d.	1.6	1.8	n.a.	n.a.	n.a.	n.a.	n.a.	(Lee et al., 2021)
	81	n.d.	29	n.d.	n.d.	n.d.	n.d.	1.5	1.8	n.a.	n.a.	n.a.	n.a.	n.a.	
Recombinant *C. necator* P(3HB)-4	73-83	5-17	10-12	n.d.	n.d.	n.d.	n.d.	16.0-18.4	2.0-2.2	n.a.	141-143	n.d.	n.a.	14.5-27.5	(Ye et al., 2010)
	66-94	3-32	2-7	n.d.	n.d.	n.d.	n.d.	3.3-4.6	2.0-2.6	-4.7 to -0.8	91-129	139-148	n.a.	19.2-45.2	(Bhubalan et al., 2010)
Recombinant *A. hydrophila* 4AK4	85	4	11	n.d.	n.d.	n.d.	n.d.	30.3	1.8	-1.3	113	n.d.	256	19.5	(Hu et al., 2009)
	48-75	13-24	12-28	n.d.	n.d.	n.d.	n.d.	8.1-12.7	1.7-2.9	-1.9 to -12.5	54.2-101	n.d.	247-258	n.a.	(H. Zhang et al., 2009)

* - These terpolyemers have a P(4HB) content between 3 and 16 mol%.

Cont. - mcl-PHA Polymers

Microbial source	Composition (mol%)							M_w ($\times 10^5$ Da)	PDI	T_g (°C)	T_{m1} (°C)	T_{m2} (°C)	T_{deg} (°C)	X_c (%)	References
	3HB	3HV	3HHx	3HO	3HD	3HDd	3HTd								
P. chlororaphis subsp. *aurantiaca* DSM 19604	*n.d.*	*n.d.*	*4*	*24*	*61*	*6*	*5*	*0.4*	*1.7*	*-46*	*44.9*	*n.d.*	*274*	*18.2*	*This study*
	15	n.d.	4	18	42.7	10	11	1.3	2.7	-40.9	42	n.d.	300	12.6	(Pereira et al., 2021)
	n.d.	n.d.	3	17	50	13	17	1.3	1.5	-49.9	45	n.d.	288	27	(de Meneses et al., 2020)
P. chlororaphis 555	n.d.	n.d.	n.d.	15	56	28	n.d.	1.2	2.3	-42.1	38.2	n.d.	284	n.a.	(Cerrone et al., 2015)
	n.d.	n.d.	4-6	27-29	44-48	18-24	n.d.	1.0	1.7	-66 to -55	n.a.	n.a.	290	n.a.	(Walsh et al., 2015)
P. chlororaphis PA23	n.d.	n.d.	6	49	33	10	3	n.a.	n.a.	n. a.	n.a.	n.a.	n.a.	n.a.	(P. K. Sharma et al., 2017)
P. citronellolis NRRL B-2504	n.d.	n.d.	1	22	68	5	4	3.7	2.1	-12	53	n.d.	296	n.a.	(Rebocho et al., 2019)
	n.d.	n.d.	10-14	36 to 48	32 to 40	12 to 14	<1	0.3	1.5	-14	25	n.d.	n.a.	1	(Cruz, Araújo, et al., 2016)
P. resinovorans NRRL B-2649	n.d.	n.d.	11-19	43-44	28-33	9-12	<1	0.2-0.3	1.3 to 1.5	-29 to -16	36-43	n.d.	n.a.	6-7	(Cruz, Araújo, et al., 2016; Cruz, Freitas, et al., 2016)
P. putida KT2440	n.d.	n.d.	5	89	5	n.d.	n.d.	0.8	2.2	-36	57	n.d.	n.a.	n.a.	(Derippe et al., 2024)
P. mediterranea CFBP 5447	n.d.	n.d.	4	17	61	18	n.d.	0.6	1.3	-45.1	40.6	n.d.	n.a.	6.4	(Pappalardo et al., 2014)
P. umsongensis GO16	8-14	n.d.	3-8	77-88	1	n.d.	n.d.	n.a.	n.a.	-25	29	164	257	n.a.	(Cerrone et al., 2023)

2.4.1.2 Fourier-Transform Infrared Spectroscopy

Through the observation of the FTIR spectra it is visible that for all the PHA polymers (P(3HB), P(3HB-co-3HV-co-3HHx) and mcl-PHA) there is a similar absorption pattern (Figure 2.1 A, B and C, respectively). They show an intense absorption peak at around 1720 cm^{-1} corresponding to the stretching band of the ester carbonyl group (C=O) (Deng et al., 2024; Dubey et al., 2018; Singh et al., 2021). In all PHA spectra this band is always the strongest, corresponding to a characteristic band of PHA polymers (Rebocho et al., 2020). More specifically, the FTIR spectra of the P(3HB) homopolymer (Figure 2.1 A) showed the weakest band in the spectra near 2936-2974 cm^{-1} which corresponds to the methylene C–H elongation vibration (Dubey et al., 2018). The bands in the fingerprint region between 978 and 1453 cm^{-1} are usually related with the degree of crystallinity (Singh et al., 2021), where the peak at 1260 cm^{-1}corresponds to asymmetric C-O-C stretching vibration (G. Y. A. Tan et al., 2014; T. Volova et al., 2021). The region between 1054 and 1179 cm^{-1} shows series of absorption bands, which can be assigned to C-O and C-C stretching, respectively (Rebocho et al., 2019). Similar FTIR patterns have been found in the literature for other P(3HB) polymers produced by different bacterial strains (Dubey et al., 2018).

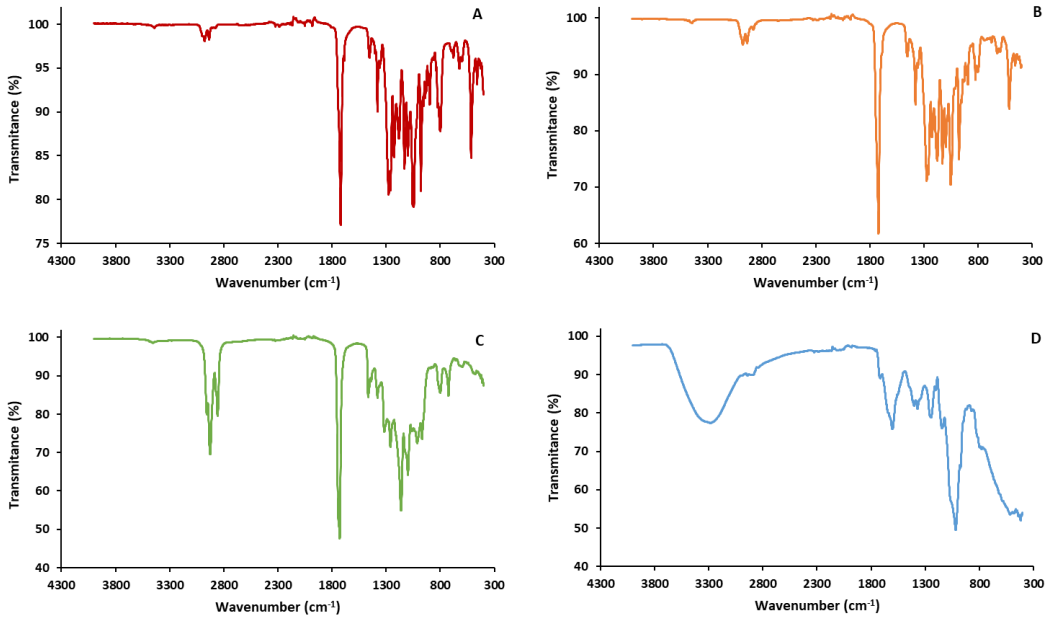

Figure 2.1 - Fourier-Transform Infrared Spectra (FTIR) of the biopolymers: P(3HB) (**A**), P(3HB-co-3HV-co-3HHx) (**B**), mcl-PHA (**C**), FucoPol (**D**).

When looking at the FTIR spectrum of P(3HB-co-3HV-co-3HHx) terpolymer it is easy to see that it also showed the weakest band near 2934-2974 cm^{-1} (for methylene C–H elongation vibration) (Sedlacek et al., 2020). It displayed an asymmetric C-O-C stretching vibration at 1261 cm^{-1}, together with C-O and C-C stretching at 1054 and 1179 cm^{-1}, respectively (T. Volova et al., 2021). When compared with the spectra attained for the P(3HB) homopolymers, both polyesters had a very similar pattern, with an equal number of absorption bands, but with distinct intensities, especially in the fingerprint region (Figure 2.1 A and B). These intensity differences could be related to the decrease in the crystallinity values revealed by the terpolymer when compared with the P(3HB) homopolymer (Table 2.1) (Sedlacek et al., 2020; Singh et al., 2021; G. Y. A. Tan et al., 2014; T. Volova et al., 2021).

Observing the FTIR spectrum of the mcl-PHA (Figure 2.1 C), it is visible that this polymer had a slightly different pattern when compared with the other PHA polymers (P(3HB) and P(3HB-co-3HV-co-3HHx)) attained in this study (Figure 2.1 A and B, respectively). One of the main differences is between 2958-2856 cm^{-1}, where three peaks can be identified which can be attributed to the asymmetric methyl group (peak at 2958 cm^{-1}), to the stretching vibration due to asymmetric -CH_2 of the lateral monomeric chains (peak at 2925 cm^{-1}) and to the symmetrical methyl group (peak at 2856 cm^{-1}) (Choonut et al., 2020; Tanikkul et al., 2020). This bands are reported in the literature to be stronger for mcl-PHA polymers and weaker when regarding P(3HB) homopolymers (Rebocho et al., 2020), as represented in Figure 2.1 A and C. Between 969 and 1466 cm^{-1}, a broad group of peaks is observed, indicating the presence of several characteristic structures within PHA polymers. For example, the peak at 1260 cm^{-1}corresponds to asymmetric C-O-C stretching vibration (Choonut et al., 2020). The region between 1013 and 1162 cm^{-1} shows series of absorption bands, which can be assigned to C-O and C-C stretching (Tanikkul et al., 2020). The presence of this broad band together with the absence of strict peaks is probably related to the decrease in the crystallinity values revealed by the mcl-PHA polyester when compared with the other two PHA polymers (the P(3HB) homopolymer and the P(3HB-co-3HV-co-3HHx) terpolymer) (Table 2.1) (Rebocho et al., 2019; G. Y. A. Tan et al., 2014). The band nearby 806 cm^{-1} is attributed to the -CH_2 bonds in the side chain of the polymer (Rebocho et al., 2019). Similar FTIR patterns have been found in the literature for other mcl-

PHA polymers produced by other bacterial strains (Choonut et al., 2020; Rebocho et al., 2019; Tanikkul et al., 2020; Wróbel-Kwiatkowska et al., 2019).

The FTIR spectrum of FucoPol has clearly different pattern when compared with the pattern observed for the PHA polymers (Figure 2.1 D), given the carbohydrate nature of the biopolymer. A broad intense band is visible around 3300 cm^{-1} that is common for samples containing polysaccharides (Fialho et al., 2021; Vázquez-González et al., 2022). This band represents O–H stretching of hydroxyls and bound water. This band overlaps in part with the C–H stretching peak of -CH_2 groups appearing between 2846-2946 cm^{-1} (Concórdio-Reis, Pereira, et al., 2020; Vázquez-González et al., 2022). The band at 1715 cm^{-1} is attributed to the C=O stretching of carbonyls in acyl groups (Araújo et al., 2023; Fialho et al., 2021). The band at 1249 cm^{-1} may also be attributed to the C–O–C vibration of acyl groups (Araújo et al., 2023). In the same way, the bands at 1602 and 1372 cm^{-1}, can be attributed to the asymmetric and symmetric stretching, respectively, of carboxylates (O=C-O) (Concórdio-Reis, Pereira, et al., 2020). Bands at 1200 and 900 cm^{-1} represent skeletal C–O and C–C vibration bands of glycosidic bonds (Vázquez-González et al., 2022). All peaks shown by FucoPol (Figure 2.1 D) in this study match those reported in previous studies attained by the same bacterial strain.

2.4.1.3 Molecular Mass Distribution

The biopolymers produced in this studied had very distinct M_w and PDI values. Among the PHAs, P(3HB) presented the highest M_w (9.15 ± 0.72 ×10^5 Da) together with a PDI value of 2.86 ± 0.54 (Table 2.1). These values were higher than those reported for the same strain grown on different carbon sources (5.0 - 5.2 ×10^5 Da and 1.8 - 2.0, respectively) and short chain length poly(hydroxyalkanoates) (scl-PHAs) (0.8 ×10^5 – 9.2 ×10^5 Da) (Table 2.1).

The P(3HB-co-3HV-co-3HHx) biopolymer had a M_w of 0.94 ± 0,14 ×10^5 Da (Table 2.1). Higher values, between 1.5 ×10^5 Da and 30.3 ×10^5 Da, were reported for the P(3HB-co-3HV-co-3HHx) synthesized by different bacteria, namely, the recombinant strains *C. necator* Re2133/pCB81 and *A. hydrophila* 4AK4 (Table 2.1). The biopolymer's PDI was 2.18 ± 0.29, which is within the average range reported for mcl-PHAs (1.3 – 2.7) and for different terpolyesters produced by the distinct bacterial strains (1.7 – 5.6) (Table 2.1).

The mcl-PHA synthesized by *P. chlororaphis* subsp. *aurantiaca* from fructose presented a M_w of 0.42 ± 0.04 ×10^5 Da, a value that is lower than those reported for polymers produced

by *P. chlororaphis* strains (1.0 – 1.3 $\times 10^5$ Da) (Table 2.1). This M_w is slightly lower than the values reported for other *Pseudomonas* sp. grown with distinct carbon sources (0.2 – 3.7 $\times 10^5$ Da) (Table 2.1). On the other hand, the mcl-PHA attained in this work had a PDI of 1.72 ± 0.08, which is within the values reported in the literature for the polymer achieved by *P. chlororaphis* strains (1.5 – 2.3) and for another *Pseudomonas* sp. (1.3 – 2.3) (Table 2.1).

The M_w and PDI values attained in this work for all PHA polymer makes them suitable to a wild range of applications, such as coatings, medical devices, drug delivery, and scaffolds for wound management (Rebocho et al., 2019). Also, the observed differences between the M_w and PDI values from this study and the ones reported in the literature can be explained by the use of the different production conditions, more specifically, the composition of the feedstock and media, cultivation mode, the microorganisms used, the stage of growth when the cells were harvested, as well as, the downstream processing (Rai et al., 2011; Sudesh et al., 2000). The monomeric composition can also influence the resulting M_w and PDI (N. Zhila & Shishatskaya, 2018). Differences the PHA's M_w and PDI have a direct impact in the preparation of polymeric solutions. Since higher M_w polymers tend to form more viscous solutions at rather lower concentrations the processability of a PHA polymer could be highly influenced by its M_w and PDI values.

The polysaccharide FucoPol had an average M_w of 1.40 ± 0.02 $\times 10^6$ Da, together with a PDI of 1.18 ± 0.01, which are similar to previously reported values (1.7 - 5.8 $\times 10^6$ Da and 1.3 – 1.9, respectively) (Baptista, Araújo, et al., 2022). The high M_w observed in FucoPol gives this biopolymer the capacity to act as a thickening and emulsifying agent to form viscous solutions and to stabilize emulsions (Baptista, Pereira, et al., 2022).

2.4.1.4 X-Ray Diffraction

The X-ray diffraction spectra for the P(3HB) homopolymer (Figure 2.2 A) exhibited peaks at 2θ equal to 13.4°, 16.8°, 20.2°, 21.5°, 22.5°, 25.5°, 27.2°, and 30.9° that were assigned to the (020), (110), (021), (101), (111), (130), (040) and (002) planes, respectively, as described by (Rincon-Granados et al., 2023). Similar XRD patterns have been described for other P(3HB) polymers (Chernozem et al., 2020; Rincon-Granados et al., 2023; Spasova et al., 2020). The P(3HB) homopolymer from this work presented the highest X_c among all the polymers tested (P(3HB), P(3HB-co-3HV-co-3HHx), mcl-PHA and FucoPol) with a value of 85.5% (Table 2.1). Slightly

lower X_c were reported for P(3HB) homopolymers (60-80%) produced by other microorganisms (Kopf et al., 2023; T. G. Volova et al., 2016; N. O. Zhila et al., 2023).

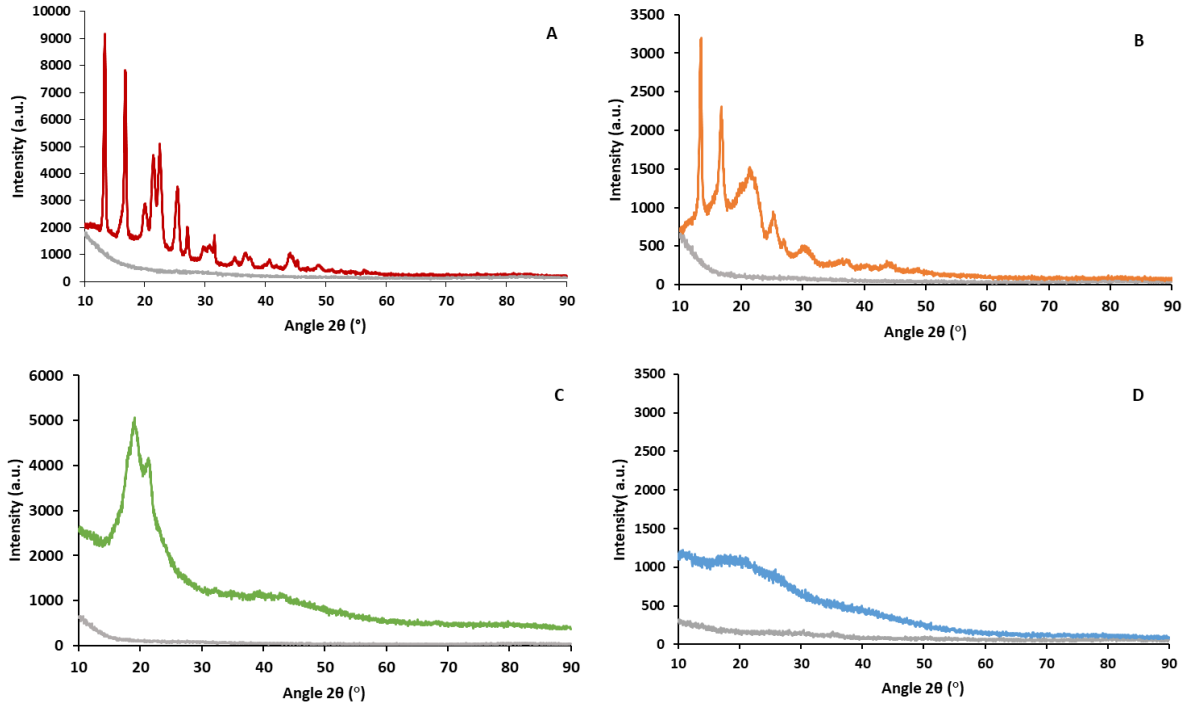

Figure 2.2 - X-ray diffractogram of the attained biopolymers: P(3HB) (**A**), P(3HB-co-3HV-co-3HHx) (**B**), mcl-PHA (**C**), FucoPol (**D**) and the silica standard used as holder (grey line).

The X-ray diffractogram of P(3HB-co-3HV-co-3HHx) (Figure 2.2 B) shows the typical behaviour of a semi-crystalline biopolymer. It exhibits peaks at 2θ qual to 13.4°, 16.8°, 22.3°, 25.5°, 27.1° and 30.7° which corresponds to the (020), (110), (111), (130), (040), and (002) lattice planes of the orthorhombic unit cell of P(3HB), as described by (Chernozem et al., 2020; Melendez-Rodriguez et al., 2018). This is representative of the crystalline fraction of the terpolymer due to its high content in 3HB monomers (59 mol%) (Martínez-Herrera et al., 2020). The presence of a broad peak at 2θ around 20° region relate to the amorphous fraction due to the incorporation of 3HV (20 mol%) and 3HHx (21 mol%) monomers, which significantly reduce the degree of crystallinity of the biopolymer (Bhubalan et al., 2008). The P(3HB-co-3HV-co-3HHx) polyester revealed to have a X_c value of 26.2% (Table 2.1), which is concomitant with the phenomenon observed in the DSC analysis (regarding the presence of two melting temperatures). This occurrence is probably due to its high contents of 3HV and 3HHx monomers (Bhubalan et al., 2008; Meléndez-Rodríguez et al., 2021). Moreover, the terpolymer also exhibited a T_g value, corroborating its semi-crystalline behaviour observed in the X-ray diffraction analysis.

It has been shown for P(3HB-co-3HHx) copolymers that increasing their content in 3HHx monomer leads to lower crystallinity degree values (Meléndez-Rodríguez et al., 2021). The observed semi-crystallinity of P(3HB-co-3HV-co-3HHx) can also be explained by the co-crystallization of 3HB and 3HV (Ye et al., 2010). A similar behaviour was reported for the P(3HB-co-3HV-co-3HHx) terpolymer produced by *A. hydrophila* 4AK4 (Ye et al., 2010).

The mcl-PHA's X-ray diffractogram shows a broad band at the 2θ region around 19°, whereas the crystalline zone displayed one diffraction peak near 21.5° (Figure 2.2 C), this spectrum is representative of an amorphous material with low crystallinity index (18.2%) (Table 2.1). This result is concomitant with the DSC analysis, where it was observed the presence of a glass transition temperature which is a characteristic of amorphous polymers (Pereira et al., 2021). Moreover, this crystallinity value is within the range of other mcl-PHA polymers produced by the same bacterial strain grown with different carbon sources but under similar bioreactor cultivation conditions (12.6% to 27%) (de Meneses et al., 2020; Pereira et al., 2021). However, this value was higher than those reported for the biopolymers produced by *P. resinovorans, P. citronellolis* and *P. mediterranea* (ranging from 1 % to 7 %) (Table 2.1). Being an amorphous material, the mcl-PHA produced in this work has a high disorder degree which makes it a less rigid and, consequently, a more flexible and elastic polymer with potential application as a coating material in the food packaging industry or in the biomedical field, for example, as wound dressing materials, for controlled drug delivery systems or for construction of 3D tissue scaffolds (Pereira et al., 2021).

The differences noticed in the X_c of all the PHA biopolymers attained in this study are related to their monomer composition, particularly with their high content in long side chain monomers (3HHx, 3HO, 3HD, 3HDd and 3HTd) (Pereira et al., 2021).

For the polysaccharide FucoPol, which was completely amorphous, no crystalline peaks were observed (Figure 2.2 D), in accordance with previous reports (Concórdio-Reis, Pereira, et al., 2020).

2.4.1.5 Thermal Properties

2.4.1.5.1 Differential Scanning Calorimetry

The DSC analysis for the P(3HB) polymer displays an endothermic peak related to polymer melting, visible at a temperature (T_m) of 174.24 ± 0.96 °C, together with a slight slope at 4.13

± 0.50 °C which is representative of the polymer's glass transition temperature (T_g) of 4.13 ± 0.50 °C (All heating cycles are shown in Appendix 2 - Figure A.1). This T_m is within the values usually reported for P(3HB) (167 to 180 °C) (Table 2.1). When compared with synthetic commercialized materials, the T_m values of P(3HB) were slightly higher than the ones observed for high density poly(ethylene) (HDPE) (112 to 132 °C), for low density poly(ethylene) (LDPE) (88 to 130 °C) (Anjum et al., 2016) and for PLA (150 to 162 °C) materials (Yousefi & Wnek, 2024). The T_g is also within the values reported for P(3HB) or P(3HB-co-3HV) polymers (4 to 5.8 °C and -7 to -0.2 °C, respectively) (Table 2.1). When compared with synthetic commercialized materials, the T_g values of P(3HB) were higher than the ones observed for HDPE (-80 °C) and for LDPE (-36 °C) (Anjum et al., 2016) but lower for PLA (45 to 60°C) materials (Yousefi & Wnek, 2024). Moreover, by observing the thermogram it is also evident the occurrence of a cold crystallization phenomena, where a clear exothermic peak (around 50 °C) is detected, this have already been reported previously for P(3HB) or P(3HB-co-3HV) polymers (Esmail, Pereira, Sevrin, et al., 2021). From all the PHA polyesters studied in this work (P(3HB), P(3HB-co-3HV-co-3HHx) and mcl-PHA) the cold crystallization was only visible for the P(3HB) polymer.

The DSC curve of P(3HB-co-3HV-co-3HHx) shows two melting endotherms at 108.51 ± 0.01 °C (T_{m1}) and at 159.72 ± 0.52 °C (T_{m2}) (All heating cycles are shown in Appendix 2 - Figure A.2). This phenomenon is observed in some P(3HB-co-3HV-co-3HHx) polyesters, probably associated with the semi-crystalline behaviour of these biopolymers due to the high contents of 3HV and 3HHx monomers (Bhubalan et al., 2008; Meléndez-Rodríguez et al., 2021). This crystallinity reduction has an impact on the polymers' melting temperatures, usually unfolding in the presence of two endothermic peaks, the first for the lowest crystalline density fractions of the terpolymer, and the second for the most thermodynamically stable 3HB-rich fractions, as described by (Meléndez-Rodríguez et al., 2021). The P(3HB-co-3HV-co-3HHx) terpolymer described by Meléndez-Rodríguez et al., 2021 had a T_{m1} and T_{m2} values of 111 °C and 173 °C, respectively, which may be related with the biopolymer's higher content in 3HB monomers. The determined T_{m1} values are within the ones reported for other terpolymers, where T_{m1} is usually between 91 - 129 °C, however, for T_{m2} the attained values are slightly higher than the ranges found previously in the literature 139 to 148 °C (Table 2.1). Nevertheless, these values are all lower than those reported for the homopolymer P(3HB) (173 to 180 °C) (Anjum et al.,

2016; Khanna & Srivastava, 2005). The lower melting temperatures might be related to the biopolymer's higher 3HHx content, since the incorporation of this monomer within 3HB domains apparently disturbs the possibility of the crystallization processes associated with 3HB, thus reducing the crystallinity of the terpolymers (Meléndez-Rodríguez et al., 2021; Zhao & Chen, 2007). The P(3HB-co-3HV-co-3HHx) biopolymer also exhibited some degree of melting transition, with a T_g of -3.8 ± 0.1 °C. This low T_g value could explain the biopolymer's elastomeric behaviour at room temperature (Zhao & Chen, 2007). The homopolymer P(3HB) is a more crystalline polymer, exhibiting small transition events, usually within 0 - 5 °C (D'Anna et al., 2022; Righetti et al., 2022; Surisaeng et al., 2022), while the terpolyesters usually display a T_g value between -4.7 °C and -0.8 °C (Table 2.1), since they have longer side chain monomers and are more amorphous (Bhubalan et al., 2010). When compared with synthetic commercialized materials, the T_m and T_g values of P(3HB-co-3HV-co-3HHx) were higher than the ones observed for HDPE and LDPE materials (Anjum et al., 2016).

The DSC thermogram of mcl-PHA shows a melting endotherm, corresponding to its T_m, at 44.91 ± 0.80 °C (All heating cycles are shown in Appendix 2 - Figure A.3). This polymer also exhibited a T_g of -46.02 ± 0.07 °C (Table 2.1), an intrinsic characteristic of amorphous materials where polymers change from a rigid glassy state to a softer and more flexible stage (Pereira et al., 2019). Similar values of Tg (-66 and -40.9 °C) and Tm (38 and 45 °C) were reported for mcl-PHAs produced by the same bacterial strain. Both values are, also, within the ranges reported for mcl-PHA polymers synthesized by other *Pseudomonas* sp. (Table 2.1). When compared with synthetic commercialized materials similar T_g (from -65 to -58 °C) and T_m (from 57 to 65 °C) values were observed by PCL materials (Yousefi & Wnek, 2024).

The thermal properties from the PHAs attained in this study (P(3HB), P(3HB-co-3HV-co-3HHx) and mcl-PHA) are intrinsically correlated with the composition and molecular weight of each polymer, which consequently, are deeply dependent on the bacterial strain, feedstock, cultivation conditions, as well as the extraction and purification processes used (Pereira et al., 2021).

2.4.1.5.2 Thermal Gravimetric Analysis

Through the observation of the thermogram from the TGA for the P(3HB) there was near 2% of weight loss until a temperature around of 265 °C, which shows the thermostability of

this polymer and the expected low water content due to the inherent hydrophobic behaviour of this biopolymer (Figure 2.3 A). However, a 5% of weight loss was attained at a temperature of 276.6 °C (T_{deg}) (Table 2.1). This value is similar to the reported ones for other P(3HB) homo-polymers (269 - 295 °C) (Table 2.1). After this step, the decomposition showed a single weight loss between 276 °C and 314 °C (as shown by the DTG curve), of approximately 82%, with a maximum degradation rate at 294.4 °C, together with a char yield of 8% at 500 °C (Figure 2.3 A). The presence of a single degradation step coupled with a very low char yield shows the high purity of the polymer. Comparable behaviour has been observed for P(3HB) polymers produced by other bacterial strains (Andler et al., 2023; Esmail, Pereira, Sevrin, et al., 2021; Rebocho et al., 2020).

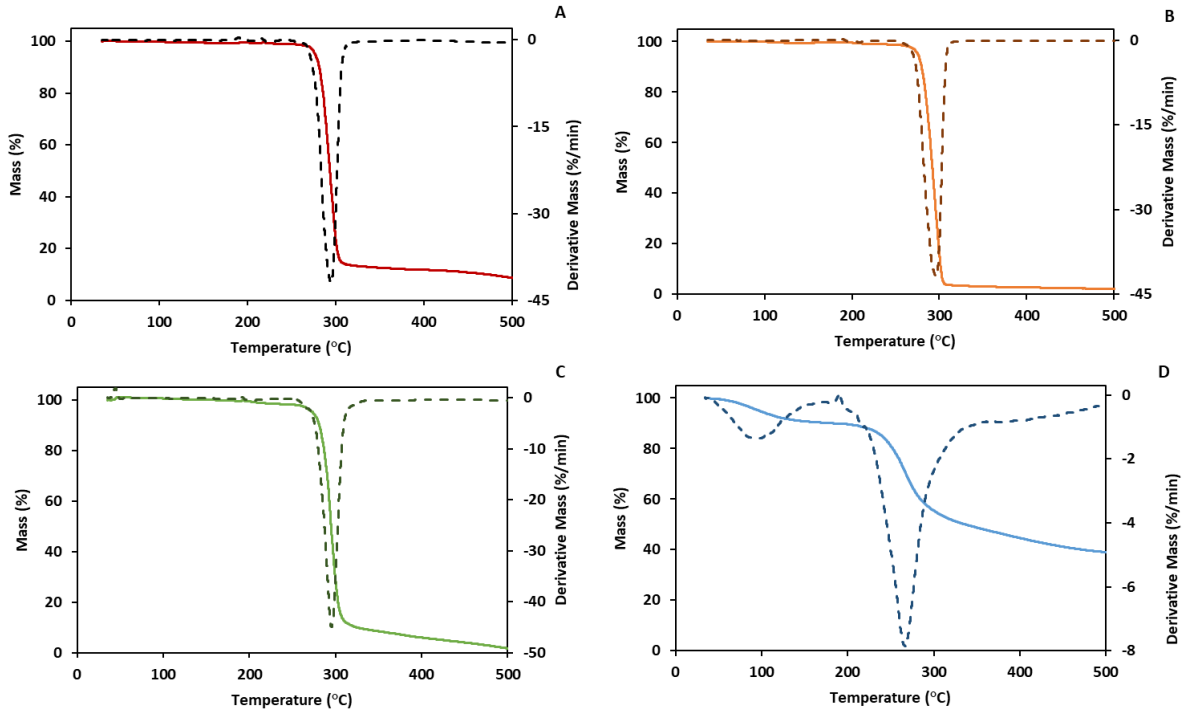

Figure 2.3 - Thermogravimetric analysis (TGA) curve with the respective first derivative of TGA curve (DTG) of the biopolymers: P(3HB) (**A**), P(3HB-co-3HV-co-3HHx) (**B**), mcl-PHA (**C**) and FucoPol (**D**).

As shown by the TGA curve for P(3HB-co-3HV-co-3HHx) (Figure 2.3 B), the decomposition of the terpolyester is a fast one-step process (also shown by the DTG curve). The curve was stable until around 260 °C, suffering a weight loss of 5% at a temperature of around 275.5 °C (T_{deg}) (Table 2.1) and a major weight loss (92%) with a single weight loss step between 276 °C and 315 °C, and a maximum degradation rate at 295.9 °C, with a char yield of approximately 2%, at 500 °C (Figure 2.3 B). These results are within those reported for other terpolymers (256

- 284 °C) (Table 2.1), somewhat higher than those reported for P(3HB-co-3HV) (224 – 268 °C) (Meléndez-Rodríguez et al., 2021; H. Zhang et al., 2009; Zhao & Chen, 2007) and P(3HB-co-3HHx) copolymers (239 - 251 °C) (Zhao & Chen, 2007), but slightly lower than for P(3HB) homopolymers (269 - 295 °C) (Table 2.1).

The TGA curve for the mcl-PHA shows a thermal stability up to 260 °C, with a weight loss of about 3%. The decomposition of the polymer was a fast one-step process (as shown by the DTG) (Figure 2.3 C). The curve exhibited a weight loss of 5% at a temperature of 274 °C (T_{deg}) (Table 2.1), followed by a major degradation step from 275 °C until 320 °C, (also shown by the DTG curve), near 85%, and a maximum degradation rate at 295.6 °C, together with a char yield of 1.5% at 500 °C. The T_{deg} of the biopolymer is within the values reported for other mcl-PHAs (257 – 300 °C) (Table 2.1). The mcl-PHA produced by the same strain when grown with other carbon sources and under similar bioreactor cultivation conditions, also had higher T_{deg} values (288 and 300 °C) (Table 2.1).

FucoPol displayed two weight loss steps in its TGA curve (as shown by the DTG curve) (Figure 2.3 D). The first occurs between 40 - 170 °C, where the sample loses around 10% of its mass, probably due to loss of the absorbed water, given the hygroscopic nature of FucoPol. Afterwards, the sample maintains its mass stable until around 200 °C, suffering a weight loss of 5% at around 240 °C. The maximum degradation rate (corresponding to the second and major step of mass loss) at 266.6 °C, where the sample loses around 30% of its mass, losing another 20% until 100 °C, resulting in a final yield of 38% at 500 °C. A similar behaviour was reported for FucoPol and for other polysaccharides (Baptista, Torres, et al., 2022b).

2.4.1.6 Cell Testing - Cytotoxicity Test

The possible cytotoxicity of PHA polymers was assessed using the indirect extract method, where these polyesters were exposed to the growth media of each cell line, at a concentration range of 1.5 to 50 mg/mL of the tested PHA sample (P(3HB), P(3HB-co-3HV-co-3HHx) and mcl-PHA), for 48h. Cell viability was observed through the colorimetric resazurin assay evaluated in cells incubated with the extracts. Viability values were normalized to the negative control (C−). According to the ISO 10993-5, cell viability below 70% of the blank is considered an indication of a cytotoxic effect (ISO10993-5:2009) (Nedeljkovic et al., 2022). However, through the observation of Figure 2.4 it is possible to conclude that all the PHA polymers tested revealed no

cytotoxic effect for fibroblasts (HFFF2) (Figure 2.4 A) and keratinocytes (HaCaT) (Figure 2.4 B) in the concentration range that was tested, since the cell viability were well above the 70%. These confirms that none of the PHA polymers leached any soluble cytotoxic compounds. The positive control (C+) revealed an extremely low cell viability, which is representative of the test's sensitivity. Therefore, these polyesters can be considered as raw materials for tissue engineering applications. These results are concordant with previously published results, since PHA polymers are well-known by their non cytotoxicity towards both cell lines (Kalia et al., 2023; Ladhari et al., 2023; Liu et al., 2024; Solarz et al., 2023).

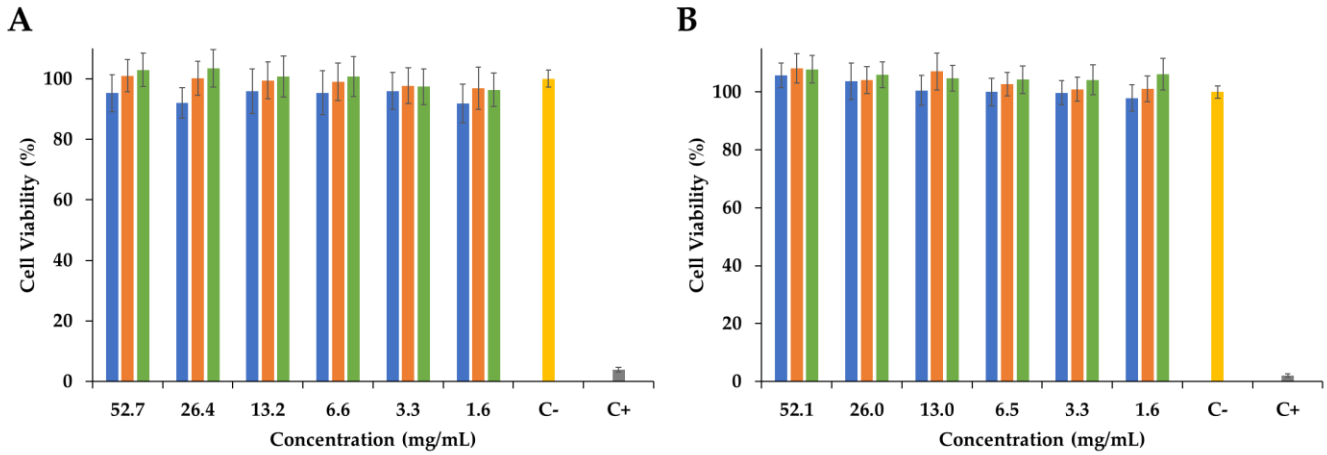

Figure 2.4 - Cell viability results for fibroblasts (HFFF2) (**A**) and keratinocytes (HaCaT) (**B**), obtained in a cytotoxicity assessment of P(3HB) (BLUE), P(3HB-co-3HV-co-3HHx) (ORANGE), mcl-PHA (GREEN) negative (YELLOW) and positive (GREY) control.

FucoPol's non-cytotoxic nature was reported in previous studies (Concórdio-Reis, Pereira, et al., 2020; Guerreiro et al., 2020). FucoPol at concentrations ranging from 0.001 to 10 mg/mL were tested for different cell lines, namely, human skin keratinocytes (HaCaT), human fibroblasts (HFFF2), human osteosarcoma (Saos-2), chronic myelogenous leukaemia (K562), monocyte leukaemia (THP1), breast and lung adenocarcinoma (MCF-7 and A549, respectively), ovarian carcinoma (A2780), mouse fibroblasts (NCTC clone L929), mouse myoblast (C2C12), Vero cells (Araújo et al., 2023; Baptista et al., 2023; Concórdio-Reis, Pereira, et al., 2020; Fialho et al., 2021; Guerreiro et al., 2020).

The cell compatibility of these polymers promotes their use as raw materials for the development of scaffolds to harbour cell adhesion and proliferation for wound management applications.

2.5 Conclusions

In this chapter, three different PHA polymers (P(3HB), P(3HB-co-3HV-co-3HHx) and mcl-PHA) were produced in bioreactor cultivation processes. The biopolymers were then extracted, purified, and characterized in terms of their physical and chemical properties. In summary, the P(3HB) that was produced had a M_w of 9.2×10^5 Da and a PDI of 2.9. It exhibited a T_m of 174.2 °C, a T_g of 4.1 °C, a T_{deg} of 276.6 °C, and a X_c of 85.5%. The P(3HB-co-3HV-co-3HHx) terpolymer, composed of 59 mol% of 3HB, 20 mol% of 3HV, and 21 mol% of 3HHx, had a M_w of 0.9×10^5 Da and a PDI of 2.2. It had two melting points at 143.7 °C (T_{m1}) and 159.7 °C (T_{m2}), a T_g of -3.8 °C, a T_{deg} of 275.5 °C, and a X_c of 26.2%. The mcl-PHA that was obtained had a composition of 4 mol% of 3HHx, 24 mol% of 3HO, 61 mol% of 3HD, 6 mol% of 3HDd, and 5 mol% of 3HTd. It had a M_w of 0.4×10^5 Da, a PDI of 1.7, a T_m of 44.9 °C, a T_g of -46 °C, a T_{deg} of 274 °C, and a X_c of 18.2%. All PHAs demonstrated to be non-cytotoxic for fibroblasts and keratinocytes.

FucoPol was produced by *Enterobacter* A47 in a standardized procedures using a bioreactor process and was recovered/purified from the cultivation broth with a diafiltration/ultrafiltration system. FucoPol was composed of fucose (34.33 mol%), glucose (33.12 mol%), galactose (26.21 mol%) and glucuronic acid (9.93 mol%). It was an amorphous biopolymer with a M_w of 1.4×10^6 Da and a PDI of 1.2 together with a T_{deg} around 240 °C. FucoPol is known to be non-cytotoxic against several cell lines including fibroblasts and keratinocytes.

The biopolymers produced in this step will be used as raw materials to develop porous structures for cellular adhesion and proliferation to evaluate their suitability for use in wound management applications.

3

DEVELOPMENT OF POLYMERIC STRUCTURES

The contents presented in this chapter are partly included in the publication "Pereira, J. R., Rafael, A. M., Esmail, A., Morais, M., Matos, M., Marques, A. C., Reis, M. A. M., & Freitas, F. (2023). Preparation of Porous Scaffold Based on Poly(3-hydroxybutyrate-co-3-hydroxyvalerate-co-3-hydroxyhexanoate) and FucoPol. *Polymers*, *15*(13), 2945. https://doi.org/10.3390/polym15132945".

3.1 Summary

The inherent non-cytotoxic behaviour of PHA polymers (P(3HB), P(3HB-co-3HV-co-3HHx) and mcl-PHA) makes them suitable materials for the development of porous scaffolds for biomedical applications (i.e., tissue engineering, dressings, or wound management). This feature is important to ensure that future porous structures produced with these materials are biocompatible and will do no harm when in contact with human skin. In addition, PHA's intrinsic structural properties provide a unique opportunity to develop scaffolds for wound management applications. Therefore, in this chapter, porous structured materials were developed using PHA polymers, namely, P(3HB), P(3HB-co-3HV-co-3HHx) and mcl-PHA, with two different strategies: the emulsion templated technique and the hot-pressing salt leaching method. Here, it became evident that the mcl-PHA polyester was unable to generate porous structures in either strategy. However, P(3HB) and P(3HB-co-3HV-co-3HHx) could be used in these two different techniques to attain 3D scaffolds. The obtained biopolymeric scaffolds were characterized in terms of their morphology, porosity, and ability to support cell adhesion and proliferation for fibroblasts. The obtained P(3HB) and P(3HB-co-3HV-co-3HHx) structures had very distinct morphologies and porosities (ranging from 49.8 to 87.1%), where the highest fibroblast proliferation values were attained after 7 days of cell cultivation observed by P(3HB) scaffolds obtained by the hot-pressing salt leaching method (178%) and the emulsion templated technique (311%). This last method revealed to be the most promising to develop 3D scaffolds based on these two PHA polymers. The main goal of this chapter was to evaluate if the produced PHA polymers could serve as raw materials to develop porous structures with the ability to support fibroblast adhesion and proliferation. It stayed clear that only with P(3HB) and P(3HB-co-3HV-co-3HHx) was it possible to attain porous structures capable of supporting cellular growth. Therefore, these two biopolymers were selected for further investigation.

3.2 Introduction

The intrinsic biocompatibility of PHAs provides a unique opportunity to develop porous biomaterials for wound management applications. The techniques used to develop porous structures play a significant role in the final applicability of the scaffold. The material processability and complexity of the method are also crucial to produce the best porous structures for wound dressing applications (Dutta et al., 2017). To achieve this, several methods have been developed to produce porous scaffolds, such as emulsion templating, freeze-drying, electrospinning (Esmail, Pereira, Zoio, et al., 2021), 3D printing (Eltom et al., 2019; Jensen & Teng, 2020), and solvent-casting particulate leaching (SCPL) (Esmail, Pereira, Zoio, et al., 2021).

Emulsion-templating is a promising approach for the fabrication of scaffolds with high porosity (up to 99%) and interconnected pores (Aldemir Dikici & Claeyssens, 2020), which are requirements for a variety of applications, including tissue engineering (Kinikoglu, 2017; Nikolova & Chavali, 2019). This technique comprises the preparation of an emulsion with two phases (one organic and one aqueous), where the aqueous phase is dispersed in the organic solution. When the organic solvent evaporates, it exposes the solid biopolymer that was previously dissolved, creating a structured material. The droplets of the aqueous phase will function as templates to produce highly porous scaffolds upon evaporation. This method not only produces structures with high porosity and interconnectivity, but it also allows for the adjustment of the scaffolds' porosity by changing the aqueous phase volume (Aldemir Dikici & Claeyssens, 2020; T. Zhang et al., 2019). This method has been used for the preparation of porous scaffolds based on different polymers, including polyhydroxyalkanoates (PHAs). Examples include the porous scaffolds based on the co-polymer P(3HB-co-3HV), characterized by having some interconnected porosity throughout the structure, together with an average pore size of 7 μm (Ruiz et al., 2011). Esmail (2021) was also able to produce porous scaffolds with the emulsion templating method using P(3HB-co-3HV) and the homopolymer P(3HB) (Esmail, Pereira, Sevrin, et al., 2021; Pereira et al., 2023).

Freeze-drying (or lyophilization) is a method to obtain porous scaffolds through solvent sublimation. In this case, the polymer is dissolved in the appropriate solvent (i.e. dioxane), then poured into a container and frozen. This structure is then subjected to sublimation in a freeze dryer. The result is a porous scaffold with numerous interconnected pores, but with physical

integrity (Ambekar & Kandasubramanian, 2019; Eltom et al., 2019). Most PHA polymers, like P(3HB) and P(3HB-co-3HV), are only soluble in harsh organic solvents (i.e. chloroform, dichloromethane) which could compromise the freeze-drying step used in this technique.

Electrospinning is a technique based on the use of an electric field for controlling the formation and deposition of polymeric fibres onto a surface. A high voltage is applied to the polymer solution, creating a charge repulsion that results in a liquid jet that travels to the target surface. The nanofibrous scaffold obtained has highly interconnected pores, but the thickness achievable with this method is still a little bit limited (Ambekar & Kandasubramanian, 2019; Jensen & Teng, 2020). The fabrication of biocompatible PHA-based electrospun scaffolds has been reported for several PHAs, namely, P(3HB), P(3HB-co-3HHx), P(3HB-4HB-3HV) and P(3HB-co-3HV), however, the scale-up of this procedure can be difficult to make (Esmail, Pereira, Zoio, et al., 2021).

3D printing is a method based in the development of porous structures through computer aid designs (CADs). This technique is a rapid prototyping technology that allows to have porous scaffolds with controlled pore structure (Ambekar & Kandasubramanian, 2019).

SCPL technique allows the formation of highly porous structures (50 – 90%), by mixing a polymeric solution with salt particles (e.g. NaCl) and casting into a surface. Then, when the solvent evaporates, the scaffold is submerged in water and the salt particles are dissolved and leached out from the structure. This method allows to attain tuneable pore dimensions, through the size of the salt particle used. However, the pore interconnectivity is still a little limited in this technique (Eltom et al., 2019; Esmail, Pereira, Zoio, et al., 2021). To overcome this issue the polymer could be melted and pressed to ensure that the produced matrix has the correct porosity and interconnected pores. This method has been explored to produce PCL scaffolds for bone tissue engineering (Gavinho et al., 2023).

The inherent biocompatibility of PHAs like P(3HB), P(3HB-co-3HV-co-3HHx) and mcl-PHAs makes them interesting materials for the development of porous scaffolds for biomedical applications (i.e., tissue engineering and wound management). This feature is important to ensure that the produced structures have reduced cytotoxicity and do not induce allergic reactions when in contact with skin. Therefore, in this chapter the main goal was to develop porous PHA scaffolds (from P(3HB), P(3HB-co-3HV-co-3HHx) and mcl-PHA) using two different

approaches, namely, the emulsion-templating technique and the hot-pressing salt leaching method. The obtained biopolymeric scaffolds were characterized in terms of their morphology, porosity and their capacity to support fibroblast adhesion and proliferation.

3.3 Materials and Methods

3.3.1 PHA Films

P(3HB), P(3HB-co-3HV-co-3HHx) and mcl-PHA films were obtained by casting 10 or 20 mL of a biopolymeric solution (at 4% (w/v), 9.5% (w/v) and 10% (w/v), respectively) in chloroform (99.5%, Sigma-Aldrich, USA) into glass petri dishes (with a diameter of 5 or 10 cm) (Figure 3.1) and placing them in the fume hood inside a desiccator, at room temperature, until complete solvent evaporation. The films were kept at room temperature in closed glass petri dishes until use.

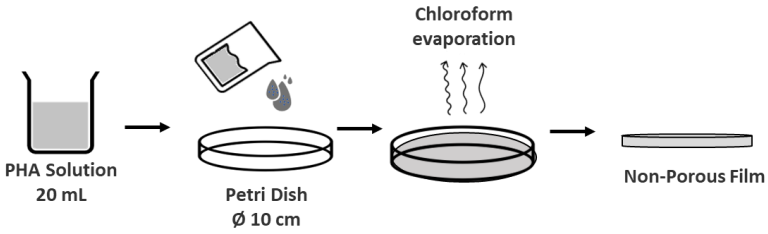

Figure 3.1 - Schematic representation of the solvent evaporation method to obtain cast films. Adapted from (Esmail, Pereira, Sevrin, et al., 2021).

3.3.2 Porous Scaffolds

In this study, two different strategies were tested to prepare porous scaffolds based on PHA polymers (P(3HB), P(3HB-co-3HV-co-3HHx) and mcl-PHA): emulsion templating and hot-pressing with salt leaching.

3.3.2.1 Emulsion Templated Scaffolds

For preparation of the porous scaffolds using P(3HB) and P(3HB-co-3HV-co-3HHx), 10 mL of the biopolymer solution in chloroform (99.5%, Sigma-Aldrich, USA) were mixed with 1 mL of deionized water and stirred with a magnetic stirrer until a stable emulsion formed (±1 hour). Different biopolymer concentrations were used, namely, 4% and 9.5% (w/v), respectively. The resulting emulsions were transferred to 5 cm petri dishes and left in the fume hood inside a desiccator, at room temperature, until complete solvent (water and chloroform) evaporation (Figure 3.2). The scaffolds were kept at room temperature in a closed glass petri dish until use. For mcl-PHA it was not possible to obtain a porous scaffold with this method because this

polyester could not form a stable emulsion, even at higher polymeric concentrations (20% and 40% (w/v)).

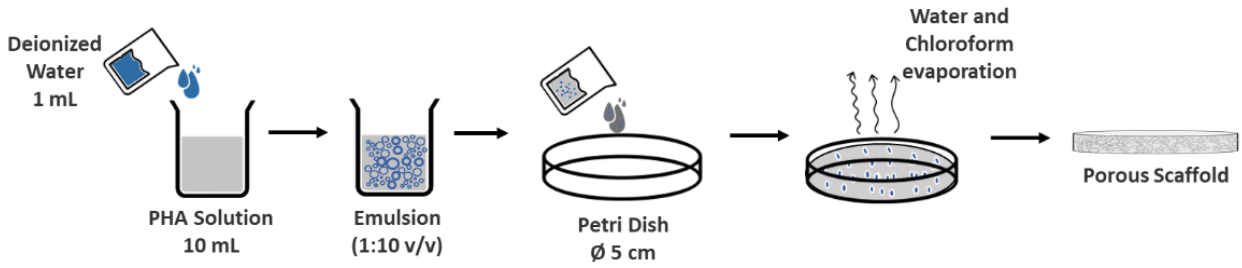

Figure 3.2 - Schematic representation of the emulsion templating technique to attain porous scaffolds. Adapted from (Esmail, Pereira, Sevrin, et al., 2021).

3.3.2.2 Hot-Pressing Salt Leaching Scaffolds

To prepare porous scaffolds through the hot-pressing salt leaching method, P(3HB), P(3HB-co-3HV-co-3HHx) and mcl-PHA biopolymers were dissolved in 30 mL of chloroform (99.5%, Sigma-Aldrich, USA) at concentrations of 5% (w/v), 10% (w/v) and 20% (w/v), respectively. This technique was adapted from a procedure used before by Gavinho et al., 2023. Briefly, to each PHA solution was added 1.5 g of salt that was previously grinded and size-selected using sieves with pore sizes of 150 µm and 200 µm. The resulting suspension (with PHA and NaCl) was then casted into a glass with a casting knife (Elcometer 3580/3, UK) and after solvent evaporation, PHA films (of P(3HB), P(3HB-co-3HV-co-3HHx) or mcl-PHA) with NaCl were obtained. Afterwards, these films were cut (using a metal punch) into circular shaped pieces with 15 mm of diameter. The obtained discs were stack into three and placed inside a metal holder, between two layers of NaCl. These structures were then compressed and heated (at 20 bar and 190 °C, respectively). After cooling down, the resulting compact material was placed in water at room temperature during 24 h for salt leaching. The porous scaffolds were left at room temperature to dry (Figure 3.3). For the mcl-PHA polyester the membranes obtained after hot-pressing were

disrupted during the salt leaching step probably due to the slow crystallization rate and low melting point displayed by this biopolymer (Reddy et al., 2022).

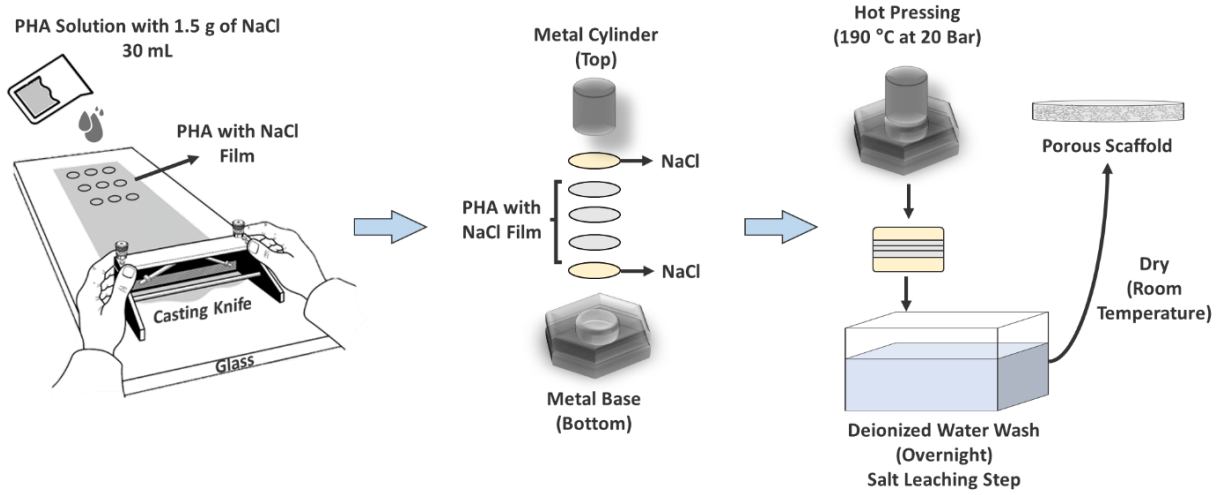

Figure 3.3 - Schematic representation the hot-pressing salt leaching method to obtain porous scaffolds.

3.3.3 Morphological Characterization

Macroscopic characteristics such as colour, texture and homogeneity were assessed visually. The thickness of the films and scaffolds was measured using a micrometer (Elcometer 124, UK).

3.3.3.1 Scanning Electron Microscopy

For the scanning electron microscopy (SEM) analysis, samples were frozen in liquid nitrogen and broken to obtain smaller pieces that were mounted for SEM observation using double sided carbon tape, aluminium stubs and sputter coated with gold-palladium (60/40%) alloy (Q150T ES, Quorum, UK). The analysis was performed using a bench top scanning electron microscope (TM3030 Plus, Hitachi, Japan) using an acceleration voltage of 15 kV. The obtained SEM images were processed by ImageJ.

3.3.3.2 Mercury Porosimetry

Mercury porosimetry was used for assessing the P(3HB) and P(3HB-co-3HV-co-3HHx) scaffolds porosity prepared by the emulsion templating technique and the hot-pressing salt leaching method. An AutoPore® IV 9500 Series apparatus was used with a range of low pressures between 4 and 345 kPa, which translates to a pore size range of 397 and 4.5 μm, and a range

of high pressure between atmospheric pressure (101 kPa) and 228 MPa, corresponding to 15 and 0.007 μm pore sizes (Appendix B.1 and Appendix B.3).

3.3.4 Cell Testing

3.3.4.1 Cell culture and Media

Fibroblast cells (HFFF2, Human Caucasian Foetal Foreskin Fibroblasts from a 14- to 18-week-old human foetus, ECACC, UK) were cultured in low-glucose DMEM with stable glutamine and sodium pyruvate (Biowest, USA) supplemented with penicillin (100 U/mL) (Life Technologies, USA), streptomycin (100 μg/mL) (Life Technologies, USA) and 10% FBS (Biowest, USA).

3.3.4.2 Adhesion and Proliferation Assay

To determine the adhesion and proliferation of HFFF2 cells seeded on the developed PHA structures, the scaffolds were cut with a 15 mm circle punch to be used as samples for cell culture. Before cell seeding, the samples were sterilized in ethanol 70% (as previously described) and soaked in complete culture medium (low glucose DMEM) for 24h. Afterwards, HFFF2 cells were seeded, at a density of 20,000 cells/cm^2, over a 1 cm^2 area over each sample inside a 24-well tissue culture plate (TCP) (Avantor, USA). Cell controls were set by seeding cells at the same density directly over the surface of the TCP wells for viability assays. After seeding, cells were incubated at 37 °C, 5% CO_2 in a humidified atmosphere incubator (MCO-19AIC(UV) Sanyo, Japan). Cell adhesion and proliferation were evaluated through the population assessment by a colorimetric viability assay with resazurin, as described previously. Briefly, a resazurin: cell culture medium solution was added to the immobilized scaffolds with adhered cells and incubated during 4 h at 37 °C, 5% CO_2 in a humidified atmosphere incubator (MCO-19AIC(UV) Sanyo, Japan). Cell viability and population was assessed through the reduction of resazurin into resorufin by viable cells and measuring the optical density in a microplate reader (BioTek ELX 800UV microplate reader) at 570 and 600 nm, respectively. This assay was performed 24 h after cell seeding (day 1 of culture) to estimate cell adhesion, and then after 4 and 7 days to assess cell proliferation. The statistical differences between the samples and the cell control were assessed by GraphPad Prism 5 through a one-way Analysis of Variance (ANOVA) with

Bonferroni's multiple comparison test (where, * $p \leq 0.05$; ** $p \leq 0.01$; *** $p \leq 0.001$) (Aghayan et al., 2022; Piironen et al., 2020) (Appendix B.2, Appendix B.4 and Appendix B.5).

3.4 Results and Discussion

The porosity and morphological properties of a structured material influence their applicability as wound management products. Low-porosity films can still be used as wound dressing materials, since they might maintain the humidity at the wound surface, preserving an impermeable layer to the microorganisms and preventing secondary infections. These materials could also be further improved to serve better their purposes. However, they will never function as 3D scaffolds for cell growth. Porous scaffolds, on the other hand, could harbour cellular adhesion, migration, proliferation, and differentiation. The structural properties of these products (pore size, interconnectivity, and porosity) affect their ability to sustain cell growth. Therefore, porous scaffolds need to have certain morphological requirements to function as suitable materials for their use in tissue engineering applications. More specifically, for fibroblasts to freely migrate and fully proliferate throughout the whole scaffold, such porous materials should have a high porosity (from 60% to 90%) (Choi et al., 2018; Khan et al., 2023). Pore interconnectivity is also quite important for cellular migration and differentiation (Choi et al., 2018; Esmail, Pereira, Sevrin, et al., 2021).

3.4.1 PHA films

3.4.1.1 Morphology

The P(3HB) films were homogenous and had a whitish translucent macroscopic appearance (Figure 3.4 A.I.) with thicknesses between 160 and 250 μm. Cast films of this homopolymer were rigid and through the observation of the SEM images, it was clear, that there was some roughness on its surface (Figure 3.4 A.II.), displaying a certain rugosity that could be related to the high crystallinity showed by this polymer. The cross-section images also displayed some irregularities and fissures that are probably a result of the fast evaporation and crystallization rate during the drying process (Figure 3.4 A.III.), with the absence of any porosity across the whole film thickness. Similar morphological features were reported for other P(3HB) and P(3HB-co-3HV) cast films (Bergstrand et al., 2012; Fabra et al., 2014).

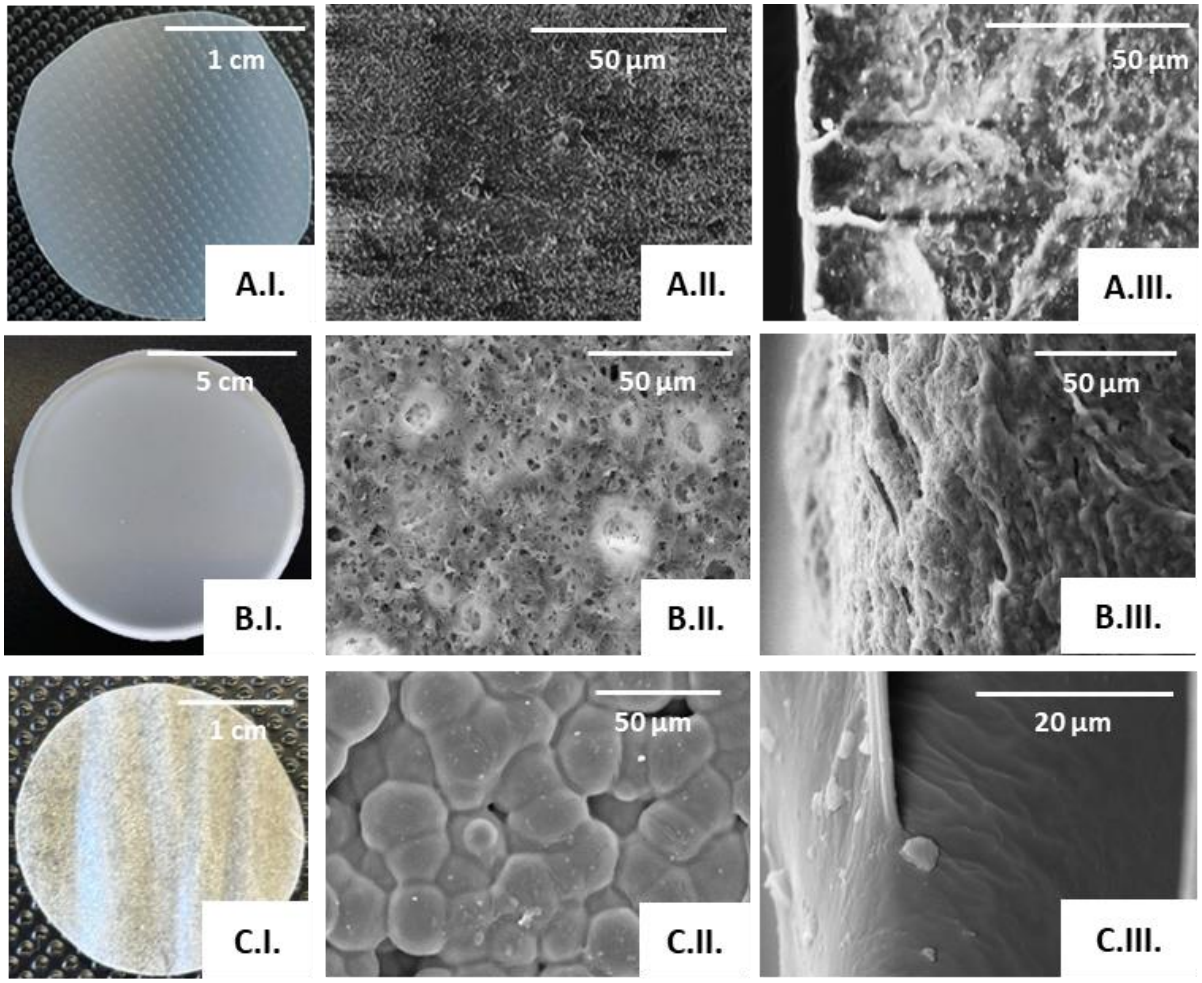

Figure 3.4 - P(3HB) (A), P(3HB-co-3HV-co-3HHx) (B) and mcl-PHA (C) film's macroscopic appearance (I) and SEM images of the surface amplified 1200× for P(3HB), 1000× for P(3HB-co-3HV-co-3HHx) and 800x for mcl-PHA (II) and cross-section amplified 1200× for P(3HB) 1000× for P(3HB-co-3HV-co-3HHx) and 4000x for mcl-PHA (III).

The P(3HB-co-3HV-co-3HHx) films obtained by solution casting and solvent evaporation were white, slightly translucid, and macroscopically homogeneous (Figure 3.4 B.I.), with a thickness ranging between 90 and 200 µm. The terpolymer cast films were more flexible when handling than the P(3HB) non-porous structures. However, the SEM analysis revealed the presence of surface roughness (Figure 3.4 B.II), similar to P(3HB) cast films, with the exception that P(3HB-co-3HV-co-3HHx) cast films exhibited an apparent porosity that was not perceivable in the cross-section image (Figure 3.4 B.III.). Similar morphological features were reported for other P(3HB-co-3HV-co-3HHx) cast films (L. Wang et al., 2010), for blends of P(3HB) and poly(butylene succinate) (Righetti et al., 2022) and blends of PLA/P(3HB) films (D'Anna et al., 2022).

The films prepared with mcl-PHA were homogeneous, opaque with a yellowish colour and macroscopically homogeneous (Figure 3.4 C.I.) with a thickness range of 150 to 300 µm. This

film was more flexible when handling than the P(3HB) homopolymer and P(3HB-co-3HV-co-3HHx) terpolymer films. The SEM imaging of the mcl-PHA film's surface revealed that this structure was composed of small overlapped polymeric spheres tightly packed to each other without any pores or holes (Figure 3.4 C.II.). The cross-section images showed that this layer was smooth and dense with the absence of air bubbles or pores (Figure 3.4 C.III.). Similar morphologies were reported for films prepared with the other mcl-PHA (Pereira et al., 2019, 2021), PLA, PCL, and poly(ethylene terephthalate) (PET) polymers (Fabra et al., 2014; Nashchekina et al., 2020; Ward et al., 2020).

Compact, dense, PHA films can be advantageous since they can function as antibacterial materials for different biomedical applications, including drug delivery and tissue engineering (H. Park et al., 2024). However, porous scaffolds allow cells to freely migrate and fully proliferate throughout the whole structure. This feature enables the possibility of achieving highly differentiated tissue, which is crucial for several medical applications including wound regeneration. This justifies why 3D porous scaffolds are considered very promising candidates for the development of wound dressing materials for wound healing applications.

3.4.2 Emulsion-templated scaffolds

PHA porous scaffolds can be prepared through different procedures. In the emulsion templating technique it is crucial to attain an emulsion able to maintain its stability throughout the whole solvent evaporation process. In this method, there are several details that could interfere with the emulsion's stability. The conditions used in this procedure such as temperature, agitation process, polymer's M_w, concentration of the polymeric solution, ratios between the dispersed and continuous phases, and the solvent evaporation rate are crucial details that interfere with the emulsion's stability, thus affecting the production and characteristics of the porous scaffolds. Studies regarding the water ratios and the concentration of the PHA solutions were published recently (Esmail, Pereira, Sevrin, et al., 2021; Pereira et al., 2023). Polymers with high M_w form viscous solutions at lower concentrations when compared with lower M_w polymers. The mcl-PHA polymer was the polyester with the lowest M_w value ($0.4x10^5$ Da) among the biopolymers tested in this study. Given this, it was not possible to attain a mcl-PHA solution with the viscosity required to sustain a good emulsion stability, even for high concentrations

up to 40% (w/v). This could be probably due to the slow crystallization rate usually displayed by these polymers (Reddy et al., 2022).

3.4.2.1 Morphology

The porous scaffolds prepared by the emulsion templating method using P(3HB) were homogeneous, had an opaque white colour (Figure 3.5 A.I.) and a thickness around 600 µm. The observation of the SEM images revealed that these scaffolds had a rough surface (Figure 3.5 A.II.), similar to the homopolymer films, without any visible microporosity, probably due to the quick solvent evaporation process. However, the cross-section images revealed the presence of pores of varied sizes with apparent interconnectivity (Figure 3.5 A.III.). The porosity determined by mercury porosimetry of this scaffold was 82.2%, which is a high value usually attained by electrospun scaffolds of bacterial cellulose and PVA (from 70% to 80%) (Khan et al., 2023), jelly fig polysaccharide structures (73.5%) for tissue engineering applications (Thangavel et al., 2024), PCL structures (74%) prepared by emulsion templating (Yadav et al., 2019) and chitosan with gelatin from fish skin cross linked with glutaraldehyde (GTA) structures obtained by electrospinning (84%) (Gomes et al., 2017). Given their high porosity, these scaffolds were more brittle and fragile when compared with the previously P(3HB) films. Analogous morphological structures have been reported for other P(3HB) homopolymer scaffolds prepared by the emulsion templating technique and by the solvent casting particulate leaching strategy (Bergstrand et al., 2012, 2014; Esmail, Pereira, Sevrin, et al., 2021). These structures also resembled the porous 3D scaffolds achieved by thermally induced phase separation of PLA polymer (Mauro et al., 2024).

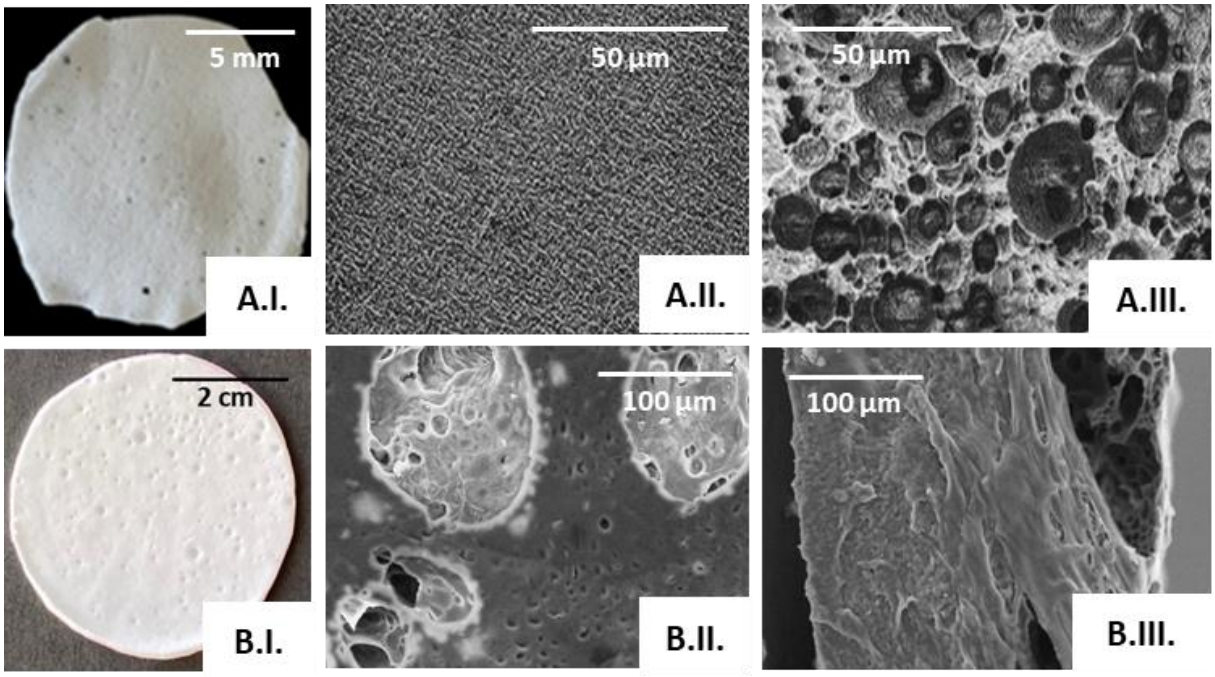

Figure 3.5 - P(3HB) (A) and P(3HB-co-3HV-co-3HHx) (B) scaffolds obtained with the emulsion-templating technique with 1 mL of water. Macroscopic appearance (I) and SEM images of the surface amplified 1200× for P(3HB) and amplified 500× for P(3HB-co-3HV-co-3HHx) (II) and cross-section amplified 1000× for P(3HB) and amplified 500× for P(3HB-co-3HV-co-3HHx) (III).

The P(3HB-co-3HV-co-3HHx) porous scaffolds achieved by the emulsion templating method, were white with an opaque appearance, and a homogeneous smooth surface (Figure 3.5 B.I.). They had thickness values ranging from 160 to 300 µm and were flexible, similarly to the terpolymer films. Being more flexible when handling than the P(3HB) porous scaffolds with macroscopic features similar to those structures. Scaffolds prepared from the terpolymer comprised pores of distinct size, including macropores with a diameter of approximately 100 µm, dispersed throughout a microporous structure (Figure 3.5 B.II.). Furthermore, the pores were interconnected through tunnel-like structures. Moreover, in the cross-section images it is also possible to observe the presence of pores of varied sizes (Figure 3.5 B.III.). The porosity of P(3HB-co-3HV-co-3HHx) structures was 49.8%, which was a much lower value when compared with P(3HB) emulsion templated scaffolds. Similar porosities have been attained for P(3HB-co-3HV) (42.2%) and PLA with P(3HO) (50.9%) structures obtained by electrospinning (De la Ossa et al., 2022; Solarz et al., 2023), for porous materials with collagen and PLA achieved by 3D printing (ranging from 52% to 63%) (Ambekar & Kandasubramanian, 2019) and for structures of poly(dimethylsiloxane) (PDMS) (60%) produced by emulsion templating (Riesco et al., 2019).

Scaffolds with equivalent morphological properties have been reported for P(3HB-co-3HV) structures obtained with the emulsion templating technique and by the solvent casting particulate leaching strategy (Esmail, Pereira, Sevrin, et al., 2021; Ruiz et al., 2011). Different polymeric materials were also reported to display such structural features, for instance scaffolds achieved with PLA (X. Zhu et al., 2015), PCL (Reignier & Huneault, 2006) and blends of chitosan with gelatin (Modaress et al., 2012).

The resulted P(3HB) and P(3HB-co-3HV-co-3HHx) scaffolds had distinct porosities (82.2% and 49.8%, respectively) that are within the ranges reported by other materials for tissue engineering applications (De la Ossa et al., 2022; Gomes et al., 2017; Rodríguez-Tobías et al., 2016). This means that these structures are promising candidates for fibroblast culture. These porous materials usually display high surface area to volume ratios allowing cells to exchange nutrients and metabolites providing them with an adequate environment for their metabolism (Vieira et al., 2019). The presence of interconnected pores is also an advantage, since it allows cells to migrate, proliferate and differentiate throughout the whole scaffold. Yet, further improvement could still be done regarding the scaffold's surface composition and roughness or hydrophilicity, since these properties can directly affect cellular behaviour (Vieira et al., 2019).

3.4.2.2 Adhesion and Proliferation Assay

Viability of fibroblasts (HFFF2) seeded over the surface of PHAs porous scaffolds and TCP wells (cell control) was evaluated through the resazurin colorimetric assay. The assessment was determined after 1 day of seeding and in the following days 4 and 7 to estimate cellular adhesion and proliferation, respectively. In Figure 3.6 (blue columns) it is possible to observe the adhesion results obtained from the ratio between the average cell viability for each PHA scaffold and the average viability of the cell control. When compared to the control, PHA emulsion templated scaffolds had statistically lower adhesion rates, around 46% for P(3HB) structures and about 29% for P(3HB-co-3HV-co-3HHx) porous materials. Similar adhesion rates in HFFF2 cells (around 50%) were observed previously for electrospun scaffolds with PU, PCL and chitosan, as well as the combination of the last two polymers (Vieira et al., 2019, 2024).

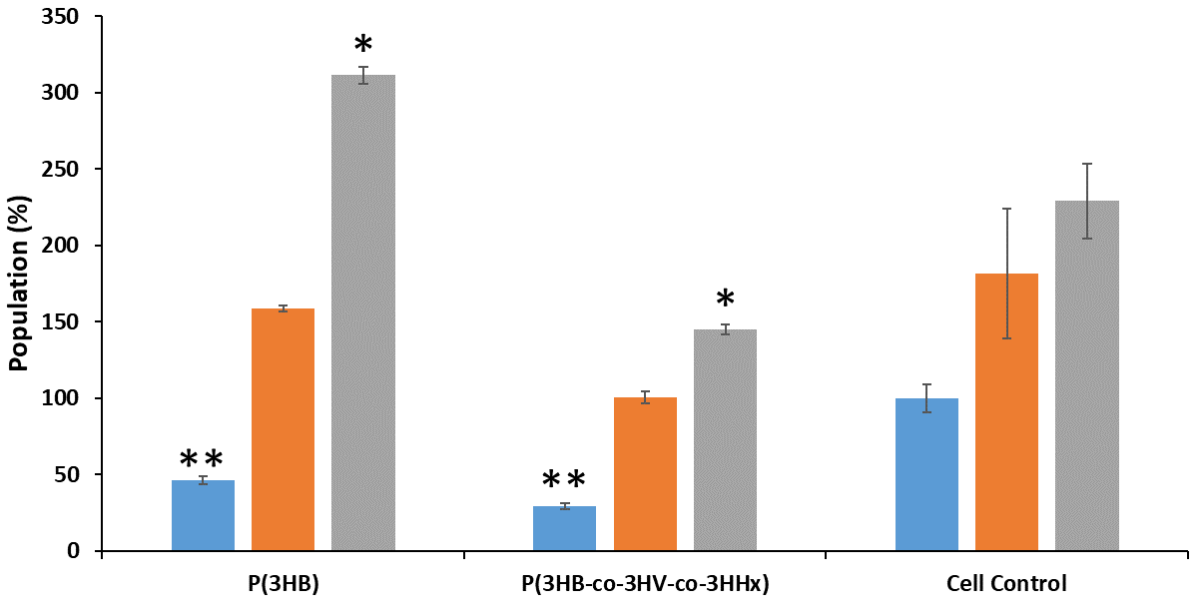

Figure 3.6 - Fibroblasts (HFFF2) relative cell population. Cells were seeded on P(3HB) and P(3HB-co-3HV-co-3HHx) porous scaffolds attained with the emulsion templating technique and TCP wells (CC) and assayed with resazurin after 1 (BLUE), 4 (ORANGE) and 7 (GREY) days of culture. Vertical lines represent the standard deviation of the mean. Statistical differences between the samples and the cell control were assessed through a one-way ANOVA with Bonferroni's multiple comparison test (where, * $p \leq 0.05$; ** $p \leq 0.01$; *** $p \leq 0.001$).

Fibroblasts proliferation was assessed from the quotient between cell viability on days 4 or 7, and day 1. During the first 4 days, cells adhered and proliferate in both PHA structures, reaching population values of 159% and 100% for P(3HB) and P(3HB-co-3HV-co-3HHx) scaffolds, respectively. The differences of cellular proliferation (after 4 days) between PHA polymers and the cell control are much less significant (with no statistical relevance) than the differences observed regarding cell adhesion ratios. This means, that the observed higher cellular population achieved by the P(3HB) emulsion templated scaffold, was due its higher cell adhesion. After 7 days of cell culture, further fibroblast proliferation was observed for both PHA scaffolds. However, P(3HB) structures achieved a population percentage significantly higher (311%) than P(3HB-co-3HV-co-3HHx) scaffolds (145%). This result was expected since P(3HB) emulsion templated scaffold had higher cell adhesion in this experiment. When compared with the cell control (228%), it stays clear that P(3HB) structures had a statistically greater proliferation, while P(3HB-co-3HV-co-3HHx) scaffolds revealed to have a significantly lower population. Despite being hydrophobic materials PHA emulsion templated scaffolds were still able to support fibroblast adhesion and proliferation due to their porosity. Similar proliferation profiles were

observed previously in P(3HB-co-4HB) scaffolds produced by solvent casting and seeded with human gingival fibroblasts (HGF) (Chen et al., 2023). Similar behaviours with P(3HB), P(3HB-co-3HV) and PCL scaffolds obtained by the solvent casting salt leaching method, also seeded with HGF, have been reported (Phuegyod et al., 2023).

3.4.3 Hot-Pressing Salt Leaching Scaffolds

To obtain porous scaffolds using PHA polymers through the hot-pressing salt leaching method, it is important to have a polymer that is slightly rigid and crystalline enough to sustain a solid structure without collapsing or disrupting with the presence of holes and pores. This means that only polymers with a certain crystallization rate can produce porous structured materials through this procedure. Given this, when mcl-PHA polyester was used in this method, the scaffolds lost their structure and disrupted during the salt leaching step. This could be explained by the slow crystallization rate, low melting point (44.9 °C) and low crystallinity (18.2%) exhibited by this biopolymer. It is known that mcl-PHAs with these properties have limited melt processability (Reddy et al., 2022). The P(3HB) and the terpolymer, on the other hand, usually have faster crystallization rates and exhibited a higher crystallinity (85.5% and 26.2%, respectively), and melting points (174.2 °C and 108.5-159.7 °C, respectively), which makes them suitable for their processing into porous scaffolds by this technique.

3.4.3.1 Morphology

The porous scaffolds that were prepared by hot-pressing salt leaching using P(3HB) were homogeneous, white, slightly translucid (Figure 3.7 A.I.) with a thickness ranging from 290 to 340 µm. Macroscopically, these structures were more resistant and flexible when handled comparing with the previously P(3HB) scaffolds obtained by the emulsion templating technique. SEM images revealed the presence of a high porosity surface (Figure 3.7 A.II.), with pore interconnectivity and with a structure morphologically different from the PHA films and scaffolds obtained using the solvent casting and the emulsion templating method, respectively. The cross-section images also showed pores of varied sizes with apparent interconnectivity (Figure 3.7 A.III.), that were also distinct from the previously achieved PHA structures. When compared with P(3HB) porous scaffolds obtained by emulsion templating process, these materials were more stiff, rigid and similar to what was obtained in the films of this homopolymer. Analogous,

morphological structures have been reported in the literature for P(3HB) scaffolds produced with tetrahydrofuran and chloroform obtained by non-solvent-induced phase separation (NIPS) (Kang et al., 2020) and for PCL porous scaffolds obtained using the hot-pressing salt leaching technique (Gavinho et al., 2023). P(3HB) porous scaffold obtained with the hot-pressing salt leaching method had a porosity of 67.7%. When compared with the porosity achieved by the PHA structures from the emulsion templating technique, this value was a lower than the one reached by P(3HB) polymer (82.2%) and higher than the porosity of P(3HB-co-3HV-co-3HHx) terpolymer (49.8%). Similar porosities have been previously reported for P(3HB-co-3HV) scaffolds produced by 3D printing (65%) (Shishatskaya et al., 2023) and for scaffolds produced by electrospinning using: P(3HB) with tricalcium phosphate (70%) (Skibiński et al., 2023), PLA (77.5%) (Ambekar & Kandasubramanian, 2019), PCL with chitosan (71%) (Gomes et al., 2017) and bacterial cellulose with PVA (from 70% to 80%) (Khan et al., 2023).

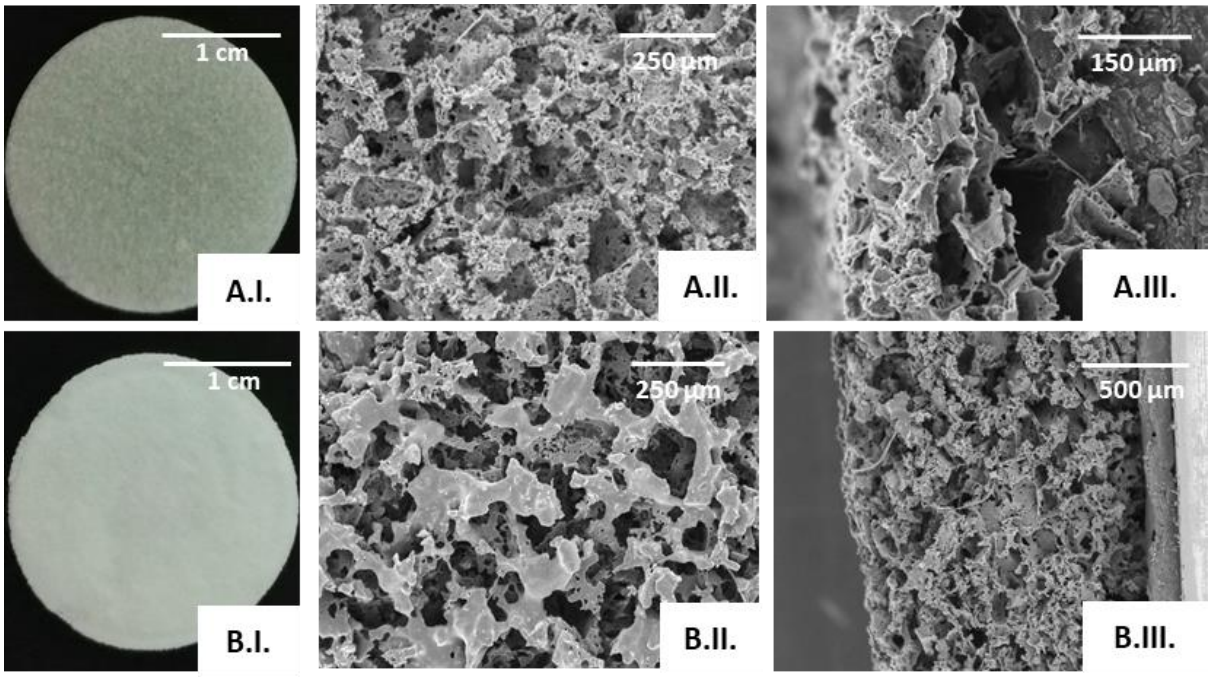

Figure 3.7 - P(3HB) (A) and P(3HB-co-3HV-co-3HHx) (B) scaffolds obtained by the hot-pressing salt leaching method macroscopic appearance (I) and SEM images of the surface amplified 150× (II) and cross-section amplified 300× for P(3HB) and amplified 80× for P(3HB-co-3HV-co-3HHx) (III).

Meanwhile, P(3HB-co-3HV-co-3HHx) porous scaffolds obtained by the hot-pressing salt leaching method were white, opaque and had a homogeneous rough surface (Figure 3.7 B.I.). This white appearance resembled the P(3HB-co-3HV-co-3HHx) scaffold previously obtained by the emulsion templating technique. The material thickness ranged from 600 to 700 µm and

were brittle with less flexibility when handled than the terpolymer's films and scaffolds achieved before. The surface SEM images showed a highly porous structure with interconnective porosity (Figure 3.7 B.II.), resembling what was observed by the P(3HB) hot-pressing scaffolds. This morphology was quite different from the structures obtained previously with the solvent casting and emulsion templating strategies for both PHA polymers. The cross-section SEM images (Figure 3.7 B.III.) revealed the presence of high pore density throughout the whole thickness of the material (with pores of varied sizes and interconnected). This was similar to the previously obtained for the P(3HB) hot-pressing scaffold, and very distinct from the formerly achieved PHA structures. Structures with equivalent morphological aspect have been reported for P(3HB-co-4HB) obtained by solvent casting (Ryltseva et al., 2023), for P(3HB), P(3HB-co-3HV) and PCL materials obtained by solvent casting salt leaching (Phuegyod et al., 2023), porous scaffold from a blend of 50% P(3HB-co-3HHx) and 50% of PCL (De Carvalho et al., 2023). P(3HB-co-3HV-co-3HHx) porous structures attained with the hot-pressing salt leaching process reached a porosity of 87.1%. This value was higher than the one obtained for the P(3HB) polymer using the same scaffold production method (67.7%). When compared with the porosity achieved for the PHA structures from the emulsion templating technique, this value was similar to the one reached by P(3HB) (82.2%) and higher than porosity of the porous structure of P(3HB-co-3HV-co-3HHx) (49.8%). Highly porous scaffolds have been previously reported for structures obtained with electrospinning with P(3HB) (85%) (Rodríguez-Tobías et al., 2016), PCL with gelatin from fish skin cross linked with GTA (90%), PCL with chitosan (90%) and gelatin with GTA (90%) (Gomes et al., 2017). Similar values were also obtained with scaffolds of P(3HB-co-3HV) (90%) obtained by the solvent casting salt leaching method (Phuegyod et al., 2023), of keratin/alginate sponges (93.5%) (Tiwari et al., 2023), and 3D printed structures of PU, triethanolamine and hydroxyapatite ranging from 80% to 90% of porosity for bone tissue engineering applications (T. Zhang et al., 2023). These porosity results suggest the presence of correlation between the fragility of a scaffold and its porosity. In both PHA polymers, when the value of porosity increased, the produced structures were apparently more brittle and fragile, non-depending on the strategy used. This was expected since the presence of pores and holes in structured materials create less dense scaffolds making them more vulnerable to mechanical stress.

Similarly to what was described for the emulsion templated scaffolds, the hot-pressing salt leaching structures could also be great candidates for fibroblast culture. Their porosity (67.7% and 87.1%) and pore interconnectivity could offer cells the opportunity to freely migrate and populate the whole scaffold volume, while exchanging nutrients for their adequate metabolic environment (Vieira et al., 2019). These structures had distinct porosities that were within the values reported for scaffolds suitable for cellular cultivation (from 60% to 90%) (Choi et al., 2018; Khan et al., 2023).

3.4.3.2 Adhesion and Proliferation Assay

The ability of P(3HB) and P(3HB-co-3HV-co-3HHx) hot-pressing salt leaching scaffolds to support fibroblast (HFFF2) adhesion and proliferation was assessed using the same procedure as for the emulsion templating porous structures. Through the observation of Figure 3.8 (blue column), it is visible that, when compared to the control, both PHA scaffolds had statistically lower adhesion rates, around 40% for P(3HB) and about 25% for P(3HB-co-3HV-co-3HHx) structures. These were slightly lower values comparing to the ones attained by the same polymers with the emulsion templating technique, 46% and 29%, respectively. Similar adhesion rates were observed previously in a bilayer scaffold of bacterial cellulose and PVA (ranging from 45% to 110%) seeded with fibroblast (NIH 3T3) (Khan et al., 2023).

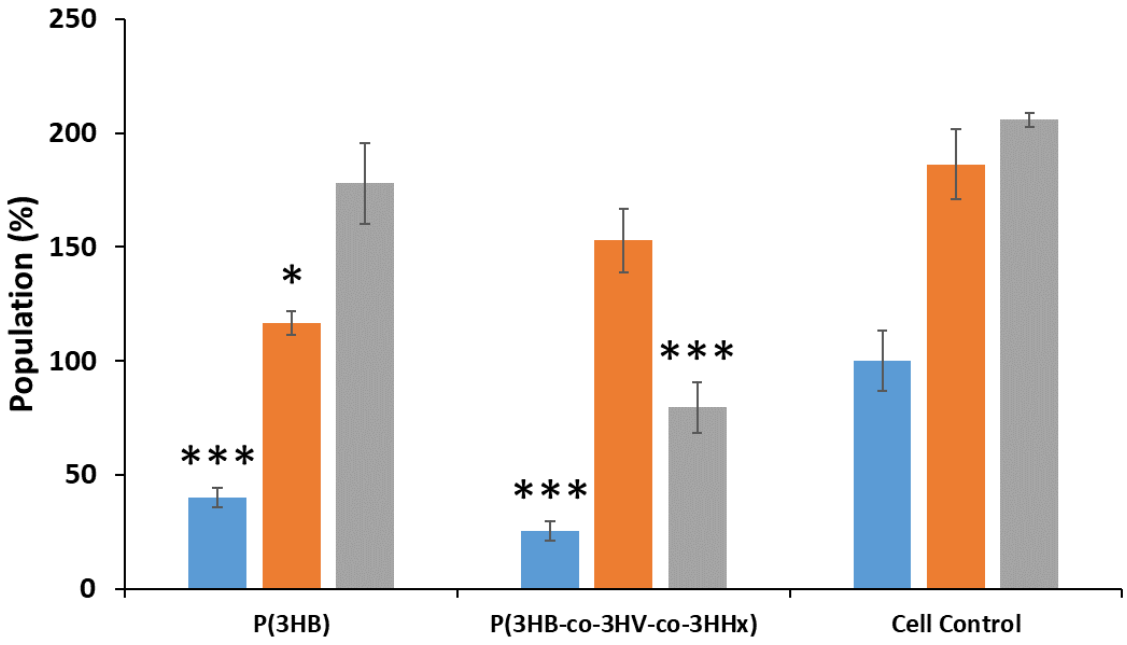

Figure 3.8 - Fibroblasts (HFFF2) relative cell population. Cells were seeded on P(3HB) and P(3HB-co-3HV-co-3HHx) porous scaffolds obtained with the hot-pressing salt leaching method and TCP wells (CC) and assayed with resazurin after 1 (BLUE), 4 (ORANGE) and 7 (GREY) days of culture. Vertical lines represent the standard deviation of the mean. Statistical differences between the samples and the cell control were assessed through a one-way ANOVA with Bonferroni's multiple comparison test (where, * $p \leq 0.05$; ** $p \leq 0.01$; *** $p \leq 0.001$).

After 4 days, HFFF2 cells had populated both PHA structures, but on opposite of what was observed in the emulsion templated scaffolds, P(3HB-co-3HV-co-3HHx) porous material reached higher population value than P(3HB) polymer, 156% and 117%, respectively. In these PHA scaffolds it is also possible to see the same behaviour as reported previously by the emulsion templating technique where the differences in cellular proliferation (after 4 days) between PHA polymers and cell control were less significant than differences observed regarding cell adhesion ratios. After 7 days of fibroblast culture, it was observed further HFFF2 proliferation in the P(3HB) scaffolds (178%), however, for P(3HB-co-3HV-co-3HHx) structures cell population significantly decreased (79%). When compared with the cell control (205%), it is visible that P(3HB) structures had a statistically similar behaviour to the TCP, while P(3HB-co-3HV-co-3HHx) scaffolds revealed to have a significantly lower population. This reduction in cell population might be explained by the thickness and 3D architecture of the P(3HB-co-3HV-co-3HHx) porous structure. Since this scaffold was thicker than the previously PHA matrices it could difficult the cell's access to nutrients throughout the whole scaffold's volume, especially in deeper parts of the structure (Choi et al., 2018; Khan et al., 2023). Moreover, smaller pores found within the structure could also be an explanation for why cells were able to adhere on the scaffold's surface and proliferate after 4 days. If pore size is reduced inside P(3HB-co-3HV-co-3HHx) porous structure, cells could migrate through scaffold and proliferate freely, but only until they reach a pore size threshold limit (Choi et al., 2018; Khan et al., 2023).

Fibroblast adhesion capacity and shape are regulated by focal adhesions mediated by integrins, transmembrane proteins that connect the scaffold and/or extracellular matrix (ECM) to the actin cytoskeleton (Khalili & Ahmad, 2015). Small connections points in the scaffold's matrix (< 1 µm) could limit the size, number, and location of focal adhesions, limiting cellular spreading throughout the scaffold (Vieira et al., 2019). The number of integrin binding domains are possibly different in all the PHA scaffolds obtained in this work, probably due to their distinct porosity and surface area, which might explain the diverse cell adhesion and proliferation values observed in the structures attained by the two strategies. Analogous proliferation profiles

were observed previously for P(3HB-co-3HV) scaffolds obtained by electrospinning seeded with fibroblasts (NIH 3T3) (Kaniuk et al., 2020), PCL, chitosan with gelatin from fish skin cross-linked with GTA structures seeded with HFFF2 (Gomes et al., 2017) and for a bilayer material of bacterial cellulose with PVA obtained by electrospinning and seeded with fibroblast (NIH 3T3) (Khan et al., 2023).

3.4.4 Comparison of adhesion and proliferation results for both emulsion templated and hot-pressing salt leaching scaffolds

The adhesion and proliferation results for the porous structures produced with P(3HB) and P(3HB-co-3HV-co-3HHx) polymers using the two different strategies had distinct results. In Figure 3.9, it is possible to observe the fibroblast population values from all the previously obtained PHA scaffolds. It also stays clear that the adhesion to the P(3HB) scaffolds was higher than for structures produced with P(3HB-co-3HV-co-3HHx). However, after 4 days, the homopolymer emulsion templated scaffold still had the highest cell population, but this value was similar when compared with the one produced by hot-pressing salt leaching with PHA terpolymer. After 7 days of cell cultivation, it is possible to see that (P3HB) polymeric scaffolds had higher cell population values than P(3HB-co-3HV-co-3HHx) porous structures (Figure 3.9). This could be explained by the higher adhesion results showed by the homopolymer in both strategies. P(3HB) emulsion templated scaffold supported a significantly higher proliferation after 7 days than all the other structures. In general, P(3HB) sustained higher adhesion and proliferation rates (after 1 and 7 days, respectively) when compared with P(3HB-co-3HV-co-3HHx) polymer, and emulsion templated scaffolds showed to have superior cell population when compared with hot-pressing salt leaching porous structures. Nevertheless, further improvement could still be done on the structures achieved with both strategies regarding their surface composition, roughness, and hydrophilicity to enhance its ability to support fibroblast adhesion, proliferation, and migration.

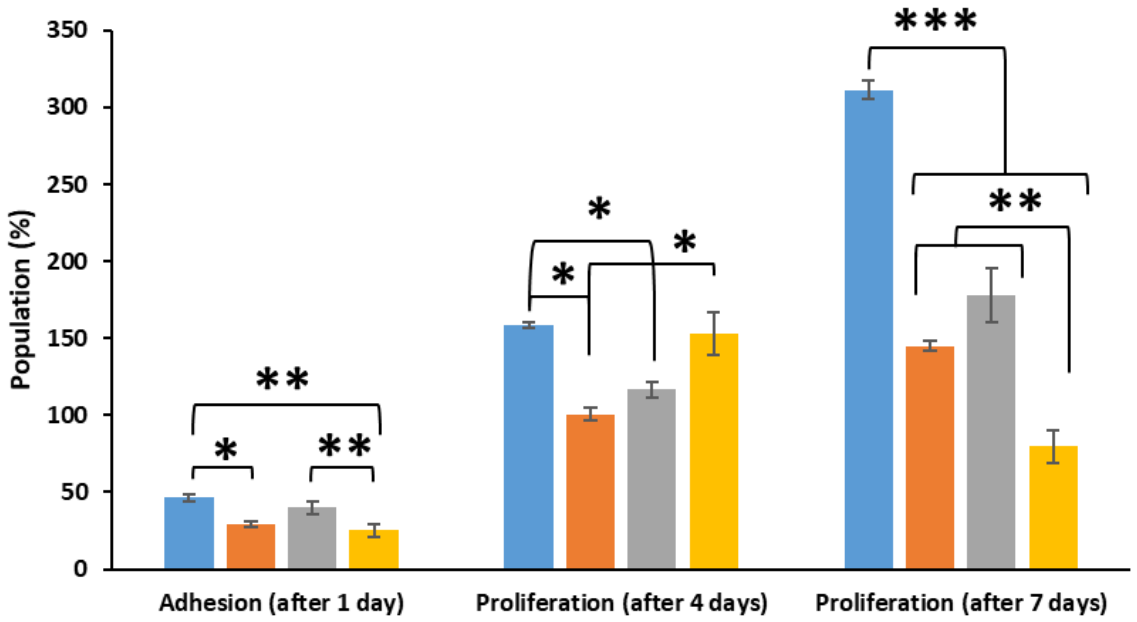

Figure 3.9 - Fibroblasts (HFFF2) relative cell population. Cells were seeded on PHA porous scaffolds obtained with the emulsion templating technique (P(3HB) in (BLUE) and P(3HB-co-3HV-co-3HHx) in (ORANGE) and hot-pressing salt leaching method (P(3HB) in (GREY) and P(3HB-co-3HV-co-3HHx) in (YELLOW), assayed with resazurin after 1, 4 and 7 days of culture. Vertical lines represent the standard deviation of the mean. Statistical differences between the samples were assessed through a one-way ANOVA with Bonferroni's multiple comparison test (where, * $p \leq 0.05$; ** $p \leq 0.01$; *** $p \leq 0.001$).

3.5 Conclusions

The intrinsic non-cytotoxic behaviour of the PHA polymers (P(3HB), P(3HB-co-3HV-co-3HHx) and mcl-PHA) provides a unique opportunity to develop materials for wound management applications. In this study, films were prepared from all the PHA polymers. Additionally, it was possible to obtain porous structured materials using PHA polymers, (P(3HB) and P(3HB-co-3HV-co-3HHx)), with two different strategies: the emulsion templated technique and the hot-pressing salt leaching method. Generally, the porous structures achieved by these procedures were macroscopically white and opaque, with thicknesses ranging from 160 to 700 µm, and porosity values from 49.8 to 87.1%, which are within the ranges reported for other scaffolds used in tissue engineering applications (De la Ossa et al., 2022; Gomes et al., 2017; Rodríguez-Tobías et al., 2016). Through the observation of the SEM images and the porosity results it stays clear that all the PHA scaffolds possessed pores of different sizes on their surface and cross section, where the highest pore densities were obtained for the emulsion templated structure of P(3HB) polymer (82.2%) and for the hot-pressing salt leaching scaffold of P(3HB-co-3HV-co-3HHx) polyester (87.1%).

The resulting PHA scaffolds showed to be able to support fibroblast adhesion and proliferation. Some of these porous structures had interconnected pores that allow cells to freely migrate and proliferate throughout the whole scaffold, while providing them with a correct exchange of nutrients to promote an appropriate metabolic environment. The adhesion values obtained for all the PHA structures were always lower when compared with the cell control (from 25% to 46%). All porous materials had lower proliferation values than the TCP, except for P(3HB) emulsion templated scaffold that achieved higher fibroblast population, after 7 days of cell cultivation (311%). In general, P(3HB) scaffolds also had higher proliferation values than P(3HB-co-3HV-co-3HHx) structures. When comparing both strategies, the emulsion templated structures attained higher cell populations after 7 days, than the hot-pressing salt leaching scaffolds. P(3HB) showed to be the most promising PHA to be used in wound dressing applications.

These results prove that the PHA scaffolds obtained with these two strategies are suitable for fibroblast cultivation. However, they need to be further improved to reach population values equal or even greater than the cell control. The addition of a biological active component

(such as, FucoPol) could enhance the bioactive properties of the PHA scaffolds, improving adhesion and proliferation, to achieve a reliable tissue engineering material for wound management applications.

4

DEVELOPMENT OF ACTIVE WOUND DRESSINGS

The contents presented in this chapter are partly included in the publication "Pereira, J. R., Rafael, A. M., Esmail, A., Morais, M., Matos, M., Marques, A. C., Reis, M. A. M., & Freitas, F. (2023). Preparation of Porous Scaffold Based on Poly(3-hydroxybutyrate-co-3-hydroxyvalerate-co-3-hydroxyhexanoate) and FucoPol. *Polymers*, *15*(13), 2945. https://doi.org/10.3390/polym15132945".

4.1 Summary

FucoPol is an amorphous, high molecular weight polysaccharide rich in Fucose. This biopolymer possesses a variety of distinctive properties, including the ability to form, films/hydrogels, provide UV protection, offer cryoprotection, act as flocculating agent, and function as thickener and as an emulsifier. FucoPol is also known to promote the *in vitro* migration of keratinocytes, which envisages its use for wound management applications. The intrinsic emulsifier capacity and skin regeneration potential of FucoPol are important properties that could improve the biological activity of porous PHA structures. The addition of this polysaccharide to PHA scaffolds could result in a hybrid material with enhanced bioactive properties suitable for wound management applications. Therefore, in this chapter, FucoPol was used with two different purposes: first, to stabilize the emulsion (of the PHA solution and water) during the solvent evaporation process when using the emulsion templating technique and, second, to improve the biological activity of the PHA porous scaffold achieved by the hot-pressing salt leaching method. In this last technique, FucoPol was added within the PHA structure through a jellification process with the help of an iron chloride solution. The resulting scaffolds were subsquently assessed for their morphology, porosity, and ability to facilitate the adhesion and proliferation of fibroblasts. The inclusion of FucoPol in the 3D scaffolds demonstrated an enhancement in fibroblast proliferation after 7 days for P(3HB) and P(3HB-co-3HV-3HHx) porous structures obtained by both strategies. It also stayed clear that the most promising strategy to obtain porous PHA scaffolds was the emulsion templating technique, mainly due to the biological properties achieved by these structures. When comparing the same PHA polymer, fibroblast proliferation values (after 7 days) achieved by the emulsion templated scaffolds were always higher than the hot-pressing salt leaching porous structures. It was also visible that P(3HB) scaffolds generally had higher fibroblast proliferation values after 7 days than porous structures produced with P(3HB-co-3HV-3HHx). Given this, the most promising candidates to be used in wound healing applications were the emulsion templated scaffolds achieved by P(3HB) with and without the presence of FucoPol.

4.2 Introduction

Emulsion systems are inherently unstable, often requiring the addition of surfactants to improve their stability (Akbari & Nour, 2018). Usually, the surfactants used in emulsion-templating techniques are either synthetic terpolymers (such as poly(ethyleneoxide) (PEO) and poly(propyleneoxide) (PPO)) or high hydrophile-lipophile molecules (for instance, Triton X-405 and Span 80 (sorbitan monooleate)) (Kimmins & Cameron, 2011). However, for tissue engineering applications, the presence of surfactants on the material can be a major issue due to their non-biodegradability, possible toxicity, and the possibility that they could induce allergic reactions when in contact with human skin (Bouyer et al., 2012), a step that can make the technique quite laborious and expensive, together with the surfactants' cost (Aldemir Dikici & Claeyssens, 2020; T. Zhang et al., 2019). Therefore, the utilization of natural biodegradable and biocompatible surfactants, such as polysaccharides, could be a major step towards the development of new materials for tissue engineering applications. Dextran has already been studied as an emulsifier agent in water-in-chloroform emulsions (Carrier et al., 2011), although the emulsions could not maintain their droplet size and stability for a long time. Another example was the use of arabic and xanthan gums for stabilization of chloroform-in-water emulsions; however, the produced emulsions lacked physico-chemical stability (Anarjan & Ping Tan, 2013). More recently, the emulsifying ability of a novel EPS produced by *Haloferax mucosum* (DSM 27191) was demonstrated in the stabilization emulsions of water and nonpolar solvents such as chloroform and n-hexane (López-Ortega et al., 2020).

FucoPol, among its various properties, has demonstrated film-forming capacity and emulsifying ability (Baptista, Pereira, et al., 2022; Concórdio-Reis, Pereira, et al., 2020). Moreover, FucoPol was shown to be non-cytotoxic towards various cell lines, including human skin keratinocytes and fibroblasts (Concórdio-Reis, Pereira, et al., 2020; Guerreiro et al., 2020), more specifically, FucoPol demonstrated to promote *in vitro* migration of keratinocytes, suggesting its use for wound dressing applications (Concórdio-Reis, Pereira, et al., 2020). Given this, the addition of FucoPol to the previously used methods could assist the emulsion templating technique into achieving better structural scaffolds. Also, given the polyanionic character of FucoPol it is possible to form gel structures through physical crosslinking via electrostatic interaction with cations (i.e. Fe^{3+} and Cu^{2+}) (Araújo et al., 2023). This procedure could be used to add

FucoPol to the previously obtained structures with the hot-pressing salt leaching method. The presence of this polysaccharide might further increase the biological activity of these scaffolds.

Therefore, in this chapter the main goal was to add FucoPol to the previously developed porous PHA scaffolds (P(3HB) and P(3HB-co-3HV-co-3HHx)) to improve their biological activity. Either by stabilizing the emulsion (of the PHA solution and water) during the solvent evaporation process (in the emulsion templating technique) or by adding FucoPol within the PHA structure through a jellification process (in the hot-pressing salt leaching method). The obtained scaffolds were then characterized in terms of their morphology, porosity, and ability to harbour fibroblasts adhesion and proliferation.

4.3 Materials and Methods

4.3.1 Active Wound Dressings

4.3.1.1 Emulsion Templating with FucoPol as Bioemulsifier

The P(3HB):FucoPol and P(3HB-co-3HV-co-3HHx):FucoPol scaffolds were prepared by emulsifying the PHA chloroform solutions with an aqueous FucoPol solution. P(3HB) and P(3HB-co-3HV-co-3HHx) were dissolved in chloroform at concentrations of 4% and 6.7% (w/v), respectively. FucoPol was dissolved in deionized water at a concentration of 0.1% (w/v). The P(3HB) and P(3HB-co-3HV-co-3HHx) solutions (10 mL) were mixed with 1 mL of the FucoPol solution, and the mixtures were stirred with a magnetic stirrer until an emulsion formed (±1 hour), with no visible phase separation. The resulting emulsions were then transferred to 5 cm Petri dishes and left in the fume hood inside a desiccator, at room temperature, until complete solvent (water and chloroform) evaporation (Figure 4.1). The biopolymers were kept at room temperature in a closed glass petri dish until use.

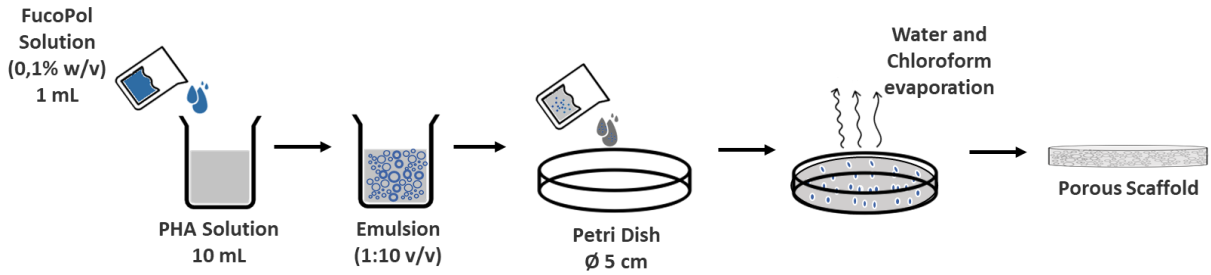

Figure 4.1 - Schematic representation of the emulsion templating technique to attain porous scaffolds with FucoPol. Adapted from (Esmail, Pereira, Sevrin, et al., 2021).

4.3.1.2 Hot-Pressing Salt Leaching Scaffolds Impregnated with Jellified FucoPol

To obtain porous scaffolds through the hot-pressing method with jellified FucoPol, first the same method previously described In Chapter 3, section 3.3.2.2. was used to prepare a porous scaffold. Afterwards, FucoPol was crosslinked by the cation mediated gelation method described by (Araújo et al., 2023). Briefly, the formerly produced porous PHA scaffolds (P3(HB) and P(3HB-co-3HV-co-3HHx)) were submerged in 50 mL of FucoPol solution (1%, w/v) at room temperature for 24 h and then soaked in 50 mL of a $FeCl_3 \cdot 6H_2O$ (98%, Sigma-Aldrich, USA) solution (with a concentration of Fe^{3+} of 1.5 g/L) also at room temperature but only for 2 h.

The obtained structures were washed with deionized water until a constant conductivity was achieved (± 1 µS/cm). After this step, the PHA with jellified FucoPol material was accomplished (Figure 4.2).

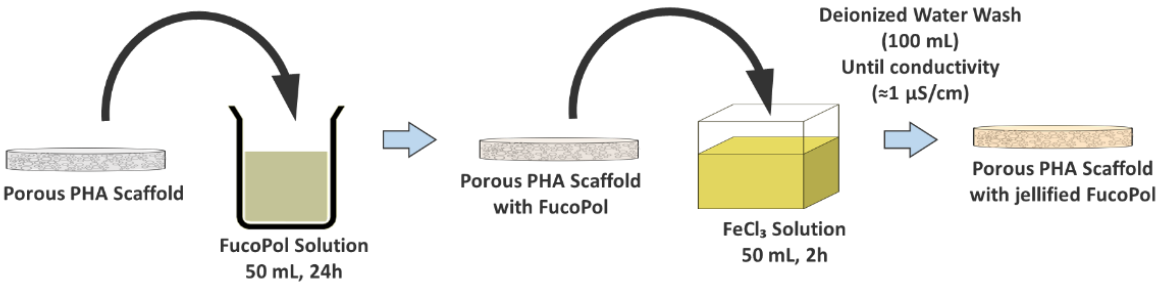

Figure 4.2 - Schematic representation of the impregnation of FucoPol on PHA scaffolds through the FucoPol jellification process.

4.3.2 Morphological Characterization

4.3.2.1 Scanning Electron Microscopy

For the scanning electron microscopy (SEM) analysis, the samples obtained hot-pressing salt leaching scaffolds with jellified FucoPol were freeze dried for water removal and then processed with the remain samples according to what was described previously in Chapter 3 - Section 3.3.3.1 of this dissertation.

4.3.2.2 Porosity Measurements

The samples porosity was assessed by mercury porosimetry as described previously in Chapter 3 - Section 3.3.3.2 of this dissertation.

4.3.3 Cell Testing

4.3.3.1 Cell culture and Media

The fibroblast cells and culture media used in this section were the same as described before in Chapter 3 - Section 3.3.4.1 of this dissertation (Appendix C.1).

4.3.3.2 Adhesion and Proliferation Assay

The adhesion and proliferation of HFFF2 cells were assessed using the same procedure as described earlier in Chapter 3 - Section 3.3.4.2 of this dissertation (Appendix C.2, Appendix C.3 and Appendix C.4).

4.4 Results and Discussion

4.4.1 Active Wound Dressings

4.4.1.1 Emulsion templated scaffolds obtained by emulsification with FucoPol

Aiming to improve the emulsions' stability during the solvent evaporation process and consequently enhance the scaffolds biological properties, FucoPol was used as a bioemulsifier. To attain this, during the emulsion process P(3HB) or a P(3HB-co-3HV-co-3HHx) solutions (4% and 6.7% w/v, respectively) in the organic phase were used, and mixed with a FucoPol solution as the aqueous phase (0.1%, w/v). The obtained emulsions showed no phase separation during the whole solvent evaporation process indicating their stability. This procedure resulted in porous PHA (P(3HB) or P(3HB-co-3HV-co-3HHx)) scaffolds with distinct porosities.

4.4.1.1.1 Morphology

The P(3HB):FucoPol porous scaffolds achieved by the emulsion templating method were slightly heterogeneous, had an opaque white colour (Figure 4.3 A.I.) with a thickness around 215 µm. The structures were rigid when handled and very similar to those obtained previously for P(3HB) polymer with the same technique. However, the P(3HB):FucoPol scaffolds were apparently more flexible and less brittle. Through the observation of SEM images, it stays clear that the scaffolds had a rough surface (Figure 4.3 A.II.), similar to the homopolymer emulsion templated scaffolds, with visible microporosity. The cross-section images, on the other hand, showed the presence of large pores, involving the whole scaffold thickness (Figure 4.3A.III.). The morphological aspect of these scaffold was completely different from the previously obtained films and porous structures of P(3HB) and P(3HB-co-3HV-co-3HHx) by either solvent casting, emulsion templating or hot-pressing salt-leaching methods. Similar morphological structures were reported for scaffolds of P(3HB) obtained by solvent casting salt leaching technique (Puppi et al., 2019) and for porous materials of hydroxyethyl-methacrylate with halloysite nanotubes/thymol (Cesarino et al., 2024). This scaffold displayed a porosity of 65.1%, when compared with the previously attained emulsion templated porous structures this value was lower for P(3HB) homopolymer (82.2%), but still higher when using P(3HB-co-3HV-co-3HHx) (49.8%). This porosity value is similar to the one obtained with the hot-pressing salt-leaching

method for P(3HB) (67.7%). Similar porosity values have been reported for P(3HB-co-3HV) with olive leaf extract obtained by electrospinning (63.3%) (De la Ossa et al., 2022), PCL gels (65%) (Tiwari et al., 2023), and PLA scaffolds produced with 3D printing and gas foaming method (ranging from 57% to 70%) (Ambekar & Kandasubramanian, 2019).

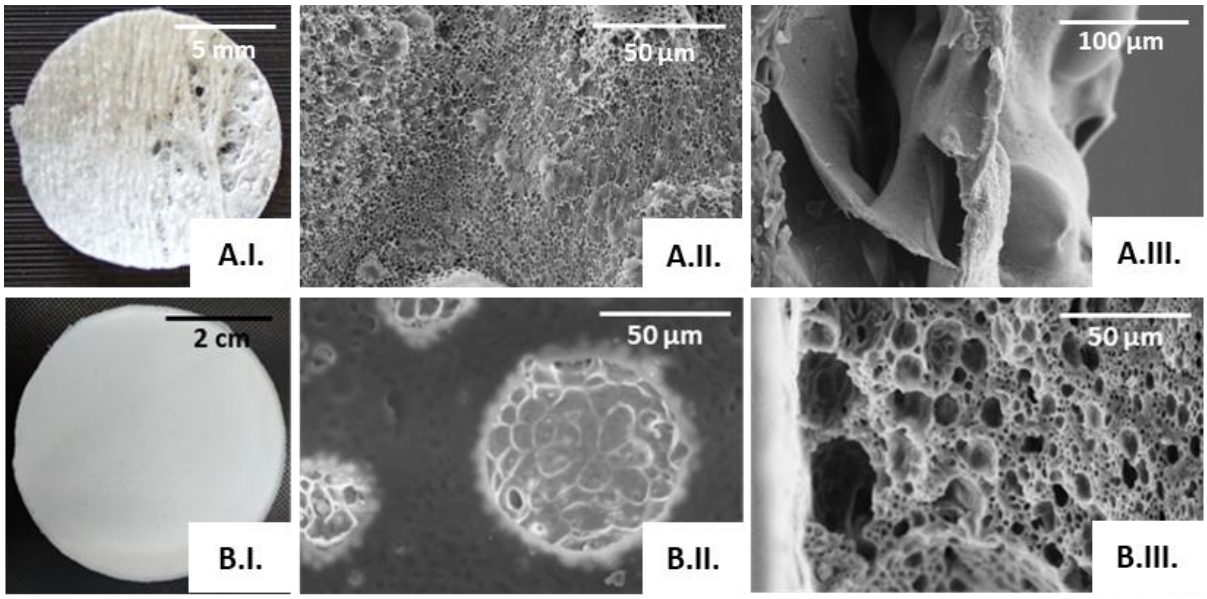

Figure 4.3 - P(3HB) (A) and P(3HB-co-3HV-co-3HHx) (B) scaffolds attained by the emulsion templating technique with FucoPol at 0.1% macroscopic appearance (I) and SEM images of the surface amplified 1000× (II) and cross-section amplified 500× for P(3HB) and 1000× for P(3HB-co-3HV-co-3HHx) (III).

The porous P(3HB-co-3HV-co-3HHx):FucoPol scaffolds were white and opaque, with an homogeneous mostly smooth surface (Figure 4.3 B.I.). They presented a thickness around 145 µm and were less flexible when handling, compared to the terpolymer's porous scaffolds attained with the emulsion templating strategy. The surface SEM image (Figure 4.3 B.II.) showed the presence of different sized pores, with visible interconnectivity, similarly to what was observed by the terpolymer's emulsion templated scaffold. In the cross-section images, pores with different diameters decreasing in size along the thickness of the scaffold were also perceivable (Figure 4.3 B.III.), which resembled the porous PHA structures achieved with the emulsion strategy. Due to the presence of FucoPol in the dispersed phase, the solutions displayed a higher viscosity when compared with water, which may have led to a small coalescent effect of the internal phase of the emulsion resulting in larger pores close to the scaffold's surface (Figure 4.3 B.III.), and smaller pores at the bottom (Figure 4.3 B.III.), this could also be explained by the lack of emulsion stability during the solvent evaporation process. Scaffolds with equivalent

morphological properties have been reported for P(3HB-co-3HV) with 5% of poly(ethylene glycol) (PEG) (Tomietto et al., 2020), for poly(dimethylsiloxane)(PDMS) and PCL structures obtained by the emulsion templating technique (Riesco et al., 2019; Yadav et al., 2019). The porosity of P(3HB-co-3HV-co-3HHx):FucoPol structures was 41.7%, which was the lowest value when compared with all the previously obtained PHA scaffolds (with and without FucoPol). The presence of FucoPol in the dispersed phase led to an evident decrease in porosity. This behaviour was also observed for the P(3HB) polymer. Similar porosities have been reported for P(3HB-co-3HV) porous structure produced with selective laser sintering (46%) (Patel et al., 2024) and for PLA produced by electrospinning (40.6%) for tissue engineering applications (Solarz et al., 2023).

4.4.1.1.2 Adhesion and Proliferation Assay

The ability of P(3HB):FucoPol and P(3HB-co-3HV-co-3HHx):FucoPol emulsion templated scaffolds to support fibroblast (HFFF2) adhesion and proliferation was assessed following the same procedure used in previously in Chapter 3. Briefly, cells were seeded over the surface of the scaffolds and TCP wells (cell control) and their viability evaluated through the resazurin colorimetric assay. After 1 day of seeding, it was possible to estimate cellular adhesion and in the following days 4 and 7, proliferation was assessed. In Figure 4.4 (blue columns) it is visible that the adhesion results obtained for the PHA emulsion templated scaffolds (with and without the use of FucoPol) were similar for both structures (around 40%), but significantly lower than the cell control. It is also visible a slightly increase in cellular adhesion of the P(3HB-co-3HV-co-3HHx) porous structure when FucoPol was used (from 29% to 39 %). Similar adhesion rates (around 50%) were obtained by PCL (56%) (Querido et al., 2022) and PCL with chitosan (ranging from 32% to 48%) (Gomes et al., 2017; Querido et al., 2022) scaffolds produced by electrospinning and seeded with HFFF2.

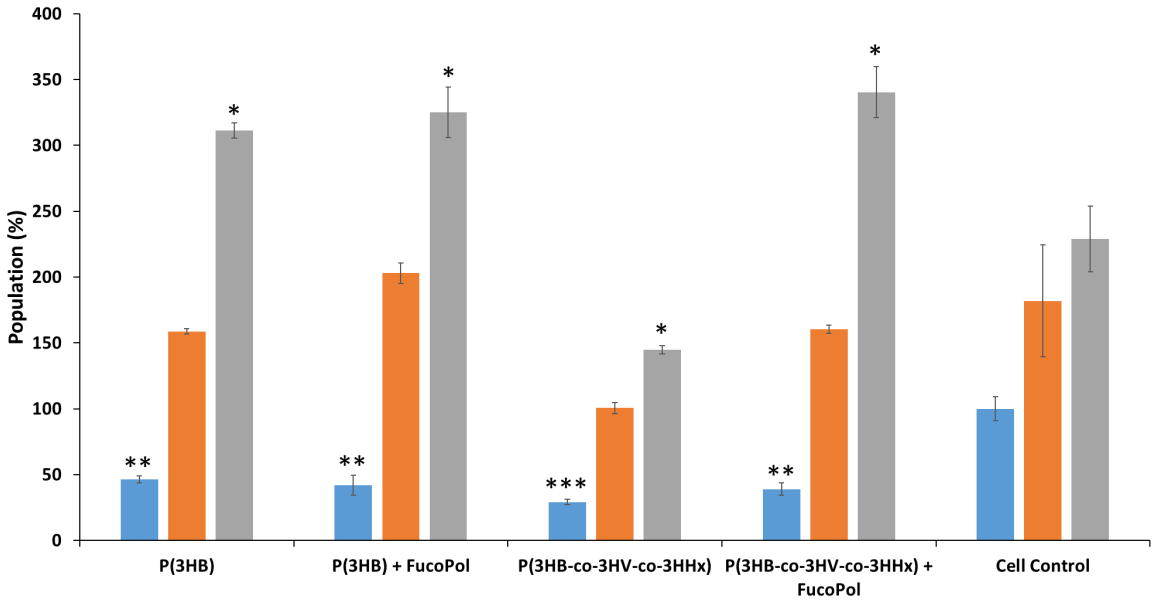

Figure 4.4 - Fibroblasts (HFFF2) relative cell population. Cells were seeded on P(3HB) and P(3HB-co-3HV-co-3HHx) porous scaffolds with and without FucoPol obtained with the emulsion templating technique and TCP wells (CC) and assayed with resazurin after 1 (BLUE), 4 (ORANGE) and 7 (GREY) days of culture. Vertical lines represent the standard deviation of the mean. Statistical differences between the samples and the cell control were assessed through a one-way ANOVA with Bonferroni's multiple comparison test (where, * $p \leq 0.05$; ** $p \leq 0.01$; *** $p \leq 0.001$).

Figure 4.4 illustrates a noticeable increase in fibroblast population after 4 days across all scaffolds, both with and without the inclusion of FucoPol. It is also clear that structures obtained using FucoPol exhibited higher proliferation rates within 4 days for both PHA polyesters compared to scaffolds achieved without the use of this EPS. These values increased from 159% to 203% and from 100% to 160% for P(3HB) and P(3HB-co-3HV-co-3HHx), respectively. Moreover, similarly to what was seen in Chapter 3 (in the absence of FucoPol), with the use of this EPS, the PHA homopolymer showed a higher cell population than the PHA terpolymer, also slightly higher than the cell control (182%). In addition, when compared to the TCP control after 4 days, the fibroblast proliferation for all the PHA scaffolds had no statistical differences. During the following days (until day 7), the HFFF2 cells continued to proliferate in all the PHA scaffolds, however, for P(3HB) structures obtained with FucoPol there was a slight increase in fibroblast population when compared to what was previously achieved (from 311% to 325%), but for P(3HB-co-3HV-co-3HHx) scaffolds produced with EPS there was a significantly increase in proliferation (from 145% to 340%), which was the highest result obtained for the emulsion templated scaffolds and statistically higher than the cell population achieved by the TCP control after 7 days. Similar proliferation profiles were observed previously for P(3HB-co-3HV)

scaffolds obtained by electrospinning seeded with fibroblasts (NIH 3T3) (Kaniuk et al., 2021) and PCL structures produced by electrospinning with gelatin from fish skin cross linked with GTA seeded with HFFF2 (Gomes et al., 2017).

In general, the adhesion values are similar between the structures produced with and without the addition of FucoPol, revealing a small impact of this EPS in these results. However, scaffolds obtained in the presence of FucoPol increased fibroblast population when compared to the ones prepared without this polysaccharide and these values were higher for both PHA polymers after 4 and 7 days (Figure 4.4). These results were somehow expected, since the presence of FucoPol was previously reported to be beneficial when in contact with different cell lines (Baptista et al., 2023; Concórdio-Reis, Pereira, et al., 2020; Guerreiro et al., 2020).

4.4.1.2 Hot-Pressing Salt Leaching Scaffolds with Jellified FucoPol

To improve the hot-pressing salt leaching scaffold's biological properties, FucoPol was added to these structures it is a bioactive polymer. To achieve this, the previously obtained P(3HB) and P(3HB-co-3HV-co-3HHx) scaffolds were submerged in a FucoPol solution (1%, w/v) for FucoPol impregnation within the PHA porous materials that were then soaked in $FeCl_3$ solution (with a concentration of Fe^{3+} of 1.5 g/L) to cause FucoPol crosslinking by cation mediated gelation within the scaffolds. The result were hybrid materials composed of either P(3HB) or P(3HB-co-3HV-co-3HHx) with jellified FucoPol.

4.4.1.2.1 Morphology

The porous P(3HB) scaffolds with jellified FucoPol were homogeneous, with a slightly orange opaque colour. These materials had an outside FucoPol layer with a rigid P(3HB) core. Figure 4.5 A.I. shows the dried structure before SEM analysis. It is visible that FucoPol detached from both top and bottom of the porous structure. Before SEM analysis the structures must be completely dry. After scaffold freeze drying, due to the physical properties and lack of interaction between P(3HB) and FucoPol, small sheets of the EPS polymer did not remain attached to the PHA porous structure (Figure 4.5 A.I.). This explains why in Figure 4.5 A.II. it is not possible to observe the presence of FucoPol on the scaffold's surface SEM image. Here, it is visible a slightly distinct structure when compared to what was observed previously for the P(3HB) hot-pressing salt leaching scaffold. However, in the cross-section SEM image (Figure 4.5 A.III.) it is perceivable the presence of small FucoPol sheets at the bottom of the scaffold embedded within the

P(3HB) porous structure. This confirms that this EPS was able to diffuse and jellify inside the PHA material, which could be crucial for improving cellular proliferation. Similarly, structures have been reported for P(3HB) scaffolds produced with tetrahydrofuran and chloroform obtained by non-solvent-induced phase separation (NIPS) (Kang et al., 2020) and the FucoPol sheets resembles the morphological aspect of jelly fig polysaccharide scaffolds produced for skin tissue engineering applications (Thangavel et al., 2024).

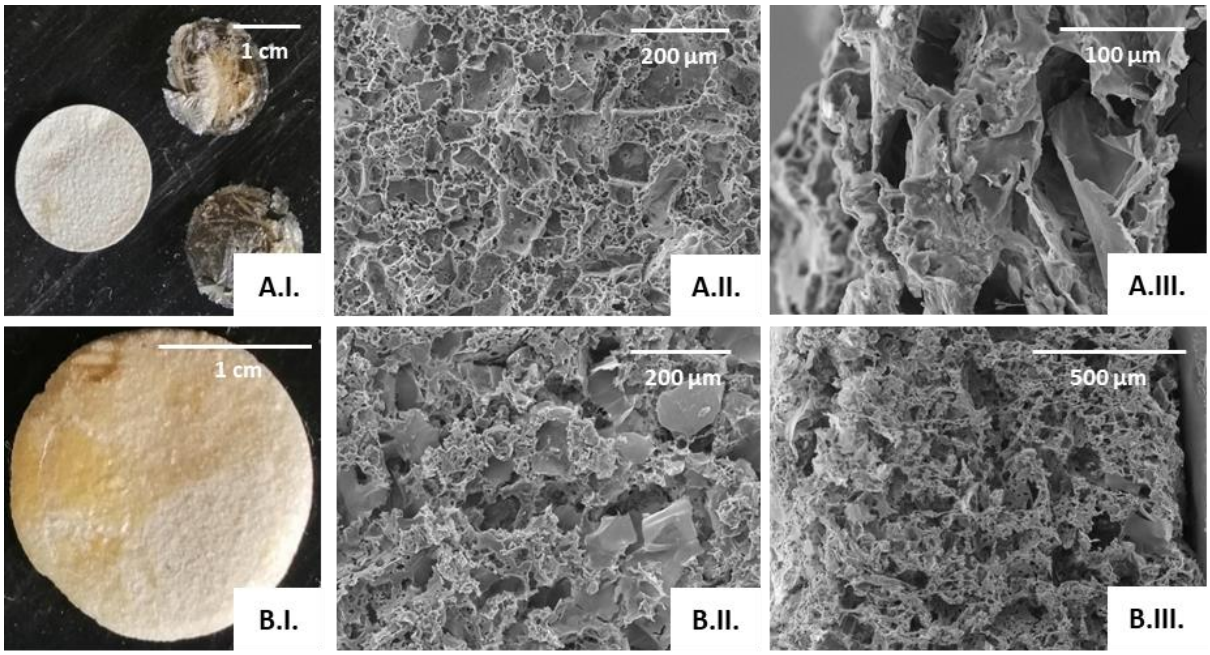

Figure 4.5 - P(3HB) (A) and P(3HB-co-3HV-co-3HHx) (B) scaffolds obtained by the hot-pressing salt leaching method with jellified FucoPol macroscopic appearance (I) and SEM images of the surface amplified 200×. (II) and cross-section amplified 500× for P(3HB) and amplified 120× for P(3HB-co-3HV-co-3HHx) (III).

On the other hand, P(3HB-co-3HV-co-3HHx):FucoPol porous scaffolds attained by the hot-pressing salt leaching method were slightly orange, completely opaque and had an homogeneous gel-like surface with a brittle and less rigid PHA core. Similar to what happen previously with the hybrid material of P(3HB) and FucoPol, this scaffold also needed to be freeze dried. This revealed that the surface of this structure was slightly rough (Figure 4.5 B.I.). However, on the opposite to what occurred with the homopolymer and EPS material, in P(3HB-co-3HV-co-3HHx) structure FucoPol was able to remain on the surface and bottom of the scaffold. Here, the high thickness of the structure (between 600 and 700 µm) could be an important property to ensure that FucoPol stays embedded within the structure during the freeze-drying step. The presence of the EPS polymer was visible to the naked eye due to its yellow/orange colour

(Figure 4.5 B.I.) and observable in the SEM images (Figure 4.5 B.II.), as small FucoPol sheets spread throughout the whole surface of the scaffold. By looking at the cross-section images of this hybrid material (Figure 4.5 B.III.), similar to what happened with the P(3HB) homopolymer and EPS, here it is also possible to detect minor segments of FucoPol present within the scaffold's thickness. Structures with equivalent morphological properties have been reported for scaffolds made from blends of 50% P(3HB) with 50% of PCL (De Carvalho et al., 2023), for collagen porous materials achieved by the freeze-drying technique (Kiany et al., 2024), for poly-L-lactic acid (PLLA) foams, and for PLLA porous structures with 10 %wt. of PHA, both obtained by direct quenching method (Lopresti et al., 2022).

4.4.1.2.2 Adhesion and Proliferation Assay

Fibroblasts viability was assessed through the same procedure as before. In Figure 4.6 (blue columns), it is possible to observe the adhesion results for P(3HB) and P(3HB-co-3HV-co-3HHx) hot-pressing salt leaching scaffolds (with and without the incorporation of FucoPol). When compared with the control, PHA hot-pressing salt leaching scaffolds had statistically lower adhesion rates. The fibroblast adhesion for P(3HB) structures with FucoPol were similar to those previously obtained for P(3HB) scaffolds without FucoPol (35% and 40%, respectively). The same behaviour was observed for P(3HB-co-3HV-co-3HHx) scaffolds where the values were also identical (a slight decrease from 25% to 27%). Similar adhesion rates (around 35%) were observed previously for PCL mats with chitosan flakes seeded with HFFF2 (Querido et al., 2022).

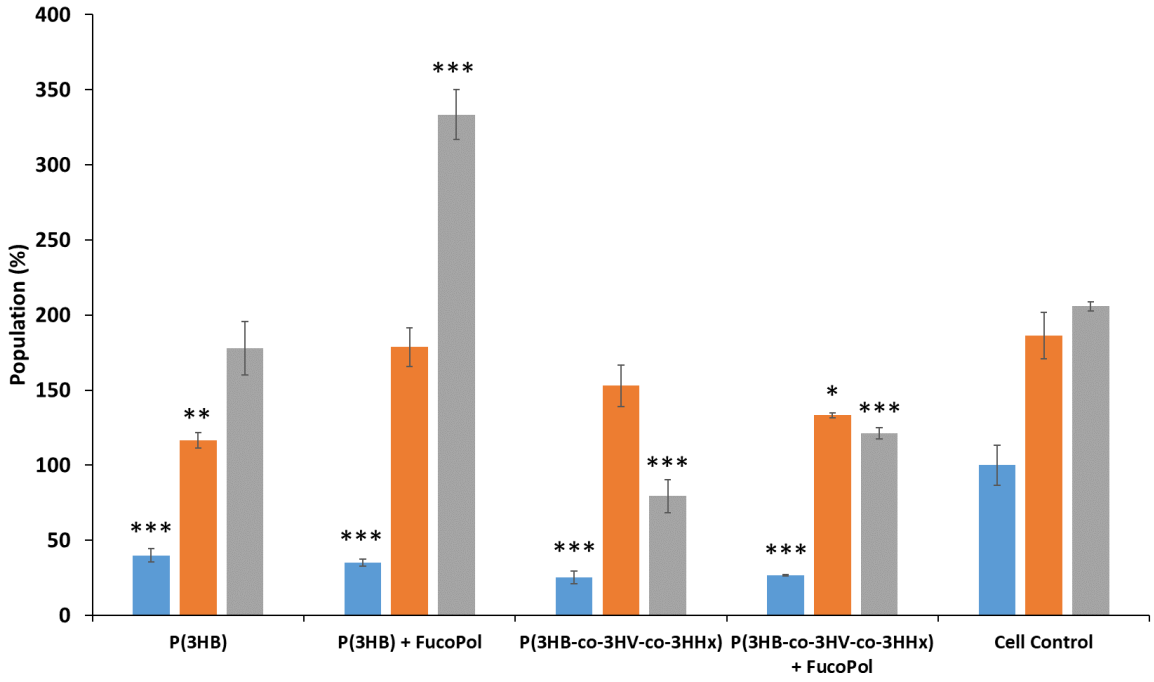

Figure 4.6 - Fibroblasts (HFFF2) relative cell population. Cells were seeded on P(3HB) and P(3HB-co-3HV-co-3HHx) porous scaffolds with and without FucoPol obtained with the hot-pressing salt leaching method and TCP wells (CC) and assayed with resazurin after 1 (BLUE), 4 (ORANGE) and 7 (GREY) days of culture. Vertical lines represent the standard deviation of the mean. Statistical differences between the samples and the cell control were assessed through a one-way ANOVA with Bonferroni's multiple comparison test (where, * $p \leq 0.05$; ** $p \leq 0.01$; *** $p \leq 0.001$).

After 4 days, the HFFF2 population on the P(3HB) scaffold with FucoPol was 179%, which was the highest value among the PHA hot-pressing salt leaching scaffolds, identical to that of the cell control (186%). The cell proliferation on P(3HB-co-3HV-co-3HHx) scaffolds was smaller in the presence of FucoPol (from 153% to 133%). Nevertheless, the differences of cellular proliferation (after 4 days) between PHA polymers and the cell control were much less significant than differences observed regarding cell adhesion ratios. After 7 days of fibroblast cultivation, a decrease in cell proliferation on P(3HB-co-3HV-co-3HHx) scaffolds with FucoPol was observed, this behaviour was very similar to what happened before without the presence of this EPS. However, for both PHA polymers the presence of FucoPol proved beneficial in attaining higher cell populations when compared with structures without the EPS, increasing from 178% to 333% for the P(3HB) homopolymer, and from 80% to 121% for the P(3HB-co-3HV-co-3HHx) terpolymer. The result achieved by the P(3HB) hot-pressing salt leaching scaffold surpassed the fibroblast proliferation attained by the cell control (206%). This value resembled the cell population that was reached by the emulsion templating structures with FucoPol for both

P(3HB) (325%) and P(3HB-co-3HV-co-3HHx) (340%). Analogous proliferation profiles were observed previously for collagen and P(3HB-co-4HB) scaffolds grown with HGF cells (Chen et al., 2023) and for P(3HB) blended with its functionalized oligomers in fibroblasts (NIH 3T3) (Boyandin et al., 2024).

4.4.1.3 Comparison of adhesion and proliferation results for both emulsion templated and hot-pressing salt leaching scaffolds with FucoPol

The adhesion and proliferation results for the P(3HB) and P(3HB-co-3HV-co-3HHx) scaffolds with FucoPol produced with the two different methods are presented in figure 4.7. Through the observation of the adhesion results, it is clear that all the PHA:FucoPol structures had very similar adhesion values with no statistically significant difference. However, after 4 days the scaffolds produced with the P(3HB) homopolymer revealed a higher proliferation when compared to the structures obtained with P(3HB-co-3HV-co-3HHx). At day 7 of HFFF2 cultivation, the scaffolds of the homopolymer with FucoPol achieved by both methods had similar cell population values when compared with the terpolymer porous structures produced only with the emulsion templating technique. This behaviour was seen earlier in Chapter 3, where P(3HB) scaffolds revealed to have a higher proliferation after 7 days than all the other structures, however, with the presence of FucoPol, P(3HB-co-3HV-co-3HHx) emulsion templated scaffold could significantly increase its fibroblast population reaching values close to what was attained for P(3HB) porous structures. In general, all the materials reported similar adhesion rates. Regarding fibroblast proliferation, only the P(3HB-co-3HV-co-3HHx):FucoPol attained with the hot-pressing salt leaching method supported a lower cell population when compared with the remaining scaffolds. It stays clear that the presence of FucoPol increased the cell population in the scaffolds especially for the structures produced with the P(3HB) homopolymer.

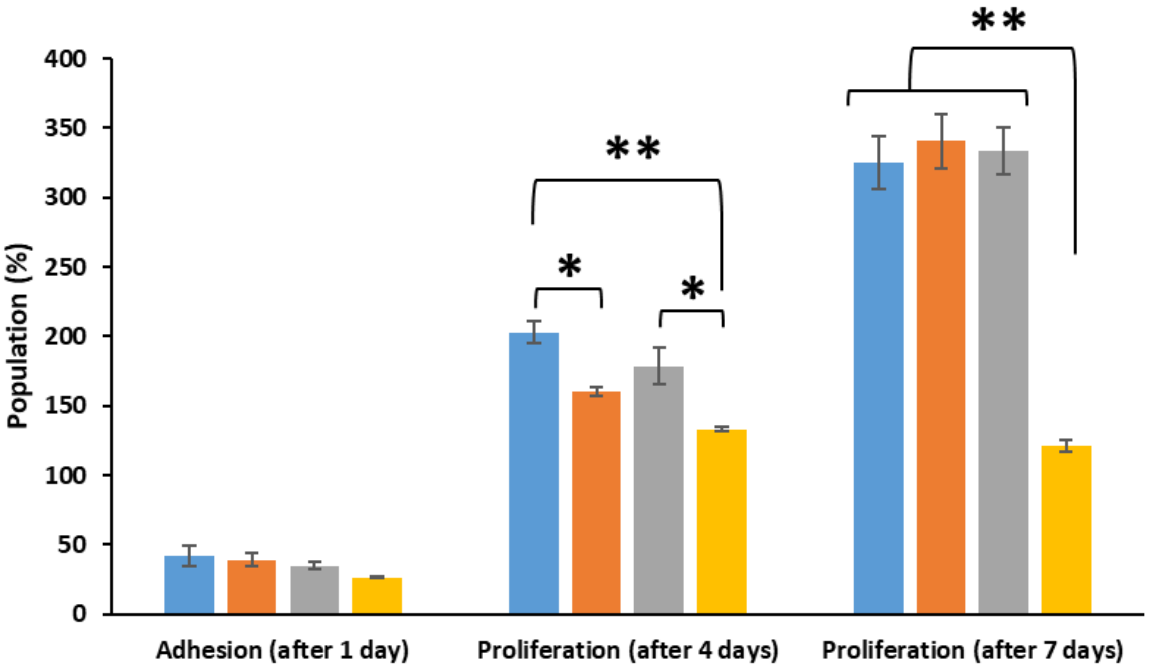

Figure 4.7 - Fibroblasts (HFFF2) relative cell population. Cells were seeded on PHA porous scaffolds obtained with the emulsion templating technique (P(3HB) in (BLUE) and P(3HB-co-3HV-co-3HHx) in (ORANGE) and hot-pressing salt leaching method (P(3HB) in (GREY) and P(3HB-co-3HV-co-3HHx) in (YELLOW) with FucoPol, assayed with resazurin after 1, 4 and 7 days of culture. Vertical lines represent the standard deviation of the mean. Statistical differences between the samples were assessed through a one-way ANOVA with Bonferroni's multiple comparison test (where, * $p \leq 0.05$; ** $p \leq 0.01$; *** $p \leq 0.001$).

4.5 Conclusions

PHA and FucoPol are very versatile materials with potential use in wound healing systems. This study showed that it is possible to achieve porous scaffolds based on two natural biopolymers (PHA and FucoPol) through two different methods. These structures exhibited convenient biological properties (revealed by *in vitro* results with fibroblasts) suitable for soft tissue engineering purposes, for instance in skin regeneration for wound treatment applications. The inclusion of FucoPol in 3D scaffolds was found to enhance the proliferation of fibroblasts after 7 days for both P(3HB) and P(3HB-co-3HV-3HHx) porous structures, regardless of the production method used. The emulsion templating technique emerged as the most effective method for creating porous PHA scaffolds, primarily due to the biological properties these structures exhibited. When the same PHA polymer was compared, the fibroblast proliferation rates (after 7 days) for scaffolds created using the emulsion templating technique consistently surpassed those of the hot-pressing salt leaching porous structures. Moreover, P(3HB) scaffolds typically demonstrated higher fibroblast proliferation rates after 7 days, when compared to porous structures made with P(3HB-co-3HV-3HHx). Consequently, the most promising candidates for wound healing applications were the emulsion templated scaffolds made from P(3HB), both with and without FucoPol. However, to make a deeper evaluation of the potential of this material for wound management, the mechanical properties should be assessed, as well as specific *in vitro* and *in vivo* research should be performed.

5

General Conclusions and Future Perspectives

5.1 General Conclusions

In this dissertation, three different PHA polymers P(3HB), P(3HB-co-3HV-co-3HHx), and mcl-PHA (composed by 3HHx, 3HO, 3HD, 3HDd and 3HTd monomers), were tested for the preparation of porous scaffolds with properties adequate for their use as active wound dressings, namely, non-cytotoxic behaviour, porosity, pore interconnectivity and ability to support fibroblast adhesion and proliferation.

The biopolyesters had distinct molecular weights (ranging from 0.4 to 9.2 $x10^5$ Da), different crystallinities (from 18.2 to 85.5%), diverse melting points (between 44.9 and 174.2 °C), various glass transition temperatures (from -46 to 4.1 °C), and similar degradation temperatures (around 275 °C). They were demonstrated to be not cytotoxic towards fibroblasts and keratinocytes.

FucoPol, an amorphous high molecular weight exopolysaccharide (1.4 $x10^6$ Da), rich in fucose (34.33 mol%), with high degradation temperature (240 °C) and non-cytotoxic for fibroblasts and keratinocytes, was used as bioemulsifier and/or bioactive component for the preparation of active scaffolds.

Films of each PHA polymers were prepared previously through solution casting and solvent evaporation and used for comparison. Porous structured materials based on P(3HB) and P(3HB-co-3HV-co-3HHx), were prepared by two different strategies: the emulsion templated technique and the hot-pressing salt leaching method. Generally, the porous structures achieved by these procedures were macroscopically white and opaque, with thicknesses ranging from 160 to 700 μm, and porosity values from 49.8 to 87.1% which are within the ranges reported by other materials for tissue engineering applications (De la Ossa et al., 2022; Gomes et al., 2017; Rodríguez-Tobías et al., 2016).

Through the observation of the SEM images and the porosity results it stayed clear that all the PHA scaffolds revealed pores of different sizes on their surface and cross section layer, where the higher porosities were attained by an emulsion templated structure for the P(3HB) polymer (82.2%) and by a hot-pressing salt leaching scaffold for P(3HB-co-3HV-co-3HHx) polyester (87.1%). The morphological appearance of these structures resembled those of porous scaffolds obtained with synthetic polymers, such as, PLA, PCL and PET, which are examples of polymers commonly used in wound dressing applications. However, the use of these polymers

due to their inherent low biocompatibility and biodegradability, revealed to be disadvantageous when compared with PHA porous materials (Borbolla-Jiménez et al., 2023; Sadeghi-Aghbash et al., 2023; Zahra et al., 2023).

The produced PHA scaffolds were able to support fibroblast adhesion and proliferation. The adhesion values for all the PHA structures were always lower when compared with the cell control (from 25% to 46%). All porous materials had lower proliferation rates than the TCP, except for P(3HB) emulsion templated scaffold that achieved higher fibroblast population after 7 days of cell cultivation (311%). Focal adhesion regulates the capacity and shape of fibroblast attachment. It is controlled by transmembrane proteins called integrins, which link the actin in the cytoskeleton to the scaffold or extracellular matrix (ECM) (Khalili & Ahmad, 2015). The size, number, and position of focal adhesions may be restricted by small connection points (< 1 μm) in the scaffold matrix, which would prevent cells from spreading across the scaffold (Vieira et al., 2019). The differences in cell adhesion and proliferation values between all the structures could be explained by the distinct number of integrin binding domains found in the PHA scaffolds, due to their distinct porosities and surface area.

PHA and FucoPol, as previously showed, are highly adaptable polymers with potential applications in wound healing systems. This dissertation demonstrated the use of these biopolymers in two separated methods (emulsion templating and hot-pressing salt leaching) to develop structures with enhanced biological properties. It was shown that FucoPol served as a bioemulsifier for emulsion stabilisation during the solvent evaporation process when using the emulsion templating technique, producing 3D porous structures with improved biological features, achieving relative fibroblast populations after 7 days of 325% and 340% for P(3HB) and P(3HB-co-3HV-co-3HHx), respectively. FucoPol was used as a bioactive material when using the hot-pressing salt leaching method to develop structures with improved biological activity, which also proved to be advantageous for the scaffolds made of P(3HB) polymer, reaching a proliferation rate of 333%.

The PHA scaffolds produced in this work revealed superior proliferation profiles than the ones described for structures produced with PCL, PU and chitosan cultured with the same cell line (Querido et al., 2022; Vieira et al., 2018, 2019, 2024). This proliferation performance was similar to that previously reported for other PHA structures and collagen membranes, also

seeded with fibroblasts (Boyandin et al., 2024; Chen et al., 2023). Given this, the most promising candidates for wound treatment applications revealed to be the emulsion templated porous structures obtained with P(3HB), P(3HB):FucoPol, P(3HB-co-3HV-co-3HHx):FucoPol and the hot-pressing salt leaching scaffolds of P(3HB):FucoPol. These results suggest that the most promising PHA polymer to produce 3D scaffolds was the homopolymer P(3HB), while the emulsion templating technique proved to be the most favourable method to produce porous structures for all the PHA polymers tested. The two procedures used to develop porous scaffolds in this study, namely the emulsion templating process and the hot-pressing salt leaching method, hold potential for industrial production. However, there are some possible scale-up constraints that must be considered. The main limitation would be the use of chloroform that is needed to dissolve the PHA polymers in both procedures. To overcome this issue, it is imperative to find innovative processing procedures that either, do not require the use of organic solvents, or involves the use of environmentally friendly ones that can solubilize these biopolymers to facilitate their applicability on an industrial scale.

To conclude, this work revealed that it is possible to achieve porous scaffolds based on two natural biopolymers, PHA and FucoPol, through two different methods and with convenient biological properties (revealed by *in vitro* results with fibroblasts) suitable for soft tissue engineering purposes, for instance in skin regeneration for wound treatment applications. This sustains that these biopolymers have very interesting physical, chemical, and biological properties that makes them suitable materials to develop new products (for high-end applications) in a wide variety of areas, ranging from fine chemicals to medical products.

5.2 Future Perspectives

The forefront of scientific development is always made of new improvement strategies, therefore, despite of all the results attained in this dissertation, there is still a lot of work to be done to ensure the use of PHA scaffolds as wound healing products. PHA processing typically uses chloroform, which is a toxic organic solvent with a recognized environmental footprint and generally not recommended for industrialized procedures. Given this, it could be advantageous exploring new methodologies for an eco-friendlier manipulation of these biopolymers. The incorporation of less hazardous and more sustainable solvents in PHA processing might be beneficial, to minimize the environmental footprint and to facilitate their implementation on an industrial scale.

PHAs are very versatile materials with many distinct properties, ranging from rigid and brittle to soft and elastic polyesters. These polymers are also known for their intrinsic great structural properties, biocompatibility, and biodegradability. Therefore, that are many ways to process these polymers to achieve different structured products. This would increase the economic competitiveness of PHAs and discover novel applications for these polymers in many distinct areas (such as packaging, biomedical, drug delivery, tissue engineering). 3D porous structures with the ability to support cellular adhesion and proliferation are crucial for soft tissue engineering applications. Therefore, it is extremely important to not only improve the strategies already used to produce these scaffolds, but also to find novel approaches and methodologies to achieve this type of materials. Some of these techniques could be difficult to apply at a larger scale, however, for an industrial production, it is crucial that these processes have unique scale up ability. Procedures such as the emulsion templating technique and the hot-pressing salt leaching process are a great example of promising strategies that could be further improved. For instance, the successful production of a PHA scaffold through the emulsion templating technique is clearly dependent on the viscosity/concentration of the biopolymeric solution in the organic phase and on the amount of water used in the dispersed phase. Therefore, to improve this strategy it is vital to study different PHA concentrations, as well as different water quantities, to evaluate if it is possible to obtain structures with higher porosity. Regarding the hot-pressing salt leaching method, it could be interesting to study different sizes and amounts of salt grains, to achieve scaffolds with tailored pore sizes and densities. By controlling

the porosity of these structures, the materials produced could overcome some limitations of cellular proliferation, by providing an adequate pore size. Surface modification to promote hydrophilicity and cellular adhesion could also be a viable approach to apply in both strategies (emulsion templating and hot-pressing salt leaching) to improve cell compatibility. Blending PHA scaffolds with other polymers, namely collagen or gelatin, could be another technique to promote a better cell interaction. Different techniques, such 3D printing, electrospinning are thermal induced phase separation (TIPS) can also be studied to find new innovative methodologies to achieve tailormade porous scaffolds, with a defined pore size and precise porosity for tissue engineering applications. This would ensure that the produced structures have the correct properties and requirements for wound healing applications. Another advantage is the increased range of applications that these scaffolds would make feasible, since each cell line has an appropriate pore size to proliferate, controlling the scaffold's porosity provides a wide range of applicability for these materials in skin, cardiac, bone, or even, in neuronal tissue (Choi et al., 2018).

In this dissertation FucoPol was used as a bioemulsifier and a bioactive material to be impregnated in PHA scaffolds. However, to further improve the porous structures biological activity, various products could be introduced in PHA scaffolds, such as, pharmaceuticals, metallic nanoparticles (MNPs), or proteins, to add new physical and biological properties to expand their applicability to different areas. These novel smart materials could have noble applications especially in the biomedical field, for instance in cancer treatment, in drug delivery, as biomedical materials or as biosensors.

To ensure that all these scaffolds can be used in wound treatment systems and as a biomedical product, further mechanical and permeability tests (especially for water vapor, O_2 and CO_2) need to be performed. This would evaluate if these structures fulfilled the physical requirements needed for this type of applications. Further *in vivo* studies are also required, to correctly assess the material's ability to be used as a biomedical product.

BIBLIOGRAPHY

Aghayan, S., Seyedjafari, E., & Hamidi, S. (2022). Effects of Nanofiber Scaffolds Coated with Nanoparticulate and Microparticulate Freeze Dried Bone Allograft on the Morphology, Adhesion, and Proliferation of Human Mesenchymal Stem Cells. *Iranian Biomedical Journal*, *26*(3), 193–201. https://doi.org/10.52547/ibj.26.3.193

Akbari, S., & Nour, A. H. (2018). Emulsion types, stability mechanisms and rheology: A review. In *International Journal of Innovative Research and Scientific Studies* (Vol. 1, Issue 1). https://ssrn.com/abstract=3324905

Aldemir Dikici, B., & Claeyssens, F. (2020). Basic Principles of Emulsion Templating and Its Use as an Emerging Manufacturing Method of Tissue Engineering Scaffolds. In *Frontiers in Bioengineering and Biotechnology* (Vol. 8). Frontiers Media S.A. https://doi.org/10.3389/fbioe.2020.00875

Ali, A., Bairagi, S., Ganie, S. A., & Ahmed, S. (2023). Polysaccharides and proteins based bionanocomposites as smart packaging materials: From fabrication to food packaging applications a review. In *International Journal of Biological Macromolecules* (Vol. 252). Elsevier B.V. https://doi.org/10.1016/j.ijbiomac.2023.126534

Ambekar, R. S., & Kandasubramanian, B. (2019). Progress in the Advancement of Porous Biopolymer Scaffold: Tissue Engineering Application. *Industrial and Engineering Chemistry Research*, *58*(16), 6163–6194. https://doi.org/10.1021/acs.iecr.8b05334

Anarjan, N., & Ping Tan, C. (2013). Physico-chemical stability of astaxanthin nanodispersions prepared with polysaccharides as stabilizing agents. *International Journal of Food Sciences and Nutrition*, *64*(6), 744–748. https://doi.org/10.3109/09637486.2013.783001

Anaya Mancipe, J. M., Boldrini Pereira, L. C., de Miranda Borchio, P. G., Dias, M. L., & da Silva Moreira Thiré, R. M. (2023). Novel polycaprolactone (PCL)-type I collagen core-shell

electrospun nanofibers for wound healing applications. *Journal of Biomedical Materials Research Part B: Applied Biomaterials*, *111*(2), 366–381. https://doi.org/10.1002/jbm.b.35156

Andler, R., Rojas, V., Pino, V., Castro, R. I., Valdés, C., Kumar, V., Peña, C., & Díaz-Barrera, A. (2023). Efficient production of a polyhydroxyalkanoate by Azotobacter vinelandii OP using apple residues as promising feedstock. *International Journal of Biological Macromolecules*, *242*. https://doi.org/10.1016/j.ijbiomac.2023.124626

Anjum, A., Zuber, M., Zia, K. M., Noreen, A., Anjum, M. N., & Tabasum, S. (2016). Microbial production of polyhydroxyalkanoates (PHAs) and its copolymers: A review of recent advancements. In *International Journal of Biological Macromolecules* (Vol. 89, pp. 161–174). Elsevier B.V. https://doi.org/10.1016/j.ijbiomac.2016.04.069

Anwer, A. H., Ahtesham, A., Shoeb, M., Mashkoor, F., Ansari, M. Z., Zhu, S., & Jeong, C. (2023). State-of-the-art advances in nanocomposite and bio-nanocomposite polymeric materials: A comprehensive review. In *Advances in Colloid and Interface Science* (Vol. 318). Elsevier B.V. https://doi.org/10.1016/j.cis.2023.102955

Araújo, D., Martins, M., Concórdio-Reis, P., Roma-Rodrigues, C., Morais, M., Alves, V. D., Fernandes, A. R., & Freitas, F. (2023). Novel Hydrogel Membranes Based on the Bacterial Polysaccharide FucoPol: Design, Characterization and Biological Properties. *Pharmaceuticals*, *16*(7). https://doi.org/10.3390/ph16070991

Balusamy, B., Senthamizhan, A., & Uyar, T. (2017). Electrospun nanofibrous materials for wound healing applications. In *Electrospun Materials for Tissue Engineering and Biomedical Applications* (pp. 147–177). Elsevier. https://doi.org/10.1016/B978-0-08-101022-8.00012-0

Baptista, S., Araújo, D., Concórdio-Reis, P., Marques, A. C., Fortunato, E., Alves, V. D., & Freitas, F. (2022). Deacetylation and Desuccinylation of the Fucose-Rich Polysaccharide Fucopol: Impact on Biopolymer Physical and Chemical Properties. *Molecules*, *27*(21). https://doi.org/10.3390/molecules27217165

Baptista, S., Pereira, J. R., Gil, C. V., Torres, C. A. V., Reis, M. A. M., & Freitas, F. (2022). Development of Olive Oil and α-Tocopherol Containing Emulsions Stabilized by FucoPol: Rheological and Textural Analyses. *Polymers*, *14*(12). https://doi.org/10.3390/polym14122349

Baptista, S., Pereira, J. R., Guerreiro, B. M., Baptista, F., Silva, J. C., & Freitas, F. (2023). Cosmetic emulsion based on the fucose-rich polysaccharide FucoPol: Bioactive properties and sensorial evaluation. *Colloids and Surfaces B: Biointerfaces*, *225*. https://doi.org/10.1016/j.colsurfb.2023.113252

Baptista, S., Torres, C. A. V., Sevrin, C., Grandfils, C., Reis, M. A. M., & Freitas, F. (2022a). Extraction of the Bacterial Extracellular Polysaccharide FucoPol by Membrane-Based Methods: Efficiency and Impact on Biopolymer Properties. *Polymers*, *14*(3). https://doi.org/10.3390/polym14030390

Baptista, S., Torres, C. A. V., Sevrin, C., Grandfils, C., Reis, M. A. M., & Freitas, F. (2022b). Extraction of the Bacterial Extracellular Polysaccharide FucoPol by Membrane-Based Methods: Efficiency and Impact on Biopolymer Properties. *Polymers*, *14*(3). https://doi.org/10.3390/polym14030390

Bergstrand, A., Andersson, H., Cramby, J., Sott, K., & Larsson, A. (2012). Preparation of Porous Poly(3-Hydroxybutyrate) Films by Water-Droplet Templating. *Journal of Biomaterials and Nanobiotechnology*, *03*(04), 431–439. https://doi.org/10.4236/jbnb.2012.34043

Bergstrand, A., Uppström, S., & Larsson, A. (2014). Permeability of porous poly(3-hydroxybutyrate) barriers of single and bilayer type for implant applications. *International Journal of Polymer Science*, *2014*. https://doi.org/10.1155/2014/958975

Bhubalan, K., Lee, W. H., Loo, C. Y., Yamamoto, T., Tsuge, T., Doi, Y., & Sudesh, K. (2008). Controlled biosynthesis and characterization of poly(3-hydroxybutyrate-co-3-hydroxyvalerate-co-3-hydroxyhexanoate) from mixtures of palm kernel oil and 3HV-precursors. *Polymer Degradation and Stability*, *93*(1), 17–23. https://doi.org/10.1016/j.polymdegradstab.2007.11.004

Bhubalan, K., Rathi, D. N., Abe, H., Iwata, T., & Sudesh, K. (2010). Improved synthesis of P(3HB-co-3HV-co-3HHx) terpolymers by mutant Cupriavidus necator using the PHA synthase gene of Chromobacterium sp. USM2 with high affinity towards 3HV. *Polymer Degradation and Stability*, *95*(8), 1436–1442. https://doi.org/10.1016/j.polymdegradstab.2009.12.018

Borbolla-Jiménez, F. V., Peña-Corona, S. I., Farah, S. J., Jiménez-Valdés, M. T., Pineda-Pérez, E., Romero-Montero, A., Del Prado-Audelo, M. L., Bernal-Chávez, S. A., Magaña, J. J., & Leyva-Gómez, G. (2023). Films for Wound Healing Fabricated Using a Solvent Casting Technique.

In *Pharmaceutics* (Vol. 15, Issue 7). Multidisciplinary Digital Publishing Institute (MDPI). https://doi.org/10.3390/pharmaceutics15071914

Bouyer, E., Mekhloufi, G., Rosilio, V., Grossiord, J. L., & Agnely, F. (2012). Proteins, polysaccharides, and their complexes used as stabilizers for emulsions: Alternatives to synthetic surfactants in the pharmaceutical field? In *International Journal of Pharmaceutics* (Vol. 436, Issues 1–2, pp. 359–378). https://doi.org/10.1016/j.ijpharm.2012.06.052

Boyandin, A. N., Dvoinina, L. M., Sukovatyi, A. G., Sukhanova, A. A., & Ertiletskaya, N. L. (2024). Improvement of biocompatibility of high molecular weight poly-3-hydroxybutyrate by blending with its functionalized oligomers. *Chimica Techno Acta*, *11*(1). https://doi.org/10.15826/chimtech.2024.11.1.01

Carrier, O., Covis, R., Marie, E., & Durand, A. (2011). Inverse emulsions stabilized by a hydrophobically modified polysaccharide. *Carbohydrate Polymers*, *84*(1), 599–604. https://doi.org/10.1016/j.carbpol.2010.12.031

Castro, K. C., Campos, M. G. N., & Mei, L. H. I. (2021). Hyaluronic acid electrospinning: Challenges, applications in wound dressings and new perspectives. In *International Journal of Biological Macromolecules* (Vol. 173, pp. 251–266). Elsevier B.V. https://doi.org/10.1016/j.ijbiomac.2021.01.100

Casula, L., Zidar, A., Kristl, J., Jeras, M., Kralj, S., Fadda, A. M., & Zupančič, Š. (2023). Development of Nanofibers with Embedded Liposomes Containing an Immunomodulatory Drug Using Green Electrospinning. *Pharmaceutics*, *15*(4). https://doi.org/10.3390/pharmaceutics15041245

Cerrone, F., Davis, R., Kenny, S. T., Woods, T., O'Donovan, A., Gupta, V. K., Tuohy, M., Babu, R. P., O'Kiely, P., & O'Connor, K. (2015). Use of a mannitol rich ensiled grass press juice (EGPJ) as a sole carbon source for polyhydroxyalkanoates (PHAs) production through high cell density cultivation. *Bioresource Technology*, *191*, 45–52. https://doi.org/10.1016/j.biortech.2015.04.128

Cerrone, F., Zhou, B., Mouren, A., Avérous, L., Conroy, S., Simpson, J. C., O'Connor, K. E., & Narancic, T. (2023). Pseudomonas umsongensis GO16 as a platform for the in vivo synthesis of short and medium chain length polyhydroxyalkanoate blends. *Bioresource Technology*, *387*. https://doi.org/10.1016/j.biortech.2023.129668

Cesarino, I., Moroz, I., Carbonera, A. F., Martins, G. de O., Fernandes, L. G. L., & Leao, A. L. (2024). PHA/PHB/PHBV-based composites: development and biomedical applications. In *Bioresorbable Polymers and their Composites* (pp. 107–123). Elsevier. https://doi.org/10.1016/B978-0-443-18915-9.00001-X

Chen, F., Liu, X., Ge, X., Wang, Y., Zhao, Z., Zhang, X., Chen, G. Q., & Sun, Y. (2023). Porous polydroxyalkanoates (PHA) scaffolds with antibacterial property for oral soft tissue regeneration. *Chemical Engineering Journal*, *451*. https://doi.org/10.1016/j.cej.2022.138899

Chernozem, R. V., Guselnikova, O., Surmeneva, M. A., Postnikov, P. S., Abalymov, A. A., Parakhonskiy, B. V., De Roo, N., Depla, D., Skirtach, A. G., & Surmenev, R. A. (2020). Diazonium chemistry surface treatment of piezoelectric polyhydroxybutyrate scaffolds for enhanced osteoblastic cell growth. *Applied Materials Today*, *20*. https://doi.org/10.1016/j.apmt.2020.100758

Choi, D. J., Park, S. J., Gu, B. K., Kim, Y. J., Chung, S., & Kim, C. H. (2018). Effect of the pore size in a 3D bioprinted gelatin scaffold on fibroblast proliferation. *Journal of Industrial and Engineering Chemistry*, *67*, 388–395. https://doi.org/10.1016/j.jiec.2018.07.013

Choonut, A., Prasertsan, P., Klomklao, S., & Sangkharak, K. (2020). Study on mcl-PHA Production by Novel Thermotolerant Gram-Positive Isolate. *Journal of Polymers and the Environment*, *28*(9), 2410–2421. https://doi.org/10.1007/s10924-020-01779-8

Concórdio-Reis, P., Pereira, J. R., Alves, V. D., Nabais, A. R., Neves, L. A., Marques, A. C., Fortunato, E., Moppert, X., Guézennec, J., Reis, M. A. M., & Freitas, F. (2022). Characterisation of Films Based on Exopolysaccharides from Alteromonas Strains Isolated from French Polynesia Marine Environments. *Polymers*, *14*(20). https://doi.org/10.3390/polym14204442

Concórdio-Reis, P., Pereira, J. R., Torres, C. A. V., Sevrin, C., Grandfils, C., & Freitas, F. (2018). Effect of mono- and dipotassium phosphate concentration on extracellular polysaccharide production by the bacterium Enterobacter A47. *Process Biochemistry*, *75*, 16–21. https://doi.org/10.1016/j.procbio.2018.09.001

Concórdio-Reis, P., Pereira, C. V., Batista, M. P., Sevrin, C., Grandfils, C., Marques, A. C., Fortunato, E., Gaspar, F. B., Matias, A. A., Freitas, F., & Reis, M. A. M. (2020). Silver nanocomposites based on the bacterial fucose-rich polysaccharide secreted by Enterobacter A47 for wound dressing applications: Synthesis, characterization and in vitro bioactivity.

International Journal of Biological Macromolecules, *163*, 959–969. https://doi.org/10.1016/j.ijbiomac.2020.07.072

Concórdio-Reis, P., Reis, M. A. M., & Freitas, F. (2020). Biosorption of heavy metals by the bacterial exopolysaccharide fucopol. *Applied Sciences (Switzerland)*, *10*(19). https://doi.org/10.3390/APP10196708

Criollo-Mendoza, M. S., Contreras-Angulo, L. A., Leyva-López, N., Gutiérrez-Grijalva, E. P., Jiménez-Ortega, L. A., & Heredia, J. B. (2023). Wound Healing Properties of Natural Products: Mechanisms of Action. *Molecules*, *28*(2), 598. https://doi.org/10.3390/molecules28020598

Cruz, M. V., Araújo, D., Alves, V. D., Freitas, F., & Reis, M. A. M. (2016). Characterization of medium chain length polyhydroxyalkanoate produced from olive oil deodorizer distillate. *International Journal of Biological Macromolecules*, *82*, 243–248. https://doi.org/10.1016/j.ijbiomac.2015.10.043

Cruz, M. V., Freitas, F., Paiva, A., Mano, F., Dionísio, M., Ramos, A. M., & Reis, M. A. M. (2016). Valorization of fatty acids-containing wastes and byproducts into short- and medium-chain length polyhydroxyalkanoates. *New Biotechnology*, *33*(1), 206–215. https://doi.org/10.1016/j.nbt.2015.05.005

Dam, P., Celik, M., Ustun, M., Saha, S., Saha, C., Kacar, E. A., Kugu, S., Karagulle, E. N., Tasoglu, S., Buyukserin, F., Mondal, R., Roy, P., Macedo, M. L. R., Franco, O. L., Cardoso, M. H., Altuntas, S., & Mandal, A. K. (2023). Wound healing strategies based on nanoparticles incorporated in hydrogel wound patches. In *RSC Advances* (Vol. 13, Issue 31, pp. 21345–21364). Royal Society of Chemistry. https://doi.org/10.1039/d3ra03477a

D'Anna, A., Arrigo, R., & Frache, A. (2022). Rheology, Morphology and Thermal Properties of a PLA/PHB/Clay Blend Nanocomposite: The Influence of Process Parameters. *Journal of Polymers and the Environment*, *30*(1), 102–113. https://doi.org/10.1007/s10924-021-02186-3

De Carvalho, E., Chebil, M., Fay, F., Renard, E., & Langlois, V. (2023). A solvent-free process to design low density polyhydroxyalkanoate. *Polymers from Renewable Resources*, *14*(2), 61–75. https://doi.org/10.1177/20412479231165454

De la Ossa, J. G., Danti, S., Esposito Salsano, J., Azimi, B., Tempesti, V., Barbani, N., Digiacomo, M., Macchia, M., Uddin, M. J., Cristallini, C., Di Stefano, R., & Lazzeri, A. (2022). Electrospun

Poly(3-Hydroxybutyrate-Co-3-Hydroxyvalerate)/Olive Leaf Extract Fiber Mesh as Prospective Bio-Based Scaffold for Wound Healing. *Molecules*, *27*(19). https://doi.org/10.3390/molecules27196208

de Meneses, L., Pereira, J. R., Sevrin, C., Grandfils, C., Paiva, A., Reis, M. A. M., & Freitas, F. (2020). Pseudomonas chlororaphis as a multiproduct platform: Conversion of glycerol into high-value biopolymers and phenazines. *New Biotechnology*, *55*, 84–90. https://doi.org/10.1016/j.nbt.2019.10.002

Deng, B., Rao, L., & Rodriguez-Freire, L. (2024). Evaluation and optimization of FTIR spectroscopy to quantify PHA production by municipal wastewater sludge. *Spectrochimica Acta Part A: Molecular and Biomolecular Spectroscopy*, *312*, 124012. https://doi.org/10.1016/j.saa.2024.124012

Derippe, G., Philip, L., Lemechko, P., Eyheraguibel, B., Meistertzheim, A. L., Pujo-Pay, M., Conan, P., Barbe, V., Bruzaud, S., & Ghiglione, J. F. (2024). Marine biodegradation of tailor-made polyhydroxyalkanoates (PHA) influenced by the chemical structure and associated bacterial communities. *Journal of Hazardous Materials*, *462*. https://doi.org/10.1016/j.jhazmat.2023.132782

Dhivya, S., Padma, V. V., & Santhini, E. (2015). Wound dressings - A review. In *BioMedicine (Netherlands)* (Vol. 5, Issue 4, pp. 24–28). China Medical University. https://doi.org/10.7603/s40681-015-0022-9

Diniz, M. S. da F., Mourão, M. M., Xavier, L. P., & Santos, A. V. (2023). Recent Biotechnological Applications of Polyhydroxyalkanoates (PHA) in the Biomedical Sector—A Review. *Polymers*, *15*(22), 4405. https://doi.org/10.3390/polym15224405

Dubey, S., Bharmoria, P., Gehlot, P. S., Agrawal, V., Kumar, A., & Mishra, S. (2018). 1-Ethyl-3-methylimidazolium Diethylphosphate Based Extraction of Bioplastic "polyhydroxyalkanoates" from Bacteria: Green and Sustainable Approach. *ACS Sustainable Chemistry and Engineering*, *6*(1), 766–773. https://doi.org/10.1021/acssuschemeng.7b03096

Dutta, R. C., Dey, M., Dutta, A. K., & Basu, B. (2017). Competent processing techniques for scaffolds in tissue engineering. In *Biotechnology Advances* (Vol. 35, Issue 2, pp. 240–250). Elsevier Inc. https://doi.org/10.1016/j.biotechadv.2017.01.001

Eltom, A., Zhong, G., & Muhammad, A. (2019). Scaffold Techniques and Designs in Tissue Engineering Functions and Purposes: A Review. In *Advances in Materials Science and Engineering* (Vol. 2019). Hindawi Limited. https://doi.org/10.1155/2019/3429527

Esmail, A., Pereira, J. R., Sevrin, C., Grandfils, C., Menda, U. D., Fortunato, E., Oliva, A., & Freitas, F. (2021). Preparation and characterization of porous scaffolds based on poly(3-hydroxybutyrate) and poly(3-hydroxybutyrate-co-3-hydroxyvalerate). *Life*, *11*(9). https://doi.org/10.3390/life11090935

Esmail, A., Pereira, J. R., Zoio, P., Silvestre, S., Menda, U. D., Sevrin, C., Grandfils, C., Fortunato, E., Reis, M. A. M., Henriques, C., Oliva, A., & Freitas, F. (2021). Oxygen plasma treated-electrospun polyhydroxyalkanoate scaffolds for hydrophilicity improvement and cell adhesion. *Polymers*, *13*(7). https://doi.org/10.3390/polym13071056

Fabra, M. J., Lopez-Rubio, A., & Lagaron, J. M. (2014). Nanostructured interlayers of zein to improve the barrier properties of high barrier polyhydroxyalkanoates and other polyesters. *Journal of Food Engineering*, *127*, 1–9. https://doi.org/10.1016/j.jfoodeng.2013.11.022

Farazin, A., Shirazi, F. A., & Shafiei, M. (2023). Natural biomarocmolecule-based antimicrobial hydrogel for rapid wound healing: A review. In *International Journal of Biological Macromolecules* (Vol. 244). Elsevier B.V. https://doi.org/10.1016/j.ijbiomac.2023.125454

Ferrari, F., Striani, R., Fico, D., Alam, M. M., Greco, A., & Esposito Corcione, C. (2022). An Overview on Wood Waste Valorization as Biopolymers and Biocomposites: Definition, Classification, Production, Properties and Applications. In *Polymers* (Vol. 14, Issue 24). MDPI. https://doi.org/10.3390/polym14245519

Fialho, L., Araújo, D., Alves, V. D., Roma-Rodrigues, C., Baptista, P. V., Fernandes, A. R., Freitas, F., & Reis, M. A. M. (2021). Cation-mediated gelation of the fucose-rich polysaccharide FucoPol: preparation and characterization of hydrogel beads and their cytotoxicity assessment. *International Journal of Polymeric Materials and Polymeric Biomaterials*, *70*(2), 90–99. https://doi.org/10.1080/00914037.2019.1695205

Fosse, C., Esposito, A., Lemechko, P., Salim, Y. S., Causin, V., Gaucher, V., Bruzaud, S., Sudesh, K., Delbreilh, L., & Dargent, E. (2023). Effect of Chemical Composition on Molecular Mobility and Phase Coupling in Poly(3-hydroxybutyrate-co-3-hydroxyvalerate) and Poly(3-

hydroxybutyrate-co-3-hydroxyhexanoate) with Different Comonomer Contents. *Journal of Polymers and the Environment*, *31*(10), 4430–4447. https://doi.org/10.1007/s10924-023-02882-2

Freitas, F., Torres, C. A. V., Araújo, D., Farinha, I., Pereira, J. R., Concórdio-Reis, P., & Reis, M. A. M. (2021). Advanced Microbial Polysaccharides. In *Biopolymers for Biomedical and Biotechnological Applications* (pp. 19–62). Wiley. https://doi.org/10.1002/9783527818310.ch2

Gaur, M., Dobke, M., & Lunyak, V. V. (2017). Mesenchymal stem cells from adipose tissue in clinical applications for dermatological indications and skin aging. In *International Journal of Molecular Sciences* (Vol. 18, Issue 1). MDPI AG. https://doi.org/10.3390/ijms18010208

Gautam, S., Purohit, S. D., Singh, H., Dinda, A. K., Potdar, P. D., Sharma, C., Chou, C. F., & Mishra, N. C. (2023). Surface modification of PCL-gelatin-chitosan electrospun scaffold by nano-hydroxyapatite for bone tissue engineering. *Materials Today Communications*, *34*. https://doi.org/10.1016/j.mtcomm.2022.105237

Gavinho, S. R., Pádua, A. S., Sá-Nogueira, I., Silva, J. C., Borges, J. P., Costa, L. C., & Graça, M. P. F. (2023). Fabrication, Structural and Biological Characterization of Zinc-Containing Bioactive Glasses and Their Use in Membranes for Guided Bone Regeneration. *Materials*, *16*(3). https://doi.org/10.3390/ma16030956

Gianino, E., Miller, C., & Gilmore, J. (2018). Smart wound dressings for diabetic chronic wounds. In *Bioengineering* (Vol. 5, Issue 3). MDPI AG. https://doi.org/10.3390/bioengineering5030051

Gomes, S., Rodrigues, G., Martins, G., Henriques, C., & Silva, J. C. (2017). Evaluation of nanofibrous scaffolds obtained from blends of chitosan, gelatin and polycaprolactone for skin tissue engineering. *International Journal of Biological Macromolecules*, *102*, 1174–1185. https://doi.org/10.1016/j.ijbiomac.2017.05.004

Guerreiro, B. M., Freitas, F., Lima, J. C., Silva, J. C., Dionísio, M., & Reis, M. A. M. (2020). Demonstration of the cryoprotective properties of the fucose-containing polysaccharide FucoPol. *Carbohydrate Polymers*, *245*. https://doi.org/10.1016/j.carbpol.2020.116500

Guerreiro, B. M., Silva, J. C., Lima, J. C., Reis, M. A. M., & Freitas, F. (2021). Antioxidant potential of the bio-based fucose-rich polysaccharide fucopol supports its use in oxidative stress-inducing systems. *Polymers*, *13*(18). https://doi.org/10.3390/polym13183020

Haraguchi, K. (2014). Biocomposites. In *Encyclopedia of Polymeric Nanomaterials* (pp. 1–8). Springer Berlin Heidelberg. https://doi.org/10.1007/978-3-642-36199-9_316-1

Hernández-Herreros, N., Rivero-Buceta, V., Pardo, I., & Prieto, M. A. (2023). Production of poly(3-hydroxybutyrate)/poly(lactic acid) from industrial wastewater by wild-type Cupriavidus necator H16. *Water Research*, 120892. https://doi.org/10.1016/j.watres.2023.120892

Holloway, S., & Harding, K. G. (2022). Wound dressings. *Surgery (Oxford)*, *40*(1), 25–32. https://doi.org/10.1016/j.mpsur.2021.11.002

Hu, Y. J., Wei, X., Zhao, W., Liu, Y. S., & Chen, G. Q. (2009). Biocompatibility of poly(3-hydroxybutyrate-co-3-hydroxyvalerate-co-3-hydroxyhexanoate) with bone marrow mesenchymal stem cells. *Acta Biomaterialia*, *5*(4), 1115–1125. https://doi.org/10.1016/j.actbio.2008.09.021

Jensen, C., & Teng, Y. (2020). Is It Time to Start Transitioning From 2D to 3D Cell Culture? In *Frontiers in Molecular Biosciences* (Vol. 7). Frontiers Media S.A. https://doi.org/10.3389/fmolb.2020.00033

Jung, H. R., Jeon, J. M., Yi, D. H., Song, H. S., Yang, S. Y., Choi, T. R., Bhatia, S. K., Yoon, J. J., Kim, Y. G., Brigham, C. J., & Yang, Y. H. (2019). Poly(3-hydroxybutyrate-co-3-hydroxyvalerate-co-3-hydroxyhexanoate) terpolymer production from volatile fatty acids using engineered Ralstonia eutropha. *International Journal of Biological Macromolecules*, *138*, 370–378. https://doi.org/10.1016/j.ijbiomac.2019.07.091

Kalia, V. C., Patel, S. K. S., & Lee, J.-K. (2023). Exploiting Polyhydroxyalkanoates for Biomedical Applications. *Polymers*, *15*(8), 1937. https://doi.org/10.3390/polym15081937

Kang, J., Hwang, J. Y., Huh, M., & Yun, S. Il. (2020). Porous Poly(3-hydroxybutyrate) Scaffolds Prepared by Non-Solvent-Induced Phase Separation for Tissue Engineering. *Macromolecular Research*, *28*(9), 835–843. https://doi.org/10.1007/s13233-020-8109-x

Kaniuk, Ł., Ferraris, S., Spriano, S., Luxbacher, T., Krysiak, Z., Berniak, K., Zaszczynska, A., Marzec, M. M., Bernasik, A., Sajkiewicz, P., & Stachewicz, U. (2021). Time-dependent effects on

physicochemical and surface properties of PHBV fibers and films in relation to their interactions with fibroblasts. *Applied Surface Science*, *545*. https://doi.org/10.1016/j.apsusc.2021.148983

Kaniuk, Ł., Krysiak, Z. J., Metwally, S., & Stachewicz, U. (2020). Osteoblasts and fibroblasts attachment to poly(3-hydroxybutyric acid-co-3-hydrovaleric acid) (PHBV) film and electrospun scaffolds. *Materials Science and Engineering C*, *110*. https://doi.org/10.1016/j.msec.2020.110668

Khalili, A. A., & Ahmad, M. R. (2015). A Review of cell adhesion studies for biomedical and biological applications. In *International Journal of Molecular Sciences* (Vol. 16, Issue 8, pp. 18149–18184). MDPI AG. https://doi.org/10.3390/ijms160818149

Khan, R., Aslam Khan, M. U., Stojanović, G. M., Javed, A., Haider, S., & Abd Razak, S. I. (2023). Fabrication of Bilayer Nanofibrous-Hydrogel Scaffold from Bacterial Cellulose, PVA, and Gelatin as Advanced Dressing for Wound Healing and Soft Tissue Engineering. *ACS Omega*. https://doi.org/10.1021/acsomega.3c06613

Khanna, S., & Srivastava, A. K. (2005). Recent advances in microbial polyhydroxyalkanoates. *Process Biochemistry*, *40*(2), 607–619. https://doi.org/10.1016/j.procbio.2004.01.053

Khoroushi, M., Foroughi, M. R., Karbasi, S., Hashemibeni, B., & Khademi, A. A. (2018). Effect of Polyhydroxybutyrate/Chitosan/Bioglass nanofiber scaffold on proliferation and differentiation of stem cells from human exfoliated deciduous teeth into odontoblast-like cells. *Materials Science and Engineering C*, *89*, 128–139. https://doi.org/10.1016/j.msec.2018.03.028

Kiany, F., Sarafraz, N., Tanideh, N., Bordbar, H., Andisheh-Tadbir, A., Zare, S., Farshidfar, N., & Zarei, M. (2024). Bone repair potential of collagen-poly(3-hydroxybutyrate)-carbon nanotubes scaffold loaded with mesenchymal stem cells for the reconstruction of critical-sized mandibular defects. *Journal of Stomatology, Oral and Maxillofacial Surgery*, *125*(2). https://doi.org/10.1016/j.jormas.2023.101670

Kimmins, S. D., & Cameron, N. R. (2011). Functional Porous Polymers by Emulsion Templating: Recent Advances. *Advanced Functional Materials*, *21*(2), 211–225. https://doi.org/10.1002/adfm.201001330

Kinikoglu, B. (2017). A Comparison of Scaffold-free and Scaffold-based Reconstructed Human Skin Models as Alternatives to Animal Use. *Alternatives to Laboratory Animals*, *45*(6), 309–316. https://doi.org/10.1177/026119291704500607

Koehler, J., Brandl, F. P., & Goepferich, A. M. (2018). Hydrogel wound dressings for bioactive treatment of acute and chronic wounds. In *European Polymer Journal* (Vol. 100, pp. 1–11). Elsevier Ltd. https://doi.org/10.1016/j.eurpolymj.2017.12.046

Koller, M., & Mukherjee, A. (2022). A New Wave of Industrialization of PHA Biopolyesters. In *Bioengineering* (Vol. 9, Issue 2). MDPI. https://doi.org/10.3390/bioengineering9020074

Kopf, S., Åkesson, D., & Skrifvars, M. (2023). Textile Fiber Production of Biopolymers–A Review of Spinning Techniques for Polyhydroxyalkanoates in Biomedical Applications. In *Polymer Reviews* (Vol. 63, Issue 1, pp. 200–245). Taylor and Francis Ltd. https://doi.org/10.1080/15583724.2022.2076693

Kuddushi, M., Shah, A. A., Ayranci, C., & Zhang, X. (2023). Recent advances in novel materials and techniques for developing transparent wound dressings. *Journal of Materials Chemistry B*, *11*(27), 6201–6224. https://doi.org/10.1039/D3TB00639E

Ladhari, S., Vu, N. N., Boisvert, C., Saidi, A., & Nguyen-Tri, P. (2023). Recent Development of Polyhydroxyalkanoates (PHA)-Based Materials for Antibacterial Applications: A Review. In *ACS Applied Bio Materials* (Vol. 6, Issue 4, pp. 1398–1430). American Chemical Society. https://doi.org/10.1021/acsabm.3c00078

Las Heras, K., Igartua, M., Santos-Vizcaino, E., & Hernandez, R. M. (2020). Chronic wounds: Current status, available strategies and emerging therapeutic solutions. In *Journal of Controlled Release* (Vol. 328, pp. 532–550). Elsevier B.V. https://doi.org/10.1016/j.jconrel.2020.09.039

Lee, H. S., Lee, S. M., Park, S. L., Choi, T. R., Song, H. S., Kim, H. J., Bhatia, S. K., Gurav, R., Kim, Y. G., Kim, J. H., Choi, K. Y., & Yang, Y. H. (2021). Tung oil-based production of high 3-hydroxyhexanoate-containing terpolymer poly(3-hydroxybutyrate-co-3-hydroxyvalerate-co-3-hydroxyhexanoate) using engineered ralstonia eutropha. *Polymers*, *13*(7). https://doi.org/10.3390/polym13071084

Liu, J., Zhou, Z., Li, H., Yang, X., Wang, Z., Xiao, J., & Wei, D. X. (2024). Current status and challenges in the application of microbial PHA particles. In *Particuology* (Vol. 87, pp. 286–302). Elsevier B.V. https://doi.org/10.1016/j.partic.2023.08.011

López-Ortega, M. A., Rodríguez-Hernández, A. I., Camacho-Ruíz, R. M., Córdova, J., López-Cuellar, M. del R., Chavarría-Hernández, N., & González-García, Y. (2020). Physicochemical characterization and emulsifying properties of a novel exopolysaccharide produced by haloarchaeon Haloferax mucosum. *International Journal of Biological Macromolecules*, *142*, 152–162. https://doi.org/10.1016/j.ijbiomac.2019.09.087

Lopresti, F., Liga, A., Capuana, E., Gulfi, D., Zanca, C., Inguanta, R., Brucato, V., La Carrubba, V., & Carfì Pavia, F. (2022). Effect of Polyhydroxyalkanoate (PHA) Concentration on Polymeric Scaffolds Based on Blends of Poly-L-Lactic Acid (PLLA) and PHA Prepared via Thermally Induced Phase Separation (TIPS). *Polymers*, *14*(12). https://doi.org/10.3390/polym14122494

Ma, L., Zhang, H., Liu, Q., Chen, J., Zhang, J., & Chen, G.-Q. (2009). Production of two monomer structures containing medium-chain-length polyhydroxyalkanoates by β-oxidation-impaired mutant of Pseudomonas putida KT2442. *Bioresource Technology*, *100*(20), 4891–4894. https://doi.org/10.1016/j.biortech.2009.05.017

Martínez-Herrera, R. E., Alemán-Huerta, M. E., Almaguer-Cantú, V., Rosas-Flores, W., Martínez-Gómez, V. J., Quintero-Zapata, I., Rivera, G., & Rutiaga-Quiñones, O. M. (2020). Efficient recovery of thermostable polyhydroxybutyrate (PHB) by a rapid and solvent-free extraction protocol assisted by ultrasound. *International Journal of Biological Macromolecules*, *164*, 771–782. https://doi.org/10.1016/j.ijbiomac.2020.07.101

Massella, D., Argenziano, M., Ferri, A., Guan, J., Giraud, S., Cavalli, R., Barresi, A. A., & Salaün, F. (2019). Bio-functional textiles: Combining pharmaceutical nanocarriers with fibrous materials for innovative dermatological therapies. In *Pharmaceutics* (Vol. 11, Issue 8). MDPI AG. https://doi.org/10.3390/pharmaceutics11080403

Mauro, N., Calabrese, G., Sciortino, A., Rizzo, M. G., Messina, F., Giammona, G., & Cavallaro, G. (2024). Microporous Fluorescent Poly(D,L-lactide) Acid–Carbon Nanodot Scaffolds for Bone Tissue Engineering Applications. *Materials*, *17*(2). https://doi.org/10.3390/ma17020449

Melendez-Rodriguez, B., Castro-Mayorga, J. L., Reis, M. A. M., Sammon, C., Cabedo, L., Torres-Giner, S., & Lagaron, J. M. (2018). Preparation and Characterization of Electrospun Food Biopackaging Films of Poly(3-hydroxybutyrate-co-3-hydroxyvalerate) Derived From Fruit Pulp Biowaste. *Frontiers in Sustainable Food Systems*, *2*. https://doi.org/10.3389/fsufs.2018.00038

Meléndez-Rodríguez, B., Torres-Giner, S., Reis, M. A. M., Silva, F., Matos, M., Cabedo, L., & Lagarón, J. M. (2021). Blends of poly(3-hydroxybutyrate-co-3-hydroxyvalerate) with fruit pulp biowaste derived poly(3-hydroxybutyrate-co-3- hydroxyvalerate-co-3-hydroxyhexa-noate) for organic recycling food packaging. *Polymers*, *13*(7). https://doi.org/10.3390/polym13071155

Modaress, M. P., Mirzadeh, H., & Zandi, M. (2012). Fabrication of a porous wall and higher interconnectivity scaffold comprising gelatin/chitosan via combination of salt-leaching and lyophilization methods. *Iranian Polymer Journal (English Edition)*, *21*(3), 191–200. https://doi.org/10.1007/s13726-012-0019-0

Muhr, A., Rechberger, E. M., Salerno, A., Reiterer, A., Malli, K., Strohmeier, K., Schober, S., Mittelbach, M., & Koller, M. (2013). Novel Description of mcl-PHA Biosynthesis by Pseudomonas chlororaphis from Animal-Derived Waste. *Journal of Biotechnology*, *165*(1), 45–51. https://doi.org/10.1016/j.jbiotec.2013.02.003

Muhr, A., Rechberger, E. M., Salerno, A., Reiterer, A., Schiller, M., Kwiecień, M., Adamus, G., Kowalczuk, M., Strohmeier, K., Schober, S., Mittelbach, M., & Koller, M. (2013). Biodegradable latexes from animal-derived waste: Biosynthesis and characterization of mcl-PHA accumulated by Ps. citronellolis. *Reactive and Functional Polymers*, *73*(10), 1391–1398. https://doi.org/10.1016/j.reactfunctpolym.2012.12.009

Nashchekina, Y., Chabina, A., Nashchekin, A., & Mikhailova, N. (2020). Polycaprolactone films modified by L-Arginine for mesenchymal stem cell cultivation. *Polymers*, *12*(5). https://doi.org/10.3390/POLYM12051042

Nedeljkovic, I., Doulabi, B. Z., Abdelaziz, M., Feilzer, A. J., Exterkate, R. A. M., Szafert, S., Gulia, N., Krejci, I., & Kleverlaan, C. J. (2022). Cytotoxicity and anti-biofilm properties of novel hybrid-glass-based caries infiltrant. *Dental Materials*, *38*(12), 2052–2061. https://doi.org/10.1016/j.dental.2022.11.018

Nguyen, H. M., Ngoc Le, T. T., Nguyen, A. T., Thien Le, H. N., & Pham, T. T. (2023). Biomedical materials for wound dressing: recent advances and applications. In *RSC Advances* (Vol. 13, Issue 8, pp. 5509–5528). Royal Society of Chemistry. https://doi.org/10.1039/d2ra07673j

Niculescu, A. G., & Grumezescu, A. M. (2022). An Up-to-Date Review of Biomaterials Application in Wound Management. In *Polymers* (Vol. 14, Issue 3). MDPI. https://doi.org/10.3390/polym14030421

Nikolova, M. P., & Chavali, M. S. (2019). Recent advances in biomaterials for 3D scaffolds: A review. *Bioactive Materials*, *4*, 271–292. https://doi.org/10.1016/j.bioactmat.2019.10.005

Obruca, S., Sedlacek, P., Slaninova, E., Fritz, I., Daffert, C., Meixner, K., Sedrlova, Z., & Koller, M. (2020). Novel unexpected functions of PHA granules. In *Applied Microbiology and Biotechnology* (Vol. 104, Issue 11, pp. 4795–4810). Springer. https://doi.org/10.1007/s00253-020-10568-1

Özcan Bülbül, E., Okur, M. E., Üstündağ Okur, N., & Siafaka, P. I. (2022). Traditional and advanced wound dressings: physical characterization and desirable properties for wound healing. In *Natural Polymers in Wound Healing and Repair* (pp. 19–50). Elsevier. https://doi.org/10.1016/B978-0-323-90514-5.00020-1

Pang, Q., Jiang, Z., Wu, K., Hou, R., & Zhu, Y. (2023). Nanomaterials-Based Wound Dressing for Advanced Management of Infected Wound. In *Antibiotics* (Vol. 12, Issue 2). MDPI. https://doi.org/10.3390/antibiotics12020351

Pappalardo, F., Fragalà, M., Mineo, P. G., Damigella, A., Catara, A. F., Palmeri, R., & Rescifina, A. (2014). Production of filmable medium-chain-length polyhydroxyalkanoates produced from glycerol by Pseudomonas mediterranea. *International Journal of Biological Macromolecules*, *65*, 89–96. https://doi.org/10.1016/j.ijbiomac.2014.01.014

Park, H., He, H., Yan, X., Liu, X., Scrutton, N. S., & Chen, G. Q. (2024). PHA is not just a bioplastic! In *Biotechnology Advances* (Vol. 71). Elsevier Inc. https://doi.org/10.1016/j.biotechadv.2024.108320

Park, S., Baker, J. O., Himmel, M. E., Parilla, P. A., & Johnson, D. K. (2010). Cellulose crystallinity index: measurement techniques and their impact on interpreting cellulase performance. *Biotechnology for Biofuels*, *3*(1), 10. https://doi.org/10.1186/1754-6834-3-10

Patel, R., Gómez-Cerezo, M. N., Huang, H., Grøndahl, L., & Lu, M. (2024). Degradation behaviour of porous poly(hydroxybutyrate-co-hydroxyvalerate) (PHBV) scaffolds in cell culture. *International Journal of Biological Macromolecules*, *257*. https://doi.org/10.1016/j.ijbiomac.2023.128644

Peregrina, A., Martins-Lourenço, J., Freitas, F., Reis, M. A. M., & Arraiano, C. M. (2021). Post-transcriptional control in the regulation of polyhydroxyalkanoates synthesis. In *Life* (Vol. 11, Issue 8). MDPI AG. https://doi.org/10.3390/life11080853

Pereira, J. R., Araújo, D., Freitas, P., Marques, A. C., Alves, V. D., Sevrin, C., Grandfils, C., Fortunato, E., Reis, M. A. M., & Freitas, F. (2021). Production of medium-chain-length polyhydroxyalkanoates by Pseudomonas chlororaphis subsp. aurantiaca: Cultivation on fruit pulp waste and polymer characterization. *International Journal of Biological Macromolecules*, *167*, 85–92. https://doi.org/10.1016/j.ijbiomac.2020.11.162

Pereira, J. R., Araújo, D., Marques, A. C., Neves, L. A., Grandfils, C., Sevrin, C., Alves, V. D., Fortunato, E., Reis, M. A. M., & Freitas, F. (2019). Demonstration of the adhesive properties of the medium-chain-length polyhydroxyalkanoate produced by Pseudomonas chlororaphis subsp. aurantiaca from glycerol. *International Journal of Biological Macromolecules*, *122*, 1144–1151. https://doi.org/10.1016/j.ijbiomac.2018.09.064

Pereira, J. R., Rafael, A. M., Esmail, A., Morais, M., Matos, M., Marques, A. C., Reis, M. A. M., & Freitas, F. (2023). Preparation of Porous Scaffold Based on Poly(3-hydroxybutyrate-co-3-hydroxyvalerate-co-3-hydroxyhexanoate) and FucoPol. *Polymers*, *15*(13), 2945. https://doi.org/10.3390/polym15132945

Peschel, G., Dahse, H., Konrad, A., Wieland, G. D., Mueller, P., Martin, D. P., & Roth, M. (2008). Growth of keratinocytes on porous films of poly(3-hydroxybutyrate) and poly(4-hydroxybutyrate) blended with hyaluronic acid and chitosan. *Journal of Biomedical Materials Research Part A*, *85A*(4), 1072–1081. https://doi.org/10.1002/jbm.a.31666

Phuegyod, S., Pramual, S., Wattanavichean, N., Assawajaruwan, S., Amornsakchai, T., Sukho, P., Svasti, J., Surarit, R., & Niamsiri, N. (2023). Microbial Poly(hydroxybutyrate-co-hydroxyvalerate) Scaffold for Periodontal Tissue Engineering. *Polymers*, *15*(4). https://doi.org/10.3390/polym15040855

Piironen, K., Haapala, M., Talman, V., Järvinen, P., & Sikanen, T. (2020). Cell adhesion and proliferation on common 3D printing materials used in stereolithography of microfluidic devices. *Lab on a Chip*, *20*(13), 2372–2382. https://doi.org/10.1039/d0lc00114g

Pino, P., Bosco, F., Mollea, C., & Onida, B. (2023). Antimicrobial Nano-Zinc Oxide Biocomposites for Wound Healing Applications: A Review. In *Pharmaceutics* (Vol. 15, Issue 3). MDPI. https://doi.org/10.3390/pharmaceutics15030970

Pothal, P., Pathania, K., Kumar, S., Kaur, J., Sah, S. P., Singh, R., & Pawar, S. V. (2023). Lignin-chitosan biocomposite film for antimicrobial activity: Fabrication, characterization and in-vitro evaluation. *Materials Letters*, *337*. https://doi.org/10.1016/j.matlet.2023.133956

Puppi, D., Pecorini, G., & Chiellini, F. (2019). Biomedical processing of polyhydroxyalkanoates. In *Bioengineering* (Vol. 6, Issue 4). MDPI AG. https://doi.org/10.3390/bioengineering6040108

Queirós, D., Rossetti, S., & Serafim, L. S. (2014). PHA production by mixed cultures: A way to valorize wastes from pulp industry. *Bioresource Technology*, *157*, 197–205. https://doi.org/10.1016/j.biortech.2014.01.099

Querido, D., Vieira, T., Ferreira, J. L., Henriques, C., Borges, J. P., & Silva, J. C. (2022). Study on the Incorporation of Chitosan Flakes in Electrospun Polycaprolactone Scaffolds. *Polymers*, *14*(8). https://doi.org/10.3390/polym14081496

Rai, R., Keshavarz, T., Roether, J. A., Boccaccini, A. R., & Roy, I. (2011). Medium chain length polyhydroxyalkanoates, promising new biomedical materials for the future. In *Materials Science and Engineering R: Reports* (Vol. 72, Issue 3, pp. 29–47). Elsevier Ltd. https://doi.org/10.1016/j.mser.2010.11.002

Rani Raju, N., Silina, E., Stupin, V., Manturova, N., Chidambaram, S. B., & Achar, R. R. (2022). Multifunctional and Smart Wound Dressings—A Review on Recent Research Advancements in Skin Regenerative Medicine. In *Pharmaceutics* (Vol. 14, Issue 8). MDPI. https://doi.org/10.3390/pharmaceutics14081574

Rebocho, A. T., Pereira, J. R., Freitas, F., Neves, L. A., Alves, V. D., Sevrin, C., Grandfils, C., & Reis, M. A. M. (2019). Production of medium-chain length polyhydroxyalkanoates by Pseudomonas citronellolis grown in apple pulp waste. *Applied Food Biotechnology*, *6*(1), 71–82. https://doi.org/10.22037/afb.v6i1.21793

Rebocho, A. T., Pereira, J. R., Neves, L. A., Alves, V. D., Sevrin, C., Grandfils, C., Freitas, F., & Reis, M. A. M. (2020). Preparation and characterization of films based on a natural p(3hb)/mcl-pha blend obtained through the co-culture of cupriavidus necator and pseudomonas citronellolis in apple pulp waste. *Bioengineering*, *7*(2). https://doi.org/10.3390/bioengineering7020034

Reddy, V. U. N., Ramanaiah, S. V., Reddy, M. V., & Chang, Y. C. (2022). Review of the Developments of Bacterial Medium-Chain-Length Polyhydroxyalkanoates (mcl-PHAs). In *Bioengineering* (Vol. 9, Issue 5). MDPI. https://doi.org/10.3390/bioengineering9050225

Reignier, J., & Huneault, M. A. (2006). Preparation of interconnected poly(ε{lunate}-caprolactone) porous scaffolds by a combination of polymer and salt particulate leaching. *Polymer*, *47*(13), 4703–4717. https://doi.org/10.1016/j.polymer.2006.04.029

Ribeiro, M. E. A., Checca Huaman, N. R., Gomez, J. G. C., & Rodríguez, R. J. S. (2023). Poly(3-hydroxybutyrate-co-3-hydroxyvalerate) and amino-functionalized nanodiamond bionanocomposites for bone tissue defect repair. *International Journal of Biological Macromolecules*, *226*, 1041–1053. https://doi.org/10.1016/j.ijbiomac.2022.11.221

Riesco, R., Boyer, L., Blosse, S., Lefebvre, P. M., Assemat, P., Leichle, T., Accardo, A., & Malaquin, L. (2019). Water-in-PDMS Emulsion Templating of Highly Interconnected Porous Architectures for 3D Cell Culture. *ACS Applied Materials and Interfaces*, *11*(32), 28631–28640. https://doi.org/10.1021/acsami.9b07564

Righetti, M. C., Cinelli, P., Aliotta, L., Bianchi, E., Tricoli, F., Seggiani, M., & Lazzeri, A. (2022). Immiscible PHB/PBS and PHB/PBSA blends: morphology, phase composition and modelling of elastic modulus. *Polymer International*, *71*(1), 47–56. https://doi.org/10.1002/pi.6282

Rincon-Granados, K. L., Vázquez-Olmos, A. R., Rodríguez-Hernández, A. P., Prado-Prone, G., Garibay-Febles, V., Almanza-Arjona, Y. C., Sato-Berrú, R. Y., Mata-Zamora, E., Silva-Bermúdez, P. S., & Vega-Jiménez, A. (2023). Bactericidal and Cytotoxic Study of Hybrid Films Based on NiO and NiFe2O4 Nanoparticles in Poly-3-hydroxybutyrate. *Journal of Cluster Science*. https://doi.org/10.1007/s10876-023-02467-y

Rodríguez-Tobías, H., Morales, G., Ledezma, A., Romero, J., Saldívar, R., Langlois, V., Renard, E., & Grande, D. (2016). Electrospinning and electrospraying techniques for designing novel

antibacterial poly(3-hydroxybutyrate)/zinc oxide nanofibrous composites. *Journal of Materials Science*, *51*(18), 8593–8609. https://doi.org/10.1007/s10853-016-0119-x

Ruiz, I., Hermida, É. B., & Baldessari, A. (2011). Fabrication and characterization of porous PHBV scaffolds for tissue engineering. *Journal of Physics: Conference Series*, *332*(1). https://doi.org/10.1088/1742-6596/332/1/012028

Ryltseva, G. A., Dudaev, A. E., Menzyanova, N. G., Volova, T. G., Alexandrushkina, N. A., Efimenko, A. Y., & Shishatskaya, E. I. (2023). Influence of PHA Substrate Surface Characteristics on the Functional State of Endothelial Cells. *Journal of Functional Biomaterials*, *14*(2). https://doi.org/10.3390/jfb14020085

Sadeghi-Aghbash, M., Rahimnejad, M., Adeli, H., & Feizi, F. (2023). Wound Healing: An Overview of Wound Dressings on Health Care. *Current Pharmaceutical Biotechnology*, *24*(9), 1079–1093. https://doi.org/10.2174/1389201023666220913153725

Santamaria, N., Woo, K., Beeckman, D., Alves, P., Cullen, B., Gefen, A., Lázaro-Martínez, J. L., Lev-Tov, H., Najafi, B., Sharpe, A., & Swanson, T. (2023). Clinical performance characteristics for bordered foam dressings in the treatment of complex wounds: An international wound dressing technology expert panel review. *International Wound Journal*. https://doi.org/10.1111/iwj.14217

Sedlacek, P., Pernicova, I., Novackova, I., Kourilova, X., Kalina, M., Kovalcik, A., Koller, M., Nebesarova, J., Krzyzanek, V., Hrubanova, K., Masilko, J., Slaninova, E., Trudicova, M., & Obruca, S. (2020). Introducing the newly isolated bacterium Aneurinibacillus sp. H1 as an auspicious thermophilic producer of various polyhydroxyalkanoates (PHA) copolymers-2. Material study on the produced copolymers. *Polymers*, *12*(6). https://doi.org/10.3390/POLYM12061298

Sharma, A., Dheer, D., Singh, I., Puri, V., & Kumar, P. (2023). Phytoconstituent-Loaded Nanofibrous Meshes as Wound Dressings: A Concise Review. In *Pharmaceutics* (Vol. 15, Issue 4). Multidisciplinary Digital Publishing Institute (MDPI). https://doi.org/10.3390/pharmaceutics15041058

Sharma, P. K., Munir, R. I., de Kievit, T., & Levin, D. B. (2017). Synthesis of polyhydroxyalkanoates (PHAs) from vegetable oils and free fatty acids by wild-type and mutant strains of

Pseudomonas chlororaphis. *Canadian Journal of Microbiology*, *63*(12), 1009–1024. https://doi.org/10.1139/cjm-2017-0412

Shen, M. Y., Chu, C. Y., Sawatdeenarunat, C., & Bhuyar, P. (2023). Production, downstream processing, and characterization of polyhydroxyalkanoates (PHAs) boosted by pyruvate supplement using mixed microbial culture (MMC) and organic wastewater. *Biomass Conversion and Biorefinery*, *13*(17), 15861–15869. https://doi.org/10.1007/s13399-021-02170-w

Shen, Z., Zhang, C., Wang, T., & Xu, J. (2023). Advances in Functional Hydrogel Wound Dressings: A Review. In *Polymers* (Vol. 15, Issue 9). MDPI. https://doi.org/10.3390/polym15092000

Shi, S., Wu, H., Zhi, C., Yang, J., Si, Y., Ming, Y., Fei, B., & Hu, J. (2023). A skin-like nanostructured membrane for advanced wound dressing. *Composites Part B: Engineering*, *250*, 110438. https://doi.org/10.1016/j.compositesb.2022.110438

Shishatskaya, E. I., Demidenko, A. V., Sukovatyi, A. G., Dudaev, A. E., Mylnikov, A. V., Kisterskij, K. A., & Volova, T. G. (2023). Three-Dimensional Printing of Poly(3-hydroxybutyrate-co-3-hydroxyvalerate) [P(3HB-co-3HV)] Biodegradable Scaffolds: Properties, In Vitro and In Vivo Evaluation. *International Journal of Molecular Sciences*, *24*(16). https://doi.org/10.3390/ijms241612969

Silva, F., Matos, M., Pereira, B., Ralo, C., Pequito, D., Marques, N., Carvalho, G., & Reis, M. A. M. (2022). An integrated process for mixed culture production of 3-hydroxyhexanoate-rich polyhydroxyalkanoates from fruit waste. *Chemical Engineering Journal*, *427*. https://doi.org/10.1016/j.cej.2021.131908

Singh, S., Sithole, B., Lekha, P., Permaul, K., & Govinden, R. (2021). Optimization of cultivation medium and cyclic fed-batch fermentation strategy for enhanced polyhydroxyalkanoate production by Bacillus thuringiensis using a glucose-rich hydrolyzate. *Bioresources and Bioprocessing*, *8*(1). https://doi.org/10.1186/s40643-021-00361-x

Skibiński, S., Czechowska, J. P., Guzik, M., Vivcharenko, V., Przekora, A., Szymczak, P., & Zima, A. (2023). Scaffolds based on β tricalcium phosphate and polyhydroxyalkanoates as biodegradable and bioactive bone substitutes with enhanced physicochemical properties. *Sustainable Materials and Technologies*, *38*. https://doi.org/10.1016/j.susmat.2023.e00722

Solanki, D., Vinchhi, P., & Patel, M. M. (2023). Design Considerations, Formulation Approaches, and Strategic Advances of Hydrogel Dressings for Chronic Wound Management. In *ACS Omega* (Vol. 8, Issue 9, pp. 8172–8189). American Chemical Society. https://doi.org/10.1021/acsomega.2c06806

Solarz, D., Witko, T., Karcz, R., Malagurski, I., Ponjavic, M., Levic, S., Nesic, A., Guzik, M., Savic, S., & Nikodinovic-Runic, J. (2023). Biological and physiochemical studies of electrospun polylactid/polyhydroxyoctanoate PLA/P(3HO) scaffolds for tissue engineering applications. *RSC Advances*, *13*(34), 24112–24128. https://doi.org/10.1039/d3ra03021k

Song, X., Padrão, J., Fernandes, M., Ribeiro, A. I., Melro, L., Alves, C., Yu, L., & Zille, A. (2023). Antibacterial hydrogel dressings and their applications in wound treatment. In *Antimicrobial Dressings* (pp. 153–185). Elsevier. https://doi.org/10.1016/B978-0-323-95074-9.00010-5

Spasova, M., Stoilova, O., Manolova, N., Rashkov, I., & Naydenov, M. (2020). Electrospun eco-friendly materials based on poly(3-hydroxybutyrate) (PHB) and TiO2 with antifungal activity prospective for esca treatment. *Polymers*, *12*(6). https://doi.org/10.3390/polym12061384

Sudesh, K., Abe, H., & Doi, Y. (2000). Synthesis, structure and properties of polyhydroxyalkanoates: biological polyesters. *Progress in Polymer Science*, *25*(10), 1503–1555. https://doi.org/10.1016/S0079-6700(00)00035-6

Surisaeng, J., Kanabenja, W., Passornraprasit, N., Aumnate, C., & Potiyaraj, P. (2022). Polyhydroxybutyrate/polylactic acid blends: An alternative feedstock for 3D printed bone scaffold model. *Journal of Physics: Conference Series*, *2175*(1). https://doi.org/10.1088/1742-6596/2175/1/012021

Tan, G. Y. A., Chen, C. L., Li, L., Ge, L., Wang, L., Razaad, I. M. N., Li, Y., Zhao, L., Mo, Y., & Wang, J. Y. (2014). Start a research on biopolymer polyhydroxyalkanoate (PHA): A review. In *Polymers* (Vol. 6, Issue 3, pp. 706–754). Molecular Diversity Preservation International. https://doi.org/10.3390/polym6030706

Tan, G.-Y., Chen, C.-L., Li, L., Ge, L., Wang, L., Razaad, I., Li, Y., Zhao, L., Mo, Y., & Wang, J.-Y. (2014). Start a Research on Biopolymer Polyhydroxyalkanoate (PHA): A Review. *Polymers*, *6*(3), 706–754. https://doi.org/10.3390/polym6030706

Tanikkul, P., Sullivan, G. L., Sarp, S., & Pisutpaisal, N. (2020). Biosynthesis of medium chain length polyhydroxyalkanoates (mcl-PHAs) from palm oil. *Case Studies in Chemical and Environmental Engineering*, *2*. https://doi.org/10.1016/j.cscee.2020.100045

Tawonsawatruk, T., Panaksri, A., Hemstapat, R., Praenet, P., Rattanapinyopituk, K., Boonyagul, S., & Tanadchangsaeng, N. (2023). Fabrication and biological properties of artificial tendon composite from medium chain length polyhydroxyalkanoate. *Scientific Reports*, *13*(1). https://doi.org/10.1038/s41598-023-48075-8

Thangavel, P., Saravanakumar, I., Sundaram, M. K., Rathinam, B., & Muthuvijayan, V. (2024). Preparation and characterization of a jelly fig (Ficus awkeotsang Makino) polysaccharide-based bioactive 3D scaffold for improved vascularization and skin tissue engineering applications. *International Journal of Biological Macromolecules*, *259*. https://doi.org/10.1016/j.ijbiomac.2024.129199

Tiwari, N., Kumar, D., Priyadarshani, A., Jain, G. K., Mittal, G., Kesharwani, P., & Aggarwal, G. (2023). Recent progress in polymeric biomaterials and their potential applications in skin regeneration and wound care management. In *Journal of Drug Delivery Science and Technology* (Vol. 82). Editions de Sante. https://doi.org/10.1016/j.jddst.2023.104319

Tomietto, P., Loulergue, P., Paugam, L., & Audic, J. L. (2020). Biobased polyhydroxyalkanoate (PHA) membranes: Structure/performances relationship. *Separation and Purification Technology*, *252*. https://doi.org/10.1016/j.seppur.2020.117419

Vach Agocsova, S., Culenova, M., Birova, I., Omanikova, L., Moncmanova, B., Danisovic, L., Ziaran, S., Bakos, D., & Alexy, P. (2023). Resorbable Biomaterials Used for 3D Scaffolds in Tissue Engineering: A Review. In *Materials* (Vol. 16, Issue 12). MDPI. https://doi.org/10.3390/ma16124267

Vázquez-González, Y., Prieto, C., Stojanovic, M., Torres, C. A. V., Freitas, F., Ragazzo-Sánchez, J. A., Calderón-Santoyo, M., & Lagaron, J. M. (2022). Preparation and Characterization of Electrospun Polysaccharide FucoPol-Based Nanofiber Systems. *Nanomaterials*, *12*(3). https://doi.org/10.3390/nano12030498

Vieira, T., Carvalho Silva, J., Botelho do Rego, A. M., Borges, J. P., & Henriques, C. (2019). Electrospun biodegradable chitosan based-poly(urethane urea) scaffolds for soft tissue

engineering. *Materials Science and Engineering C*, *103*. https://doi.org/10.1016/j.msec.2019.109819

Vieira, T., Rebelo, A. M., Borges, J. P., Henriques, C., & Silva, J. C. (2024). Electrospun Polycaprolactone Membranes Expanded with Chitosan Granules for Cell Infiltration. *Polymers*, *16*(4), 527. https://doi.org/10.3390/polym16040527

Vieira, T., Silva, J. C., Borges, J. P., & Henriques, C. (2018). Synthesis, electrospinning and in vitro test of a new biodegradable gelatin-based poly(ester urethane urea) for soft tissue engineering. *European Polymer Journal*, *103*, 271–281. https://doi.org/10.1016/j.eurpolymj.2018.04.005

Volova, T. G., Shumilova, A. A., Nikolaeva, E. D., Kirichenko, A. K., & Shishatskaya, E. I. (2019). Biotechnological wound dressings based on bacterial cellulose and degradable copolymer P(3HB/4HB). In *International Journal of Biological Macromolecules* (Vol. 131, pp. 230–240). Elsevier B.V. https://doi.org/10.1016/j.ijbiomac.2019.03.068

Volova, T. G., Vinogradova, O. N., Zhila, N. O., Peterson, I. V., Kiselev, E. G., Vasiliev, A. D., Sukovatiy, A. G., & Shishatskaya, E. I. (2016). Properties of a novel quaterpolymer P(3HB/4HB/3HV/3HHx). *Polymer*, *101*, 67–74. https://doi.org/10.1016/j.polymer.2016.08.048

Volova, T., Kiselev, E., Nemtsev, I., Lukyanenko, Sukovatyi, A., Kuzmin, A., Ryltseva, G., & Shishatskaya, E. (2021). Properties of degradable polyhydroxyalkanoates with different monomer compositions. *International Journal of Biological Macromolecules*, *182*, 98–114. https://doi.org/10.1016/j.ijbiomac.2021.04.008

Walsh, M., O'Connor, K., Babu, R., Woods, T., & Kenny, S. (2015). Plant oils and products of their hydrolysis as substrates for polyhydroxyalkanoate synthesis. *Chemical and Biochemical Engineering Quarterly*, *29*(2), 123–133. https://doi.org/10.15255/CABEQ.2014.2252

Wang, L., Wang, Z. H., Shen, C. Y., You, M. L., Xiao, J. F., & Chen, G. Q. (2010). Differentiation of human bone marrow mesenchymal stem cells grown in terpolyesters of 3-hydroxyalkanoates scaffolds into nerve cells. *Biomaterials*, *31*(7), 1691–1698. https://doi.org/10.1016/j.biomaterials.2009.11.053

Wang, W., Ummartyotin, S., & Narain, R. (2023). Advances and challenges on hydrogels for wound dressing. In *Current Opinion in Biomedical Engineering* (Vol. 26). Elsevier B.V. https://doi.org/10.1016/j.cobme.2022.100443

Wang, Y., Zhang, X., Tian, X., Wang, Y., Xing, X., & Song, S. (2024). Research progress on the functions, preparation and detection methods of L-fucose. In *Food Chemistry* (Vol. 433). Elsevier Ltd. https://doi.org/10.1016/j.foodchem.2023.137393

Ward, A. C., Dubey, P., Basnett, P., Lika, G., Newman, G., Corrigan, D. K., Russell, C., Kim, J., Chakrabarty, S., Connolly, P., & Roy, I. (2020). Toward a Closed Loop, Integrated Biocompatible Biopolymer Wound Dressing Patch for Detection and Prevention of Chronic Wound Infections. *Frontiers in Bioengineering and Biotechnology*, *8*. https://doi.org/10.3389/fbioe.2020.01039

Wróbel-Kwiatkowska, M., Kropiwnicki, M., Żebrowski, J., Beopoulos, A., Dymińska, L., Hanuza, J., & Rymowicz, W. (2019). Effect of mcl-PHA synthesis in flax on plant mechanical properties and cell wall composition. *Transgenic Research*, *28*(1), 77–90. https://doi.org/10.1007/s11248-018-0105-y

Xu, R., Fang, Y., Zhang, Z., Cao, Y., Yan, Y., Gan, L., Xu, J., & Zhou, G. (2023). Recent Advances in Biodegradable and Biocompatible Synthetic Polymers Used in Skin Wound Healing. In *Materials* (Vol. 16, Issue 15). Multidisciplinary Digital Publishing Institute (MDPI). https://doi.org/10.3390/ma16155459

Yadav, A., Pal, J., Nandan, B., & Srivastava, R. K. (2019). Macroporous scaffolds of cross-linked Poly(ε-caprolactone)via high internal phase emulsion templating. *Polymer*, *176*, 66–73. https://doi.org/10.1016/j.polymer.2019.05.034

Yang, J., & Wang, S. (2023). Polysaccharide-Based Multifunctional Hydrogel Bio-Adhesives for Wound Healing: A Review. In *Gels* (Vol. 9, Issue 2). MDPI. https://doi.org/10.3390/gels9020138

Ye, H. M., Wang, Z., Wang, H. H., Chen, G. Q., & Xu, J. (2010). Different thermal behaviors of microbial polyesters poly(3-hydroxybutyrate-co-3-hydroxyvalerate-co-3-hydroxyhexanoate) and poly(3-hydroxybutyrate-co-3-hydroxyhexanoate). *Polymer*, *51*(25), 6037–6046. https://doi.org/10.1016/j.polymer.2010.10.030

Yildiz, H., & Karatas, N. (2018). Microbial exopolysaccharides: Resources and bioactive properties. In *Process Biochemistry* (Vol. 72, pp. 41–46). Elsevier Ltd. https://doi.org/10.1016/j.procbio.2018.06.009

Yousefi, A. M., & Wnek, G. E. (2024). Poly(hydroxyalkanoates): Emerging Biopolymers in Biomedical Fields and Packaging Industries for a Circular Economy. *Biomedical Materials & Devices*. https://doi.org/10.1007/s44174-024-00166-4

Yu, Y., Shen, M., Song, Q., & Xie, J. (2018). Biological activities and pharmaceutical applications of polysaccharide from natural resources: A review. In *Carbohydrate Polymers* (Vol. 183, pp. 91–101). Elsevier Ltd. https://doi.org/10.1016/j.carbpol.2017.12.009

Zahra, F. T., Quick, Q., & Mu, R. (2023). Electrospun PVA Fibers for Drug Delivery: A Review. In *Polymers* (Vol. 15, Issue 18). Multidisciplinary Digital Publishing Institute (MDPI). https://doi.org/10.3390/polym15183837

Zhang, H., Ma, L., Wang, Z., & Chen, G. (2009). Biosynthesis and characterization of 3-hydroxyalkanoate terpolyesters with adjustable properties by Aeromonas hydrophila. *Biotechnology and Bioengineering*, *104*(3), 582–589. https://doi.org/10.1002/bit.22409

Zhang, T., Li, J., Wang, Y., Han, W., Wei, Y., Hu, Y., Liang, Z., Lian, X., & Huang, D. (2023). Hydroxyapatite/Polyurethane Scaffolds for Bone Tissue Engineering. *Tissue Engineering - Part B: Reviews*. https://doi.org/10.1089/ten.teb.2023.0073

Zhang, T., Sanguramath, R. A., Israel, S., & Silverstein, M. S. (2019). Emulsion Templating: Porous Polymers and beyond. In *Macromolecules* (Vol. 52, Issue 15, pp. 5445–5479). American Chemical Society. https://doi.org/10.1021/acs.macromol.8b02576

Zhao, W., & Chen, G. Q. (2007). Production and characterization of terpolyester poly(3-hydroxybutyrate-co-3-hydroxyvalerate-co-3-hydroxyhexanoate) by recombinant Aeromonas hydrophila 4AK4 harboring genes phaAB. *Process Biochemistry*, *42*(9), 1342–1347. https://doi.org/10.1016/j.procbio.2007.07.006

Zhila, N. O., Kiselev, E. G., Volkov, V. V., Mezenova, O. Y., Sapozhnikova, K. Y., Shishatskaya, E. I., & Volova, T. G. (2023). Properties of Degradable Polyhydroxyalkanoates Synthesized from New Waste Fish Oils (WFOs). *International Journal of Molecular Sciences*, *24*(19). https://doi.org/10.3390/ijms241914919

Zhila, N., & Shishatskaya, E. (2018). Properties of PHA bi-, ter-, and quarter-polymers containing 4-hydroxybutyrate monomer units. *International Journal of Biological Macromolecules*, *111*, 1019–1026. https://doi.org/10.1016/j.ijbiomac.2018.01.130

Zhou, W., Colpa, D. I., Geurkink, B., Euverink, G. J. W., & Krooneman, J. (2022). The impact of carbon to nitrogen ratios and pH on the microbial prevalence and polyhydroxybutyrate production levels using a mixed microbial starter culture. *Science of the Total Environment*, *811*. https://doi.org/10.1016/j.scitotenv.2021.152341

Zhu, J., Zhou, H., Gerhard, E. M., Zhang, S., Parra Rodríguez, F. I., Pan, T., Yang, H., Lin, Y., Yang, J., & Cheng, H. (2023). Smart bioadhesives for wound healing and closure. In *Bioactive Materials* (Vol. 19, pp. 360–375). KeAi Communications Co. https://doi.org/10.1016/j.bioactmat.2022.04.020

Zhu, X., Zhong, T., Huang, R., & Wan, A. (2015). Preparation of hydrophilic poly(lactic acid) tissue engineering scaffold via (PLA)-(PLA-b-PEG)-(PEG) solution casting and thermal-induced surface structural transformation. *Journal of Biomaterials Science, Polymer Edition*, *26*(17), 1286–1296. https://doi.org/10.1080/09205063.2015.1088125

Zhuikova, Y., Zhuikov, V., & Varlamov, V. (2022). Biocomposite Materials Based on Poly(3-hydroxybutyrate) and Chitosan: A Review. In *Polymers* (Vol. 14, Issue 24). MDPI. https://doi.org/10.3390/polym14245549

A

APPENDIX - CHAPTER 2

A.1 Gel Permeation and Size Exclusion Chromatography (GPC/SEC)

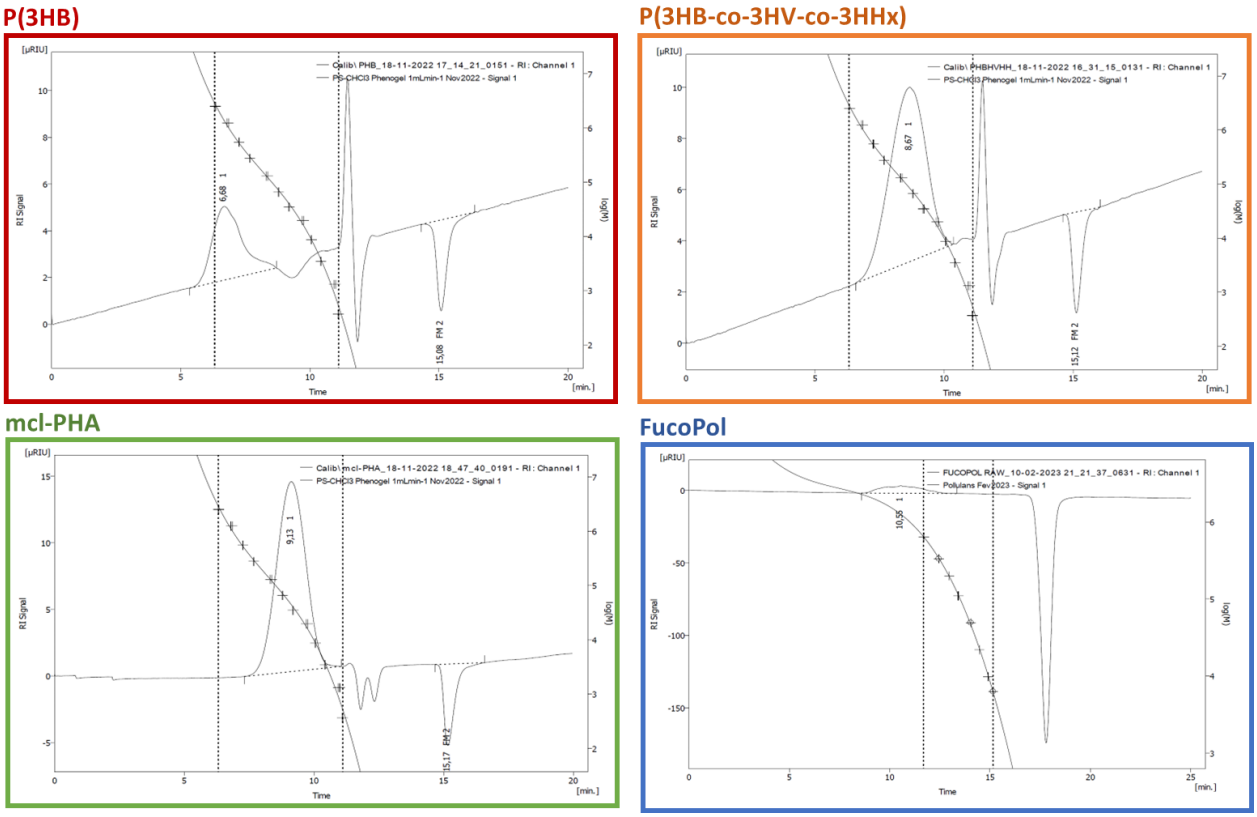

Figure A.1 - Chromatogram of molecular weight determination for P(3HB), P(3HB-co-3HV-co-3HHx), mcl-PHA and FucoPol.

A.2 Differential Scanning Calorimetry (DSC)

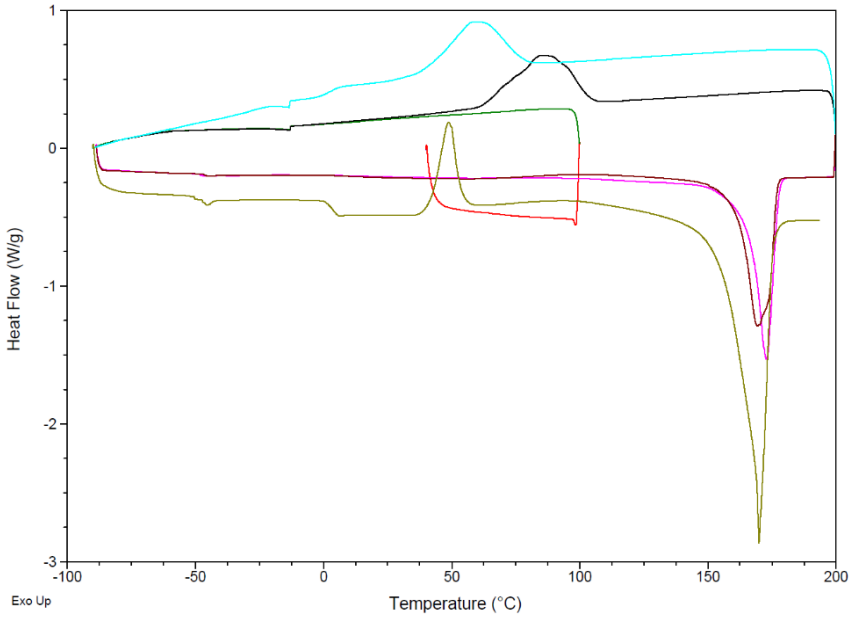

Figure A.2 - DSC scan for P(3HB) with all heating and cooling cycle, where **RED** is the first heating ramp from room temperature to 100 °C; **GREEN** is the first cooling ramp from 100 to -90 °C; **PINK** is the is the second heating ramp from -90 to 200 °C; **BLACK** is the is the second cooling ramp from 200 to -90 °C; **BROWN** is the is the third heating ramp from -90 to 200°C; **LIGHT BLUE** is the is the first cooling ramp from 200 to -90 °C; **YELLOW** is the is the last heating ramp from -90 to 200 °C.

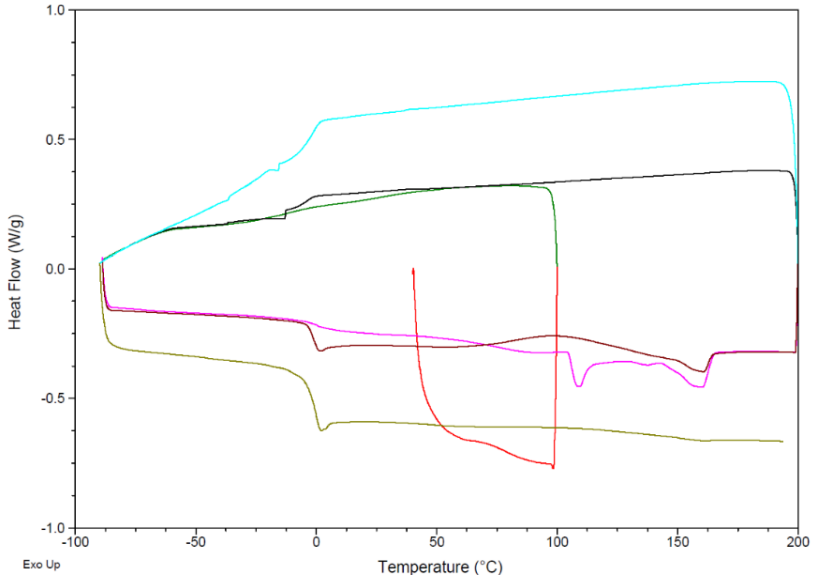

Figure A.3 - DSC scan for P(3HB-co-3HV-co-3HHx) with all heating and cooling cycle, where **RED** is the first heating ramp from room temperature to 100 °C; **GREEN** is the first cooling ramp from 100 to -90 °C; **PINK** is the is the second heating ramp from -90 to 200 °C; **BLACK** is the is the second cooling ramp from 200 to -90 °C; **BROWN** is

the is the third heating ramp from -90 to 200°C; LIGHT BLUE is the is the first cooling ramp from 200 to -90 °C; YELLOW is the is the last heating ramp from -90 to 200 °C.

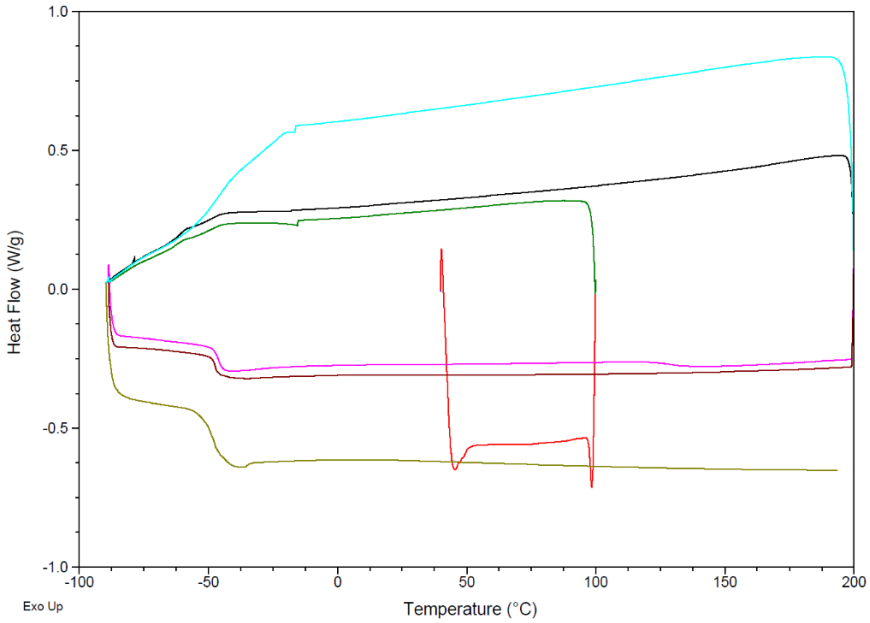

Figure A.4 - DSC scan for mcl-PHA with all heating and cooling cycle, where RED is the first heating ramp from room temperature to 100 °C; GREEN is the first cooling ramp from 100 to -90 °C; PINK is the is the second heating ramp from -90 to 200 °C; **BLACK** is the is the second cooling ramp from 200 to -90 °C; BROWN is the is the third heating ramp from -90 to 200°C; LIGHT BLUE is the is the first cooling ramp from 200 to -90 °C; YELLOW is the is the last heating ramp from -90 to 200 °C.

B

APPENDIX - CHAPTER 3

B.1 Mercury Porosimetry for Emulsion templated Scaffolds

Table B.1 - Mercury porosimetry intrusion data summary results for P(3HB) and P(3HB-co-3HV-co-3HHx) Emulsion templated Scaffolds.

P(3HB) + Water Emulsion Templating	Intrusion Data Summary
	Total Intrusion Volume = 2.7795 mL/g
	Total Pore Area = 12.565 m^2/g
	Median Pore Diameter (Volume) = 19.8481 µm
	Median Pore Diameter (Area) = 0.0409 µm
	Average Pore Diameter (4V/A) = 0.8849 µm
	Porosity = 82.1615 %
	Stem Volume Used = 27 %

P(3HB-co-3HV-co-3HHx) + Water Emulsion Templating	Intrusion Data Summary
	Total Intrusion Volume = 0.7882 mL/g
	Total Pore Area = 10.469 m^2/g
	Median Pore Diameter (Volume) = 63.0471 µm
	Median Pore Diameter (Area) = 0.0107 µm
	Average Pore Diameter (4V/A) = 0.3012 µm
	Porosity = 49.8328 %
	Stem Volume Used = 31 %

B.2 ANOVA Statistical Analysis of Adhesion and Proliferation Tests for Emulsion templated Scaffolds

Table B.2 - ANOVA statistical analysis with Bonferroni's multiple comparison test of adhesion (after 1 day of cell culture) for PHA emulsion templated scaffolds.

Table Analyzed	Adhesion after 24h
One-way analysis of variance	
P value	0,0021
P value summary	**
Are means signif. different? (P < 0.05)	Yes
Number of groups	3
F	88,71
R squared	0,9834

ANOVA Table	SS	df	MS
Treatment (between columns)	5462	2	2731
Residual (within columns)	92,35	3	30,78
Total	5554	5	

Bonferroni's Multiple Comparison Test	Mean Diff.	t	Significant?	Summary	95% CI of diff
P(3HB) vs P(3HB-3HV-3HHx)	17,18	3,097	No	ns	-9.765 to 44.13
P(3HB) vs Cell Control	-53,66	9,671	Yes	**	-80.60 to -26.71
P(3HB-3HV-3HHx) vs Cell Control	-70,84	12,77	Yes	**	-97.79 to -43.89

Table B.3 - ANOVA statistical analysis with Bonferroni's multiple comparison test of proliferation (after 4 days of cell culture) for PHA emulsion templated scaffolds.

Table Analyzed	Proliferation after 4 days
One-way analysis of variance	
P value	0,0935
P value summary	ns
Are means signif. different? (P < 0.05)	No
Number of groups	3
F	5,782
R squared	0,7940

ANOVA Table	SS	df	MS
Treatment (between columns)	7035	2	3517
Residual (within columns)	1825	3	608,4
Total	8860	5	

Bonferroni's Multiple Comparison Test	Mean Diff.	t	Significant?	Summary	95% CI of diff
P(3HB) vs P(3HB-3HV-3HHx)	58,19	2,359	No	ns	-61.60 to 178.0
P(3HB) vs Cell Control	-23,22	0,9413	No	ns	-143.0 to 96.57
P(3HB-3HV-3HHx) vs Cell Control	-81,41	3,300	No	ns	-201.2 to 38.38

Table B.4 - ANOVA statistical analysis with Bonferroni's multiple comparison test of proliferation (after 7 days of cell culture) for PHA emulsion templated scaffolds.

Table Analyzed	Proliferation after 7 days
One-way analysis of variance	
P value	0,0035
P value summary	**
Are means signif. different? (P < 0.05)	Yes
Number of groups	3
F	63,37
R squared	0,9769

ANOVA Table	SS	df	MS
Treatment (between columns)	27740	2	13870
Residual (within columns)	656,6	3	218,9
Total	28400	5	

Bonferroni's Multiple Comparison Test	Mean Diff.	t	Significant	Summary	95% CI of diff
P(3HB) vs P(3HB-3HV-3HHx)	166,6	11,26	Yes	**	94.70 to 238.4
P(3HB) vs Cell Control	82,40	5,570	Yes	*	10.55 to 154.3
P(3HB-3HV-3HHx) vs Cell Control	-84,15	5,688	Yes	*	-156.0 to -12.30

B.3 Mercury Porosimetry for Hot-Pressing Salt Leaching Scaffolds

Table B.5 - Mercury porosimetry intrusion data summary results for P(3HB) and P(3HB-co-3HV-co-3HHx) Hot-Pressing Salt Leaching Scaffolds

P(3HB) Hot-Pressing Salt Leaching	Intrusion Data Summary
	Total Intrusion Volume = 1.4168 mL/g
	Total Pore Area = 6.788 m^2/g
	Median Pore Diameter (Volume) = 97.8529 µm
	Median Pore Diameter (Area) = 0.0100 µm
	Average Pore Diameter (4V/A) = 0.8348 µm
	Porosity = 67.7301 %
	Stem Volume Used = 29 %

P(3HB-co-3HV-co-3HHx) Hot-Pressing Salt Leaching	Intrusion Data Summary
	Total Intrusion Volume = 3.9201 mL/g
	Total Pore Area = 0.590 m^2/g
	Median Pore Diameter (Volume) = 36.5067 µm
	Median Pore Diameter (Area) = 21.9329 µm
	Average Pore Diameter (4V/A) = 26.5728 µm
	Porosity = 87.1434 %
	Stem Volume Used = 40 %

B.4 ANOVA Statistical Analysis of Adhesion and Proliferation Tests for Hot-Pressing Salt Leaching Scaffolds

Table B.6 - ANOVA statistical analysis with Bonferroni's multiple comparison test of adhesion (after 1 day of cell culture) for PHA hot-pressing salt leaching scaffolds.

Table Analyzed	Adhesion after 24h
One-way analysis of variance	
P value	< 0.0001
P value summary	***
Are means signif. different? (P < 0.05)	Yes
Number of groups	3
F	79,58
R squared	0,9409

ANOVA Table	SS	df	MS
Treatment (between columns)	15470	2	7734
Residual (within columns)	971,9	10	97,19
Total	16440	12	

Bonferroni's Multiple Comparison Test	Mean Diff.	t	Significant? P < 0.05?	Summary	95% CI of diff
P(3HB) vs P(3HB-3HV-3HHx)	14,62	1,942	No	ns	-6.987 to 36.23
P(3HB) vs Cell Control	-60,01	8,609	Yes	***	-80.02 to -40.01
P(3HB-3HV-3HHx) vs Cell Control	-74,64	11,73	Yes	***	-92.90 to -56.37

Table B.7 - ANOVA statistical analysis with Bonferroni's multiple comparison test of proliferation (after 4 days of cell culture) for PHA hot-pressing salt leaching scaffolds.

Table Analyzed	Proliferation after 4 days
One-way analysis of variance	
P value	0,0111
P value summary	*
Are means signif. different? (P < 0.05)	Yes
Number of groups	3
F	16,97
R squared	0,8946

ANOVA Table	SS	df	MS
Treatment (between columns)	5869	2	2935
Residual (within columns)	691,8	4	173,0
Total	6561	6	

Bonferroni's Multiple Comparison Test	Mean Diff.	t	Significant? P < 0.05?	Summary	95% CI of diff
P(3HB) vs P(3HB-3HV-3HHx)	-36,35	2,764	No	ns	-88.44 to 15.74
P(3HB) vs Cell Control	-69,68	5,804	Yes	*	-117.2 to -22.13
P(3HB-3HV-3HHx) vs Cell Control	-33,33	2,776	No	ns	-80.88 to 14.22

Table B.8 - ANOVA statistical analysis with Bonferroni's multiple comparison test of proliferation (after 7 days of cell culture) for PHA hot-pressing salt leaching scaffolds.

Table Analyzed	Proliferation after 7 days
One-way analysis of variance	
P value	< 0.0001
P value summary	***
Are means signif. different? (P < 0.05)	Yes
Number of groups	3
F	144,0
R squared	0,9796

ANOVA Table	SS	df	MS
Treatment (between columns)	28380	2	14190
Residual (within columns)	591,2	6	98,53
Total	28970	8	

Bonferroni's Multiple Comparison Test	Mean Diff.	t	Significant	Summary	95% CI of diff
P(3HB) vs P(3HB-3HV-3HHx)	98,31	10,85	Yes	***	68.52 to 128.1
P(3HB) vs Cell Control	-27,92	3,248	No	ns	-56.18 to 0.3400
P(3HB-3HV-3HHx) vs Cell Control	-126,2	16,65	Yes	***	-151.2 to -101.3

B.5 ANOVA Statistical Analysis of Adhesion and Proliferation Tests for both Emulsion templated and Hot-Pressing Salt Leaching Scaffolds

Table B.9 - ANOVA statistical analysis with Bonferroni's multiple comparison test of adhesion (after 1 day of cell culture) for both PHA emulsion templated and hot-pressing salt leaching scaffolds.

Table Analyzed	Adhesion after 24h
One-way analysis of variance	
P value	0,0012
P value summary	**
Are means signif. different? (P < 0.05)	Yes
Number of groups	4
F	17,65
R squared	0,8832

ANOVA Table	SS	df	MS
Treatment (between columns)	757,2	3	252,4
Residual (within columns)	100,1	7	14,30
Total	857,3	10	

Bonferroni's Multiple Comparison Test	Mean Diff.	t	Significant	Summary	95% CI of diff
P(3HB) - Emulsion Templating vs P(3HB-3HV-3HHx) - Emulsion Templating	17,18	4,543	Yes	*	3.432 to 30.93
P(3HB) - Emulsion Templating vs P(3HB) - Hot-Pressing Salt Leaching	6,357	1,841	No	ns	-6.195 to 18.91
P(3HB) - Emulsion vs P(3HB-3HV-3HHx) - Hot-Pressing Salt Leaching	20,98	6,406	Yes	**	9.073 to 32.89
P(3HB-3HV-3HHx) - Emulsion Templating vs P(3HB) - Hot-Pressing Salt Leaching	-10,82	3,136	No	ns	-23.38 to 1.727
P(3HB-3HV-3HHx) - Emulsion Templating vs P(3HB-3HV-3HHx) - Hot-Pressing Salt Leaching	3,799	1,160	No	ns	-8.108 to 15.71
P(3HB) - Hot-Pressing Salt Leaching vs P(3HB-3HV-3HHx) - Hot-Pressing Salt Leaching	14,62	5,063	Yes	**	4.122 to 25.13

Table B.10 - ANOVA statistical analysis with Bonferroni's multiple comparison test of proliferation (after 4 days of cell culture) for both PHA emulsion templated and hot-pressing salt leaching scaffolds.

Table Analyzed	Proliferation after 4 days
One-way analysis of variance	
P value	0,0043
P value summary	**
Are means signif. different? (P < 0.05)	Yes
Number of groups	4
F	26,38
R squared	0,9519

ANOVA Table	SS	df	MS
Treatment (between columns)	4759	3	1586
Residual (within columns)	240,5	4	60,13
Total	5000	7	

Bonferroni's Multiple Comparison Test	Mean Diff.	t	Significant	Summary	95% CI of diff
P(3HB) - Emulsion Templating vs P(3HB-3HV-3HHx) - Emulsion Templating	58,19	7,504	Yes	*	20.57 to 95.80
P(3HB) - Emulsion Templating vs P(3HB) - Hot-Pressing Salt Leaching	42,16	5,438	Yes	*	4.548 to 79.78
P(3HB) - Emulsion vs P(3HB-3HV-3HHx) - Hot-Pressing Salt Leaching	5,816	0,7500	No	ns	-31.80 to 43.43
P(3HB-3HV-3HHx) - Emulsion Templating vs P(3HB) - Hot-Pressing Salt Leaching	-16,02	2,066	No	ns	-53.64 to 21.59
P(3HB-3HV-3HHx) - Emulsion Templating vs P(3HB-3HV-3HHx) - Hot-Pressing Salt Leaching	-52,37	6,754	Yes	*	-89.99 to -14.76
P(3HB) - Hot-Pressing Salt Leaching vs P(3HB-3HV-3HHx) - Hot-Pressing Salt Leaching	-36,35	4,688	No	ns	-73.96 to 1.268

Table B.11 - ANOVA statistical analysis with Bonferroni's multiple comparison test of proliferation (after 7 days of cell culture) for both PHA emulsion templated and hot-pressing salt leaching scaffolds.

Table Analyzed	Proliferation after 7 days
One-way analysis of variance	
P value	< 0.0001
P value summary	***
Are means signif. different? (P < 0.05)	Yes
Number of groups	4
F	182,1
R squared	0,9909

ANOVA Table	SS	df	MS
Treatment (between columns)	65870	3	21960
Residual (within columns)	602,9	5	120,6
Total	66470	8	

Bonferroni's Multiple Comparison Test	Mean Diff.	t	Significant	Summary	95% CI of diff
P(3HB) - Emulsion Templating vs P(3HB-3HV-3HHx) - Emulsion Templating	166,6	15,17	Yes	***	120.2 to 212.9
P(3HB) - Emulsion Templating vs P(3HB) - Hot-Pressing Salt Leaching	133,6	12,16	Yes	***	87.22 to 179.9
P(3HB) - Emulsion vs P(3HB-3HV-3HHx) - Hot-Pressing Salt Leaching	231,9	23,13	Yes	***	189.6 to 274.2
P(3HB-3HV-3HHx) - Emulsion Templating vs P(3HB) - Hot-Pressing Salt Leaching	-33,00	3,005	No	ns	-79.33 to 13.33
P(3HB-3HV-3HHx) - Emulsion Templating vs P(3HB-3HV-3HHx) - Hot-Pressing Salt Leaching	65,31	6,515	Yes	**	23.01 to 107.6
P(3HB) - Hot-Pressing Salt Leaching vs P(3HB-3HV-3HHx) - Hot-Pressing Salt Leaching	98,31	9,807	Yes	**	56.01 to 140.6

C

APPENDIX - CHAPTER 4

C.1 Mercury Porosimetry for Emulsion templated Scaffolds with FucoPol

Table C.12 - Mercury porosimetry intrusion data summary results for P(3HB) and P(3HB-co-3HV-co-3HHx) Emulsion templated Scaffolds with FucoPol.

P(3HB) + FucoPol Emulsion Templating	Intrusion Data Summary
	Total Intrusion Volume = 1.3007 mL/g
	Total Pore Area = 15.335 m²/g
	Median Pore Diameter (Volume) = 40.5718 µm
	Median Pore Diameter (Area) = 0.0166 µm
	Average Pore Diameter (4V/A) = 0.3393 µm
	Porosity = 65.0993 %
	Stem Volume Used = 34 %

P(3HB-co-3HV-co-3HHx) + FucoPol Emulsion Templating	Intrusion Data Summary
	Total Intrusion Volume = 0.5551 mL/g
	Total Pore Area = 8.324 m²/g
	Median Pore Diameter (Volume) = 54.8956 µm
	Median Pore Diameter (Area) = 0.0112 µm
	Average Pore Diameter (4V/A) = 0.2667 µm
	Porosity = 41.6701 %
	Stem Volume Used = 26 %

C.2 ANOVA Statistical Analysis of Adhesion and Proliferation Tests for Emulsion templated Scaffolds with and without FucoPol

Table C.13- ANOVA statistical analysis with Bonferroni's multiple comparison test of adhesion (after 1 day of cell culture) for PHA emulsion templated scaffolds with and without FucoPol.

Table Analyzed	Adhesion after 24h
One-way analysis of variance	
P value	0,0004
P value summary	***
Are means signif. different? (P < 0.05)	Yes
Number of groups	5
F	45,42
R squared	0,9732

ANOVA Table	SS	df	MS
Treatment (between columns)	6249	4	1562
Residual (within columns)	172,0	5	34,40
Total	6421	9	

Bonferroni's Multiple Comparison Test	Mean Diff.	t	Significant? P < 0.05?	Summary	95% CI of diff
P(3HB) vs P(3HB) + FucoPol	4,300	0,7332	No	ns	-23.69 to 32.29
P(3HB) vs P(3HB-3HV-3HHx)	17,18	2,930	No	ns	-10.81 to 45.18
P(3HB) vs P(3HB-3HV-3HHx) + FucoPol	7,380	1,258	No	ns	-20.61 to 35.37
P(3HB) vs Cell Control	-53,66	9,149	Yes	**	-81.65 to -25.66
P(3HB) + FucoPol vs P(3HB-3HV-3HHx)	12,88	2,196	No	ns	-15.11 to 40.88
P(3HB) + FucoPol vs P(3HB-3HV-3HHx) + FucoPol	3,080	0,5252	No	ns	-24.91 to 31.07
P(3HB) + FucoPol vs Cell Control	-57,96	9,882	Yes	**	-85.95 to -29.96
P(3HB-3HV-3HHx) vs P(3HB-3HV-3HHx) + FucoPol	-9,802	1,671	No	ns	-37.80 to 18.19
P(3HB-3HV-3HHx) vs Cell Control	-70,84	12,08	Yes	***	-98.83 to -42.84
P(3HB-3HV-3HHx) + FucoPol vs Cell Control	-61,04	10,41	Yes	**	-89.03 to -33.04

Table C.14 - ANOVA statistical analysis with Bonferroni's multiple comparison test of proliferation (after 4 days of cell culture) for PHA emulsion templated scaffolds with and without FucoPol.

Table Analyzed	Proliferation after 4 days
One-way analysis of variance	
P value	0,0227
P value summary	*
Are means signif. different? (P < 0.05)	Yes
Number of groups	5
F	7,737
R squared	0,8609

ANOVA Table	SS	df	MS
Treatment (between columns)	11730	4	2933
Residual (within columns)	1896	5	379,1
Total	13630	9	

Bonferroni's Multiple Comparison Test	Mean Diff.	t	Significant? P < 0.05?	Summary	95% CI of diff
P(3HB) vs P(3HB) + FucoPol	-44,30	2,275	No	ns	-137.2 to 48.64
P(3HB) vs P(3HB-3HV-3HHx)	58,19	2,988	No	ns	-34.75 to 151.1
P(3HB) vs P(3HB-3HV-3HHx) + FucoPol	-1,734	0,08903	No	ns	-94.67 to 91.21
P(3HB) vs Cell Control	-23,22	1,192	No	ns	-116.2 to 69.72
P(3HB) + FucoPol vs P(3HB-3HV-3HHx)	102,5	5,264	Yes	*	9.548 to 195.4
P(3HB) + FucoPol vs P(3HB-3HV-3HHx) + FucoPol	42,57	2,186	No	ns	-50.37 to 135.5
P(3HB) + FucoPol vs Cell Control	21,08	1,083	No	ns	-71.86 to 114.0
P(3HB-3HV-3HHx) vs P(3HB-3HV-3HHx) + FucoPol	-59,92	3,078	No	ns	-152.9 to 33.02
P(3HB-3HV-3HHx) vs Cell Control	-81,41	4,181	No	ns	-174.3 to 11.53
P(3HB-3HV-3HHx) + FucoPol vs Cell Control	-21,48	1,103	No	ns	-114.4 to 71.46

Table C.15 - ANOVA statistical analysis with Bonferroni's multiple comparison test of proliferation (after 7 days of cell culture) for PHA emulsion templated scaffolds with and without FucoPol

Table Analyzed	Proliferation after 7 days
One-way analysis of variance	
P value	0,0003
P value summary	***
Are means signif. different? (P < 0.05)	Yes
Number of groups	5
F	48,21
R squared	0,9747

ANOVA Table	SS	df	MS
Treatment (between columns)	54120	4	13530
Residual (within columns)	1403	5	280,6
Total	55520	9	

Bonferroni's Multiple Comparison Test	Mean Diff.	t	Significant? P < 0.05?	Summary	95% CI of diff
P(3HB) vs P(3HB) + FucoPol	-13,72	0,8190	No	ns	-93.68 to 66.25
P(3HB) vs P(3HB-3HV-3HHx)	166,6	9,942	Yes	**	86.59 to 246.5
P(3HB) vs P(3HB-3HV-3HHx) + FucoPol	-29,03	1,733	No	ns	-109.0 to 50.93
P(3HB) vs Cell Control	82,40	4,919	Yes	*	2.439 to 162.4
P(3HB) + FucoPol vs P(3HB-3HV-3HHx)	180,3	10,76	Yes	**	100.3 to 260.2
P(3HB) + FucoPol vs P(3HB-3HV-3HHx) + FucoPol	-15,32	0,9142	No	ns	-95.28 to 64.65
P(3HB) + FucoPol vs Cell Control	96,12	5,738	Yes	*	16.16 to 176.1
P(3HB-3HV-3HHx) vs P(3HB-3HV-3HHx) + FucoPol	-195,6	11,68	Yes	***	-275.6 to -115.6
P(3HB-3HV-3HHx) vs Cell Control	-84,15	5,023	Yes	*	-164.1 to -4.187
P(3HB-3HV-3HHx) + FucoPol vs Cell Control	111,4	6,652	Yes	*	31.47 to 191.4

C.3 ANOVA Statistical Analysis of Adhesion and Proliferation Tests Hot-Pressing Salt Leaching Scaffolds with and without FucoPol

Table C.16 - ANOVA statistical analysis with Bonferroni's multiple comparison test of adhesion (after 1 day of cell culture) for PHA hot-pressing salt leaching scaffolds with and without FucoPol.

Table Analyzed	Adhesion after 24h
One-way analysis of variance	
P value	< 0.0001
P value summary	***
Are means signif. different? (P < 0.05)	Yes
Number of groups	5
F	57,55
R squared	0,9505

ANOVA Table	SS	df	MS
Treatment (between columns)	18760	4	4690
Residual (within columns)	977,9	12	81,49
Total	19740	16	

Bonferroni's Multiple Comparison Test	Mean Diff.	t	Significant? P < 0.05?	Summary	95% CI of diff
P(3HB) vs P(3HB) + FucoPol	4,983	0,6047	No	ns	-23.27 to 33.24
P(3HB) vs P(3HB-3HV-3HHx)	14,62	2,121	No	ns	-9.014 to 38.26
P(3HB) vs P(3HB-3HV-3HHx) + FucoPol	13,48	1,636	No	ns	-14.77 to 41.74
P(3HB) vs Cell Control	-60,01	9,402	Yes	***	-81.90 to -38.13
P(3HB) + FucoPol vs P(3HB-3HV-3HHx)	9,640	1,233	No	ns	-17.16 to 36.44
P(3HB) + FucoPol vs P(3HB-3HV-3HHx) + FucoPol	8,500	0,9416	No	ns	-22.45 to 39.45
P(3HB) + FucoPol vs Cell Control	-65,00	8,819	Yes	***	-90.27 to -39.73
P(3HB-3HV-3HHx) vs P(3HB-3HV-3HHx) + FucoPol	-1,140	0,1458	No	ns	-27.94 to 25.66
P(3HB-3HV-3HHx) vs Cell Control	-74,64	12,81	Yes	***	-94.62 to -54.66
P(3HB-3HV-3HHx) + FucoPol vs Cell Control	-73,50	9,972	Yes	***	-98.77 to -48.23

Table C.17 - ANOVA statistical analysis with Bonferroni's multiple comparison test of proliferation (after 4 days of cell culture) for PHA hot-pressing salt leaching scaffolds with and without FucoPol.

Table Analyzed	Proliferation after 4 days
One-way analysis of variance	
P value	0,0035
P value summary	**
Are means signif. different? (P < 0.05)	Yes
Number of groups	5
F	13,82
R squared	0,9021

ANOVA Table	SS	df	MS
Treatment (between columns)	7936	4	1984
Residual (within columns)	861,2	6	143,5
Total	8797	10	

Bonferroni's Multiple Comparison Test	Mean Diff.	t	Significant? P < 0.05?	Summary	95% CI of diff
P(3HB) vs P(3HB) + FucoPol	-62,19	5,191	Yes	*	-113.9 to -10.47
P(3HB) vs P(3HB-3HV-3HHx)	-36,35	3,034	No	ns	-88.07 to 15.37
P(3HB) vs P(3HB-3HV-3HHx) + FucoPol	-16,75	1,398	No	ns	-68.47 to 34.97
P(3HB) vs Cell Control	-69,68	6,371	Yes	**	-116.9 to -22.47
P(3HB) + FucoPol vs P(3HB-3HV-3HHx)	25,85	2,157	No	ns	-25.87 to 77.56
P(3HB) + FucoPol vs P(3HB-3HV-3HHx) + FucoPol	45,45	3,793	No	ns	-6.273 to 97.17
P(3HB) + FucoPol vs Cell Control	-7,488	0,6846	No	ns	-54.70 to 39.73
P(3HB-3HV-3HHx) vs P(3HB-3HV-3HHx) + FucoPol	19,60	1,636	No	ns	-32.12 to 71.32
P(3HB-3HV-3HHx) vs Cell Control	-33,33	3,048	No	ns	-80.55 to 13.88
P(3HB-3HV-3HHx) + FucoPol vs Cell Control	-52,93	4,840	Yes	*	-100.1 to -5.721

Table C.18 - ANOVA statistical analysis with Bonferroni's multiple comparison test of proliferation (after 7 days of cell culture) for PHA hot-pressing salt leaching scaffolds with and without FucoPol.

Table Analyzed	Proliferation after 7 days
One-way analysis of variance	
P value	< 0.0001
P value summary	***
Are means signif. different? (P < 0.05)	Yes
Number of groups	5
F	195,8
R squared	0,9899

ANOVA Table	SS	df	MS
Treatment (between columns)	86930	4	21730
Residual (within columns)	888,0	8	111,0
Total	87820	12	

Bonferroni's Multiple Comparison Test	Mean Diff.	t	Significant? P < 0.05?	Summary	95% CI of diff
P(3HB) vs P(3HB) + FucoPol	-155,6	14,77	Yes	***	-196.0 to -115.2
P(3HB) vs P(3HB-3HV-3HHx)	98,31	10,22	Yes	***	61.45 to 135.2
P(3HB) vs P(3HB-3HV-3HHx) + FucoPol	56,57	5,370	Yes	**	16.19 to 96.95
P(3HB) vs Cell Control	-27,92	3,060	No	ns	-62.89 to 7.049
P(3HB) + FucoPol vs P(3HB-3HV-3HHx)	253,9	26,40	Yes	***	217.1 to 290.8
P(3HB) + FucoPol vs P(3HB-3HV-3HHx) + FucoPol	212,2	20,14	Yes	***	171.8 to 252.6
P(3HB) + FucoPol vs Cell Control	127,7	14,00	Yes	***	92.73 to 162.7
P(3HB-3HV-3HHx) vs P(3HB-3HV-3HHx) + FucoPol	-41,74	4,340	Yes	*	-78.60 to -4.879
P(3HB-3HV-3HHx) vs Cell Control	-126,2	15,69	Yes	***	-157.1 to -95.39
P(3HB-3HV-3HHx) + FucoPol vs Cell Control	-84,49	9,260	Yes	***	-119.5 to -49.52

C.4 ANOVA Statistical Analysis of Adhesion and Proliferation Tests for both Emulsion templated and Hot-Pressing Salt Leaching Scaffolds with FucoPol

Table C.19 - ANOVA statistical analysis with Bonferroni's multiple comparison test of adhesion (after 1 day of cell culture) for both PHA emulsion templated and hot-pressing salt leaching scaffolds with FucoPol.

Table Analyzed	Adhesion after 24h
One-way analysis of variance	
P value	0,0985
P value summary	ns
Are means signif. different? (P < 0.05)	No
Number of groups	4
F	4,235
R squared	0,7606

ANOVA Table	SS	df	MS
Treatment (between columns)	271,9	3	90,63
Residual (within columns)	85,60	4	21,40
Total	357,5	7	

Bonferroni's Multiple Comparison Test	Mean Diff.	t	Significant	Summary	95% CI of diff
P(3HB) + FucoPol - Emulsion Te vs P(3HB-3HV-3HHx) + FucoPol - Em	3,080	0,6658	No	ns	-19.36 to 25.52
P(3HB) + FucoPol - Emulsion Te vs P(3HB) + FucoPol - Hot-Pressin	7,040	1,522	No	ns	-15.40 to 29.48
P(3HB) + FucoPol - Emulsion Te vs P(3HB-3HV-3HHx) + FucoPol - Ho	15,54	3,359	No	ns	-6.900 to 37.98
P(3HB-3HV-3HHx) + FucoPol - Em vs P(3HB) + FucoPol - Hot-Pressin	3,960	0,8561	No	ns	-18.48 to 26.40
P(3HB-3HV-3HHx) + FucoPol - Em vs P(3HB-3HV-3HHx) + FucoPol - Ho	12,46	2,694	No	ns	-9.980 to 34.90
P(3HB) + FucoPol - Hot-Pressin vs P(3HB-3HV-3HHx) + FucoPol - Ho	8,500	1,838	No	ns	-13.94 to 30.94

Table C.20 - ANOVA statistical analysis with Bonferroni's multiple comparison test of proliferation (after 4 days of cell culture) for both PHA emulsion templated and hot-pressing salt leaching scaffolds with FucoPol.

Table Analyzed	Proliferation after 4 days
One-way analysis of variance	
P value	0,0036
P value summary	**
Are means signif. different? (P < 0.05)	Yes
Number of groups	4
F	28,90
R squared	0,9559

ANOVA Table	SS	df	MS
Treatment (between columns)	5199	3	1733
Residual (within columns)	239,9	4	59,97
Total	5439	7	

Bonferroni's Multiple Comparison Test	Mean Diff.	t	Significant	Summary	95% CI of diff
P(3HB) + FucoPol - Emulsion Te vs P(3HB-3HV-3HHx) + FucoPol - Em	42,57	5,497	Yes	*	5.001 to 80.13
P(3HB) + FucoPol - Emulsion Te vs P(3HB) + FucoPol - Hot-Pressin	24,27	3,134	No	ns	-13.30 to 61.84
P(3HB) + FucoPol - Emulsion Te vs P(3HB-3HV-3HHx) + FucoPol - Ho	69,72	9,003	Yes	**	32.15 to 107.3
P(3HB-3HV-3HHx) + FucoPol - Em vs P(3HB) + FucoPol - Hot-Pressin	-18,30	2,363	No	ns	-55.86 to 19.27
P(3HB-3HV-3HHx) + FucoPol - Em vs P(3HB-3HV-3HHx) + FucoPol - Ho	27,15	3,506	No	ns	-10.42 to 64.72
P(3HB) + FucoPol - Hot-Pressin vs P(3HB-3HV-3HHx) + FucoPol - Ho	45,45	5,869	Yes	*	7.879 to 83.01

Table C.21 - ANOVA statistical analysis with Bonferroni's multiple comparison test of proliferation (after 7 days of cell culture) for both PHA emulsion templated and hot-pressing salt leaching scaffolds with FucoPol.

Table Analyzed	Proliferation after 7 days
One-way analysis of variance	
P value	0,0004
P value summary	***
Are means signif. different? (P < 0.05)	Yes
Number of groups	4
F	86,23
R squared	0,9848

ANOVA Table	SS	df	MS
Treatment (between columns)	67480	3	22490
Residual (within columns)	1043	4	260,9
Total	68530	7	

Bonferroni's Multiple Comparison Test	Mean Diff.	t	Significant	Summary	95% CI of diff
P(3HB) + FucoPol - Emulsion Te vs P(3HB-3HV-3HHx) + FucoPol - Em	-15,32	0,9482	No	ns	-93.66 to 63.03
P(3HB) + FucoPol - Emulsion Te vs P(3HB) + FucoPol - Hot-Pressin	-8,344	0,5166	No	ns	-86.69 to 70.00
P(3HB) + FucoPol - Emulsion Te vs P(3HB-3HV-3HHx) + FucoPol - Ho	203,8	12,62	Yes	**	125.5 to 282.2
P(3HB-3HV-3HHx) + FucoPol - Em vs P(3HB) + FucoPol - Hot-Pressin	6,971	0,4316	No	ns	-71.38 to 85.32
P(3HB-3HV-3HHx) + FucoPol - Em vs P(3HB-3HV-3HHx) + FucoPol - Ho	219,2	13,57	Yes	**	140.8 to 297.5
P(3HB) + FucoPol - Hot-Pressin vs P(3HB-3HV-3HHx) + FucoPol - Ho	212,2	13,14	Yes	**	133.8 to 290.5

2024

JOÃO RICARDO ANTUNES DOS SANTOS SOARES PEREIRA

ACTIVE DRESSINGS BASED ON NATURAL POLYMERS FOR WOUND TREATMENT